UNIVERSIDADE DE SÃO PAULO
INSTITUTO DE FÍSICA DE SÃO CARLOS

GIULIA KASSAB

Pulmonary antimicrobial photodynamic therapy and the role of the lung surfactant

São Carlos
2022

GIULIA KASSAB

Pulmonary antimicrobial photodynamic therapy and the role of the lung surfactant

Thesis presented to the Graduate Program in Physics at the Instituto de Física de São Carlos, Universidade de São Paulo to obtain the degree of Doctor of Science.

Concentration area: Applied Physics
Option: Biomolecular Physics
Advisor: Prof. Dr. Vanderlei Salvador Bagnato

Corrected Version
(Original version available on the Program Unit)

São Carlos
2022

Kassab, Giulia
Pulmonary antimicrobial photodynamic therapy and the role of the lung surfactant / Giulia Kassab; advisor Vanderlei Salvador Bagnato - corrected version -- São Carlos 2022.
111 p.

Thesis (Doctorate - Graduate Program in Biomolecular Physics) -- Instituto de Física de São Carlos, Universidade de São Paulo - Brasil , 2022.

1. Pneumonia. 2. Antimicrobial photodynamic therapy. 3. Lung surfactant. I. Bagnato, Vanderlei Salvador, advisor. II. Title.

To my grandmother Bruna and my grandfather Jamil

ACKNOWLEDGEMENTS

I would like to express my deepest gratitude to all of those who were part of making this thesis a reality. To my advisor, Professor Vanderlei, who once again trusted me and allowed me to walk on my own two feet. To the Coordination for the Improvement of Higher Education Personnel (CAPES, Financial code 001) and the São Paulo Research Foundation (FAPESP, process #2018/18188-0), for the fundamental and much appreciated financial support. To Professor Cristina Kurachi, who was never my official advisor but was there every step of the way. To my colleagues from the pulmonary decontamination project, especially Johan, Ana Júlia and Samara. To every single mouse and pig that were part of this study.

To the scientific contribution of the many collaborators of this project: Professors Kleber T. de Oliveira and Clóvis W. O. de Souza from UFSCar; Professors Jeffrey Cirillo and Vladislav Yakovlev and Doctor Madeleine Moule from Texas A&M University; Professor André S. Pimentel and his students from PUC-RJ; Professor Véronique Rosilio and Doctor Jean-Phillipe Michel from Université Paris-Saclay; Professor Gang Zheng and Doctor Juan Chen from University Health Network; Professor Paulo Pêgo Fernandes and his team from InCor-USP; Professor Marcelo Amato and his team from FM-USP; Professors Eduardo Carrilho and Daniel Cardoso and their teams from IQSC-USP; and Doctor Laís C. Brazaca from Harvard University. To all the support from the CEPOF office, the IFSC graduate service, the IFSC library, and the labs LAT and LIEPO. To the support from the colleagues at the Biophotonics lab, especially the ones in microbiology, tissue culture and animal research.

And to the unending support of my friends and family, that were there for me through the hardest of times, my deepest thank you.

“The truth is we don’t know what we don’t know. We don’t even know the questions we need to ask in order to find out, but when we learn one tiny little thing, a dim light comes on in a dark hallway, and suddenly a new question appears. We spend decades, centuries, millennia, trying to answer that one question so that another dim light will come on. That’s science, but that’s also everything else, isn’t it? Try. Experiment. Ask a ton of questions.”

— Yaa Gyasi, in “Transcendent Kingdom”

ABSTRACT

KASSAB, G. **Pulmonary antimicrobial photodynamic therapy and the role of the lung surfactant**. 2022. 112p. Thesis (Doctor in Science) - Instituto de Física de São Carlos, Universidade de São Paulo, São Carlos, 2022.

Pneumonia is one of the largest causes of death worldwide and antimicrobial photodynamic therapy (aPDT) has been proposed as a broad-spectrum, resistance-proof treatment alternative for it. The initial objective of this study was to demonstrate the efficacy of indocyanine green (ICG)-based aPDT against multiple pathogens and its safety in different animal models. *In vitro*, the aPDT protocol successfully inactivated two strains of *S. aureus*, while showing no cytotoxicity to three different mammalian cell lines. *In vivo*, mice that received the treatment showed no signs of tissue damage or inflammation. However, the *in vivo* treatment of bacterial pneumonia was unsuccessful, despite multiple attempts in three different models. Further investigation of the interaction between photosensitizers and the pulmonary microenvironment showed that photosensitizers interact with the lung surfactant. This interaction does not inhibit the generation of reactive oxygen species, but instead distances them from the bacterial target, leading to a loss of activity. The clinical lung surfactant Survanta® decreases the aPDT effect of ICG, Photodithazine®, bacteriochlorin-trizma and protoporphyrin IX against *S. pneumoniae*. Methylene blue (MB) did not lose efficacy in this experimental setup, but its activity was quenched in the *in vitro* alveolar model, in which the localized concentration of lung surfactant is higher. Surface chemistry-based experiments revealed that ICG has a strong surface activity and interacts strongly with Survanta® and LPS. MB is not surface-active but has some interaction with Survanta® if mixed directly into it. The nanoemulsions neMB and nePS exhibit surface-activity as they slowly break into single molecules on the surface, and interact with the multilayered Survanta®. We have established the importance of the lung surfactant in the development of pulmonary aPDT and propose that formulation strategies can be used to overcome the lung surfactant barrier. ICG remains the most promising candidate for pulmonary PDT because of its safety and excitation range, and preliminary results indicate that combining it with the perfluorocarbon PFOB might be a viable alternative for the treatment of in-hospital patients. Additionally, preliminary results with a MB nanoemulsion have been promising and might aid the development of new pulmonary photosensitizers in the future.

Keywords: Pneumonia. Antimicrobial photodynamic therapy. Lung surfactant.

RESUMO

KASSAB, G. **Terapia fotodinâmica antimicrobiana pulmonar e o papel do surfactante pulmonar**. 2022. 112p. Tese (Doutorado em Ciências) - Instituto de Física de São Carlos, Universidade de São Paulo, São Carlos, 2022.

A pneumonia é uma das principais causas de morte no mundo, e a terapia fotodinâmica antimicrobiana (TFDa) tem sido proposta como uma alternativa de tratamento de amplo espectro e à prova de resistência. O objetivo inicial deste projeto foi demonstrar a eficácia da TFDa utilizando indocianina verde (ICG) no tratamento de múltiplos patógenos e também sua segurança em diferentes modelos animais. *In vitro*, o protocolo de TFDa proposto inativou duas cepas de *S. aureus* em condições que não foram tóxicas a três linhagens celulares de mamíferos. In vivo, camundongos que receberam o tratamento não mostraram nenhum sinal de dano tecidual ou inflamação. No entanto, o tratamento da pneumonia bacteriana *in vivo* não foi bem sucedido, apesar de múltiplas tentativas em diferentes modelos. Uma análise mais profunda revelou que fotossensibilizadores interagem com o surfactante pulmonar. Essa interação não inibe a formação de espécies reativas de oxigênio, mas as afasta do alvo bacteriano, levando a uma perda de atividade. O surfactante pulmonar de grau clínico Survanta® reduz o efeito da TFDa com ICG, Photodithazine®, bacterioclorina-trizma e protoporfirina IX contra a bactéria *S. pneumoniae*. O azul de metileno (MB) foi eficaz nesse experimento, mas não no modelo de alvéolo *in vitro*, em que a concentração de surfactante pulmonar é maior. Experimentos baseados em química de superfícies mostraram que a ICG apresenta uma forte ação surfactante e que interage com o Survanta® e com LPS. O MB não apresenta ação surfactante, mas interage com o Survanta® se misturado diretamente a ele. Já as nanoemulsões neMB e nePS apresentam ação surfactante conforme se desfazem e liberam seus componentes na superfície, e interagem com o Survanta® quando está organizado em múltiplas camadas. Nós estabelecemos a importância do surfactante pulmonar no desenvolvimento de tratamentos de TFDa pulmonar, e propusemos que estratégias de formulação podem ser utilizadas para superar a barreira imposta por ele. A ICG se mantém como melhor candidata para a TFDa pulmonar por causa de sua segurança e sua faixa de excitação, e resultados preliminares de sua combinação com o perfluorcarbono PFOB indicam que esta pode ser uma opção viável para o tratamento de pacientes internados. Além disso, resultados preliminares com a nanoemulsão neMB foram promissores e podem ajudar a direcionar o desenvolvimento de novos fotossensibilizadores para aplicação pulmonar no futuro.

Palavras-chave: Pneumonia. Terapia fotodinâmica antimicrobiana. Surfactante pulmonar.

CONTENTS

1 INTRODUCTION

Lower respiratory infections are one of the largest causes of death worldwide, especially in the elderly and children under 5 years of age.[1-2] However, antibiotic-based therapy faces a crisis due to the increase in resistance and a lack of new molecules.[3] Moreover, many antibiotics used to treat pneumonia are toxic and lead to systemic morbidity.[4] One example is the first-choice drug for methicillin-resistant *Staphylococcus aureus* (MRSA) pneumonia, vancomycin, that demonstrates treatment failure rates of up to 70% due to low tissue penetration in the lungs and high renal toxicity.[5] A promising alternative to this approach is photodynamic inactivation (PDI), the microbiological application of photodynamic therapy (PDT). Unlike antibiotic therapies, the development of resistance to PDI has been described to be highly unlikely.[6] PDI is based on the combination of a photosensitizer, light at a specific wavelength, and molecular oxygen, which generates reactive oxygen species (ROS) that cause cell death.[6] In theory, all biomolecules are possible targets, and thus the induced damage and resultant death are not dependent on a specific molecule or pathway. Another benefit of PDI is its double selectivity, from both increased photosensitizer accumulation in the microorganisms compared to hosts cells, and the restricted exposure to light on the affected area.[7] Exposure-based selectivity allows for reduction of undesired systemic effects.

With that in mind, the applicability of PDI in the treatment of streptococcal pneumonia using the photosensitizer indocyanine green (ICG) and extracorporeal activation with infrared light has been proposed and previously investigated by our research group. Initial *in vitro* studies showed that it was possible to eliminate *S. pneumoniae* using doses of ICG and light that did not show adverse effects in macrophages.[8] Then, *in vivo* studies showed reduction of the bacterial burden and increase the survival rate of previously infected mice.[9] An additional study proposed nebulization as a new pulmonary delivery method for photosensitizers, demonstrated its compatibility with ICG, and validated the delivery in a murine model.[10] The combination of ICG and infrared light has also been proposed for the treatment of other pulmonary pathogens.[11-12]

In this study, we have proposed to expand upon the proof-of-principle and perform pre-clinical studies to demonstrate the efficacy of ICG-aPDT against multiple pathogens and safety in different models, as to eventually advance it to clinical trials. Unfortunately, obtaining successful results in the *in vivo* treatment of bacterial pneumonia was a challenge, and it was eventually discovered that components of the pulmonary microenvironment were

inhibiting the expected photoactivity. The, we proposed to investigate the interaction between these components, in particular the lung surfactant, and the photosensitizers. After learning more about the nature and prevalence of this inhibition effect, we proposed alternative strategies for future photodynamic treatments of bacterial pneumonias.

2 LITERATURE REVIEW[†]

2.1 Infectious pneumonia

Lower respiratory infections are the fourth largest cause of death worldwide.[1] The most frequent lower respiratory infections are acute bronchitis and bronchiolitis, influenza, and pneumonia.[13] Pneumonia is the main infectious cause of death in Europe and the United States.[13] It is also the worldwide main cause of death of children younger than 5 years old.[14] In Brazil, pneumonia is the number one cause of hospitalization.[15] Although the number of hospitalizations has decreased over the past decades, the in-hospital mortality increased, what is mainly explained by the aging of the population and the occurrence of cases of pneumonia that are more difficult to treat.[15]

The European Respiratory Society defines pneumonia as an acute illness of the lower respiratory tract that includes cough and at least one other symptom: new focal chest signs, new lung shadowing shown by radiography, otherwise unexplained fever for more than 4 days, or otherwise unexplained tachypnea/dyspnea.[13] Until 2020, bacterial infections accounted for most of the pneumonia-related hospitalizations and deaths worldwide.[16-17] Community Acquired Pneumonia (CAP) is contracted from contact with the infection in day-to-day life.[13] It is predominantly bacterial in origin, being *Streptococcus pneumoniae* its most prevalent pathogen.[18] Other important agents are *Haemophilus influenza*, *Pseudomonas aeruginosa*, *Chlamydophila pneumoniae, Mycoplasma pneumoniae*, *Legionella pneumophila*, and *Coxiella burnetii.*[18,19] About 30% of cases present coinfections with viruses.[17,20]

Hospital Acquired Pneumonia (HAP), also called nosocomial pneumonia, is the one that develops after at least 48 hours after the patients admission to a hospital.[21] Its reported mortality rate ranges from 20 to 50%, the highest amongst nosocomial infections.[21] Ventilator-associated pneumonia (VAP) is the one contracted at least 48-72 hours after endotracheal intubation.[13] The most relevant agents of HAP and VAP are also bacteria, like *Staphylococcus aureus, Pseudomonas aeruginosa*, *Escherichia coli*, and *Klebsiella*, *Acinetobacter*, and *Enterobacter* species.[22]

The Coronavirus Disease 2019 (COVID-19) currently accounts for a large part of the morbidity and mortality of pneumonia, but is not classified as CAP, HAP, nor VAP.[23] Acute

[†] Sections 2.1 and 2.2 are updated versions of the literature review presented in the Master's dissertation of Kassab.[41]

respiratory manifestations are the most frequent feature of infection with the severe acute respiratory syndrome coronavirus 2 (SARS-CoV-2), but it is also related to many acute and long-term non-respiratory effects.[24] However, when based only on initial acute symptoms, COVID-19 might be difficult to distinguish from HAP and VAP in hospitalized patients.[25]

2.1.1 Current treatment alternatives and their limitations

In the vast majority of CAP cases, there is no investigation of the etiological agent.[15] In such situations, the treatment is based on the most prevalent microorganisms of that locality.[15] The main classes of antibiotics employed for CAP in Brazil are macrolides, beta-lactams and quinolones.[15] For COVID-19 pneumonia, the etiological agent is confirmed, but there are currently no antiviral treatments available with demonstrated efficacy in randomized clinical trials.[26] Because there is a risk of developing a secondary bacterial VAP, ventilated COVID-19 patients are often prescribed antibiotics.[25,27-28]

Knowledge of the etiological agents is of great importance in the treatment of HAP and VAP, since patients that receive the wrong initial therapy have a high risk of mortality and morbidity.[21] However, the delay in starting the treatment also leads to a poor prognostic.[21] A great concern in HAP and VAP cases is the presence of methicillin-resistant *Staphylococcus aureus* (MRSA), which is associated with elevated mortality rates and treatment costs.[5] Traditionally, the first-choice drug for MRSA infections is vancomycin, that due to its low penetration in the lungs and high renal toxicity, leads to a failure rate the can reach 70%.[5]

Even with new drugs like linezolid, tigecycline and ceftaroline, persists the difficulty in increasing the success rate of treatments, and the concern with development of resistance.[5,29] Linezolid, for example, was approved for clinical use in 2000, and cases of resistance in patients were reported as early as 2002.[30] In a study from 2014, the occurrence of non-susceptibility to this antibiotic remained relatively low, but a number of different resistance mechanisms to it had already been observed.[30]

Another approach to hinder the burden of pneumonia is vaccination. Two types of vaccines are currently available for *S. pneumoniae*, the main agent in CAP: the pneumococcal polysaccharide vaccine (PPV) has been recommended for adults since the mid-1980's, but it lacks efficacy in neonates and infants;[31] the pneumococcal conjugate vaccines (PCVs), designed to overcome that, were first approved in 2000.[32] However, pneumococcal vaccination faces two main challenges: first, each vaccine is only effective against the

serotypes contained in it; second, the reduction of the said serotypes increases the colonization of other serotypes that are not covered by the vaccines, and of other pathogen species like *S. aureus* and *H. influenza.*[31] The same challenges are true for influenza and SARS-CoV-2 vaccines.[33-34] The time it takes to distribute and deliver the vaccines to populations worldwide is much larger than the time it takes for the virus to spread and mutate.[34] Thus, new vaccines need to be developed continuously, similarly to what happens to antibiotics.[31]

2.2 Photodynamic inactivation of microorganisms

The photodynamic inactivation (PDI) of microorganisms was first described in 1900 by Oscar Raab.[35] It is based in the use of a photosensitizer that accumulates preferably in the pathogens, and that is activated by light at a specific wavelength, and in the presence of molecular oxygen generates reactive species that are toxic to the target.[3] The clinical application of PDI, denominated antimicrobial photodynamic therapy (aPDT) is particularly interesting for fighting infections because there is no evidence of cross-resistance with antibiotics, and the restriction of the light exposure offers a further degree of selectivity.[24-25] Moreover, since PDI can damage a variety of molecules, unlike the target-specific antibiotics, the development of resistance of previously-susceptible strains to this treatment is described as highly unlikely.[6]

2.2.1 Mechanism

The photodynamic process starts with an electron transfer to a higher energy orbital after the absorption of light by the photosensitizer.[38] The excited molecule may dissipate this energy emitting fluorescence, or go through an intersystem crossing and go to a triplet state.[38] From there, the energy can be dissipated non-radioactively, or generate toxicity through either of two mechanisms: in the type I reaction, the photosensitizer reacts with adjacent organic molecules and forms reactive oxygen species (ROS); in the type II reaction, there is an energy transfer to the molecular oxygen, which is a triplet in its basal state ($^3O_2$), and it goes to a singlet state ($^1O_2$).[38] Both reactions contribute to the phototoxic effect, and both singlet oxygen and the ROS have short half-life times, limiting their diffusion and therefore the effect of the PDI to the site of light exposure.[39-40] The Jablonski diagram illustrates this mechanism (Figure 1).

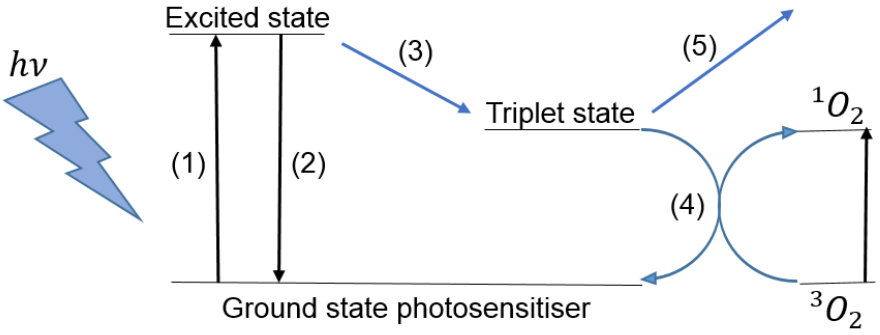

(1) Absorption; (2) Fluorescence; (3) Intersystem crossing;
(4) Type II reaction (energy transfer); (5) Type I reaction.

Figure 1 - Simplified Jablonski diagram.
Source: KASSAB *et al.*[41]

2.2.2 Photosensitizers

Indocyanine Green (ICG) is a water-soluble cyanine dye that emits fluorescence when exposed to infrared light (Figure 2).[42] Its absorption peak is 780 nm in water and 805 nm in human plasma.[43-44] ICG is approved by the FDA as a diagnostic agent for cancer, the determination of the cardiac debt and liver function, and in ophthalmic angiography.[45-46] It is not ideal for the photodynamic therapy of cancers because of its short half-life time in the blood.[45] However, studies employing ICG for the elimination of microorganisms through PDI have had promising results *in vitro* and *in vivo.*[46–48]

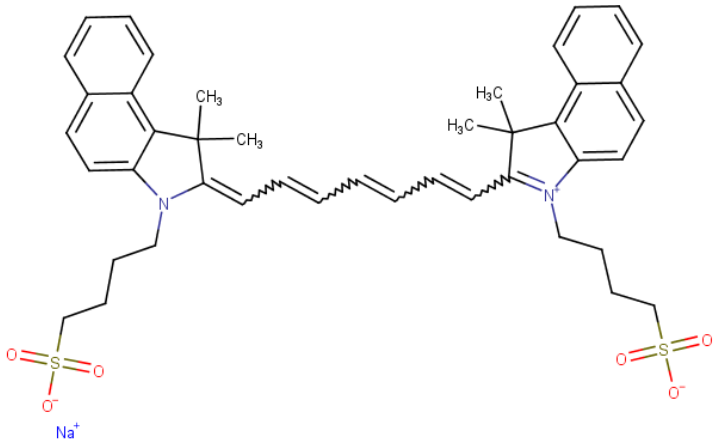

Figure 2 - Chemical structure of Indocyanine Green (ICG).
Source: KASSAB *et al.*[41]

Methylene blue (MB) is a phenothiazine dye (Figure **3**). It was first synthetized in the late 1800s and was quickly popularized as a microscopy stain and an antiseptic.[49] It is approved by the FDA as an antidote for symptomatic methemoglobinemia.[50] MB shows

maximum absorbance at 664 nm, and has a high quantum yield of singlet oxygen (ϕ_Δ~0.5).[51] As a photosensitizer, MB has been investigated for the treatment of multiple cancers and infections,[51–53] has shown encouraging results in clinical trials for wounds, autoimmune disorders and dentistry applications.[54–56]

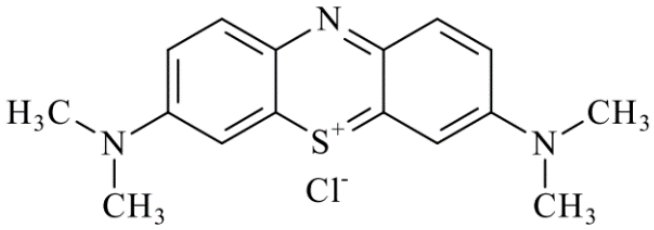

Figure 3 - Chemical Structure of Methylene Blue (MB).
Source: INTERNATIONAL…[49]

2.2.3 Light penetration into biological tissue

For aPDT to be effective, light needs to be able to reach the pathogens in sufficient dose, despite the dispersion and absorption of the adjacent layers of tissue.[3] Therefore, the choice of wavelength should take into account the depth of light penetration, the absorbance spectrum of the photosensitizer, and the location of the infectious agents.[3]

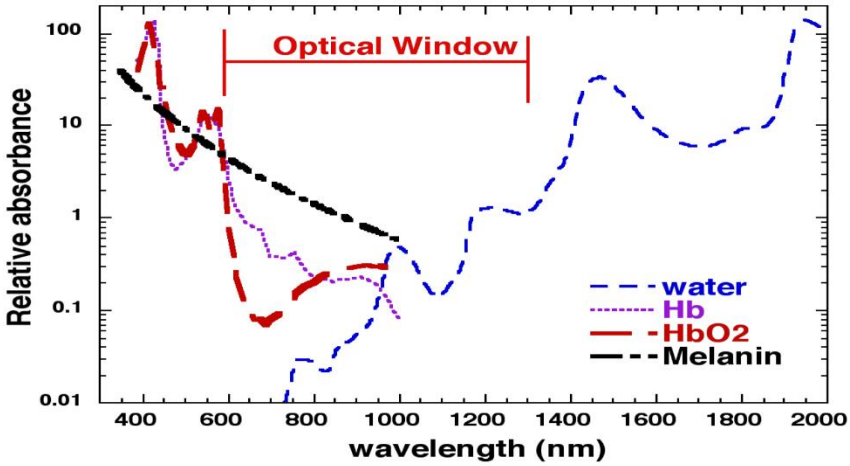

Figure 4 - The tissue optical window. Hb: hemoglobin; HbO_2: oxygenated hemoglobin. Note that the relative absorbance varies logarithmically.
Source: HUANG *et al.*[57]

It is desirable to have the light excitation at around 650 to 1000 nm, because light at this range penetrates deeper into biological tissue, since it is less absorbed by water, melanin and hemoglobin (Figure 4).[57] Because of that, this range is known as the “optical window” or the “therapeutic window” for photodynamic therapy.[57-58] However, most photosensitizer do not

absorb wavelengths greater than 800 nm, so the usual excitation sources have peaks that range from 650-850 nm.[60-61]

2.2.4 Photodynamic Inactivation of pneumonia-causing pathogens

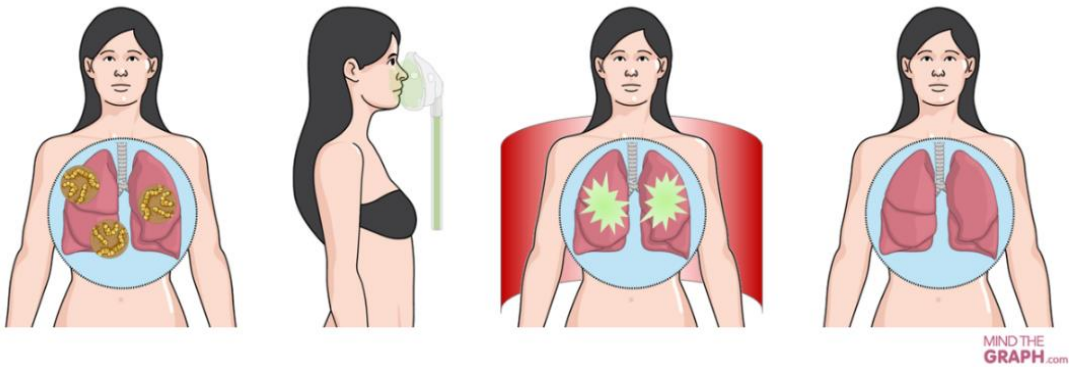

Figure 5 - Schematic representation of the proposed clinical antimicrobial photodynamic treatment of pneumonia. Upon confirmed infection, the patient would receive the photosensitizer through nebulization, then be exposed to light using an external source with peak emission in the near-infrared. The light would go through the layers of biological tissue and activate the photosensitizer in the lungs, killing the infective agent.
Source: KASSAB *et al.*[61]

The combination of the photosensitizer indocyanine green (ICG) and external activation with infrared light has been initially proposed for the treatment of pulmonary infections by our research group in 2014 (as described in Figure **5**).[63-64] In 2017, Leite *et al* showed that it was possible to eliminate *S. pneumoniae* using doses of ICG and light that were unharmful to macrophages.[8] Moreover, there was evidence that the aPDT could potentialize the antimicrobial activity of such macrophages during the infection.[8] A follow-up *in vivo* investigation made by Geralde *et al* found a reduction in the bacterial burden and an increase in the survival rate of SKH-1 hairless mice infected with *S. pneumoniae* after a single aPDT session using ICG 100 μM and 120 J/cm² of light at 780 nm.[9] In this study, the light exposure did not seem to be harmful to the animals. Additionally, the ICG alone was no different form the control, suggesting that the activation with light was essential to the observed effects. In 2019, Kassab *et al* proposed nebulization as a new delivery method, demonstrated its compatibility with ICG and validated the delivery in an animal model.[64] Pulmonary delivery using nebulization has also been proposed for other photosensitizers such as methylene blue and curcumin.[65–67] Finally, in 2021, Tovar *et al* demonstrated the activation of ICG and its PDI effect in *S. pneumoniae* when illuminated through the thoracic cage in an *ex vivo* pig carcass, proposing a model for the light distribution in this scenario and suggesting that treatment times would be compatible with a clinical context.[68]

Antimicrobial PDT has also been proposed for other pneumonia pathogens. Wong *et al* found that methicillin-resistant strains of *S. aureus* were more susceptible to ICG-aPDT than methicillin-susceptible strains. They also reported a reversion of the resistant phenotype in one of the strains after *in vitro* PDI treatment.[12] Methylene blue, radachlorin, a zinc phtalocyanine and a curcumin nanoparticle have shown efficient killing of SARS-CoV-2 *in vitro*. [69–72] In 2020, Weber *et al* reported the use of riboflavin and blue light to decontaminate the mouth and nose of COVID-19 patients, with promising results.[73] Meanwhile, Pourhajibagher and Bahador predicted using *in silico* analysis that ICG would have a high affinity for the domain responsible for cellular invasion in SARS-CoV-2.[74] Promising *in vitro* results have also been described for the photodynamic inactivation of the influenza virus.[75,76] However, there has not yet been any description of successful pulmonary aPDT treatment of any of these pathogens in *in vivo* pneumonia models.

2.3 The Lung Surfactant

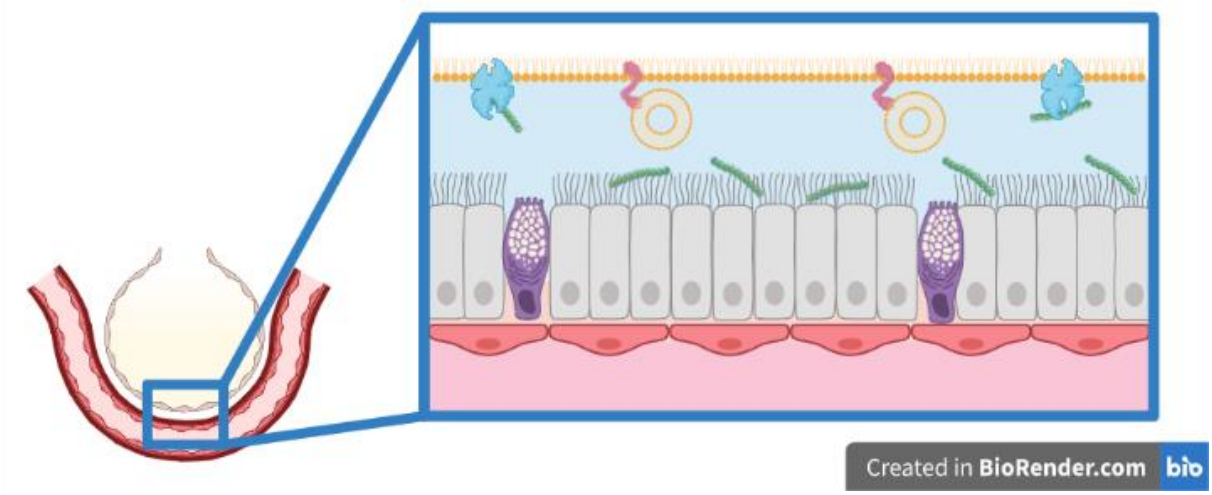

Figure 6 - Schematic representation of the alveolar microenvironment. The alveolar sac enables the exchange of gas between the blood vessel and the air (left). In detail, the endothelium (red) interfaces the type I (gray) and type II (purple) pneumocytes through extracellular matrix. Type II pneumocytes express the phospholipids (yellow) and proteins that compose the lung surfactant into the hypophase (light blue). Also in the hypophase are eventual pathogens, represented here by *S. pneumoniae* (green). The phospholipids cover the surface area but are also present in the subphase in multiple structures, represented here by unilamellar liposomes. Proteins are represented by function: mediating the transport of phospholipids to and from the surface (bright pink); and interacting with the pathogen (bright blue). Not to scale.
Source: By the author, made using www.biorender.com.

The human lung has a surface area of 1 m²/kg of weight, being composed of about 3 x 10^8 alveoli, that are covered by a thin liquid lining called the hypophase.[77] The lung surfactant (LS) is a mixture of phospholipids and proteins that prevent the alveoli from collapsing and enables the gas exchange by decreasing the surface tension of the air-water interface in the hypophase.[78-79] It also acts as a barrier, protecting the organism from contaminants in the

air.[79-80] It is synthetized, processed, packaged, secreted and recycled by type II pneumocytes.[77] Figure 6 depicts the alveolar microenvironment, in which the lung surfactant is present.

The main phospholipid component of the LS is dipalmitoyl phosphatidylcholine (DPPC), a rigid, saturated phospholipid that is not frequent in cell membranes. DPPC is able to reduce surface tension to extremely low values, but has a poor ability to respread after compression.[77] Other molecules from the phosphatidyl-choline (PC) class are present, as well as phosphatidylglycerols (PG), phosphatidyl-inositols (PI), phosphatidylserines (PS), phosphatidylethanolamines (PE), and sphingomyelins (Sph). Table 1 shows the relative composition of the endogenous lung surfactant after it has been isolated from the bronchoalveolar lavage. There are also neutral lipids present, and four surfactant proteins: SP-A, SP-B, SP-C and SP-D. SP-B and SP-C are hydrophobic and mediate the adsorption of the phospholipids into the interface and into lamellar structures in the subphase.[78,80] SP-A and SP-D are hydrophilic and have the ability to recognize infectious agents and modulate the immune response to them.[81] Despite being hydrophilic, SP-A interacts strongly with the phospholipids, and also plays a role in how they organize.[77] SP-D, on the other hand, is found in the lipid-depleted supernatant after centrifugation of the lung surfactant, and therefore is not listed on Table 1.

Table 1 – Representative composition of lavaged endogenous lung surfactant

85-90% phospholipids	DPPC (30%) Other saturated and unsaturated PC (40%) PG, PI, PS, PE, Sph are also prevalent
6-8% biophysically-active apoproteins	SP-A (5%) SP-B and SP-C (1,5% combined)
4-7% neutral lipids	Primarily cholesterol

Tabulated values are representative only (weight).

Source: Adapted from NOTTER.[77]

The interaction between the endogenous lung surfactant and pharmaceutical drugs has been previously described in the literature. In 2005, Silverman *et al* investigated why the antimicrobial daptomycin was effective against hematogenous pneumonia but not against bronchial-alveolar pneumonia, and found that it interacted with the LS and lost its efficacy.

According to them, this was “the first example of organ-specific inhibition of an antibiotic”.[82] Later, other studies found that a similar phenomenon occurs with antimicrobial peptides and multiple nanoparticles.[78,83–85] Nonetheless, exogenous LS has been proposed as a drug delivery agents for some of these and other drugs, in order to overcome poor solubility and improve biocompatibility.[84,86–88] Exogenous lung surfactant is also used as a drug itself for the treatment of respiratory distress syndrome in premature newborns, and has been proposed as an adjuvant treatment for COVID-19 pneumonia patients.[90-91]

3 EXPANDING THE PROOF-OF-PRINCIPLE AT THE PRE-CLINICAL LEVEL

Previous results had placed aPDT as a highly promising technique for the treatment of bacterial pneumonia. However, there were still several remaining questions to be answered regarding the range of pathogens that could be treated, the safety of the protocol, and pulmonary delivery of ICG. For ICG-aPDT to become a clinical treatment, it would be necessary to demonstrate its selectivity and understand the risks it could pose on patients. Thus, in this initial stage of the study, we proposed to develop a protocol that would be efficient against a pneumonia-causing pathogen, but harmless for mammalian cells types present in the lung alveoli. We then used an *in vivo* model to identify possible targets of adverse effects, and investigated the safety of the treatment.

The selectivity of ICG-PDI was initially investigated using *in vitro* bacterial and mammalian cell cultures. The study of the localization of the photosensitizer in an animal model was carried out to identify targeting efficiency using fluorescence techniques. For the safety tests, the photobleaching effect was used as an indicator of the photodynamic action on site, along with fluorescence imaging. This was followed by verification of animal behavior and general health conditions post-treatment, and histological analysis of the organs of interest. Since photobleaching is an indication of the presence of the photodynamic reaction, detecting its presence and demonstrating the integrity of the tissue provides proof of the safety of the protocol.[91] All experiments in this section were performed at the Health Science Center of Texas A&M University, under the co-supervision of Professor Jeffrey Cirillo. The results from this chapter have been published on the Journal of Biophotonics.[92]

3.1 Methodology

3.1.1 Photosensitizer and light sources

Indocyanine Green (Ophthalmos, Brazil) was weighted and diluted in sterile water to produce a stock solution (1.0 mM). For each experiment, the stock solution was used to prepare a working solution in the desired medium at each given concentration. Since ICG has a low stability in aqueous media, a fresh stock was prepared before each use. Two laser devices were custom-made for the light treatments: one for the *in vitro* experiments, composed of 6 diode lasers with emission centered at 808 nm and irradiance of 40 mW/cm^2;

and another device for the mouse experiments, composed of 18 diode lasers emitting at 808 nm, positioned in an array that produces an uniform illumination of the thorax from the back and its sides, and with a resulting irradiance of 120 mW/cm² at the surface of the region to be treated. The devices have the same design as the ones presented by Leite *et al*. and Geralde *et al*., but using 808 nm instead of 780 nm.[8-9]

3.1.2 Bacterial inactivation assays

Two strains of *Staphylococcus aureus*, Xen29 (PerkinElmer, USA) and Xen36 (PerkinElmer, USA), were grown from frozen stocks into Luria-Bertani agar containing kanamycin (200 µg/mL). Prior to each experiment, 3-5 colonies were seeded into Mueller-Hinton (MH) broth and grown overnight at 37 ºC and 220 rpm. Then, aliquots of these suspensions were transferred to fresh MH broth and grown to log-phase, with an optical density (OD600) of approximately 0.5. To assess the toxicity of ICG alone, a minimum inhibitory concentration (MIC) assay was performed. For this assay, the log-phase suspension of each strain was diluted to a final OD600 of about 0.005 in MH broth containing increasing concentrations of ICG (ranging from 0.78 to 400 µM). It was incubated at 37 ºC for 18 hours and serially diluted and plated onto MH agar, then incubated for another 18-24 hours so that the colony-forming units (CFU) could be counted. The minimum bactericidal concentration (MBC) assay was chosen to observe the effect of the light treatment and photodynamic inactivation. In this case, the Xen29 and Xen36 suspensions were diluted to a final OD of 0.05 of MH broth with or without ICG (10 µM). After 15 minutes of dark incubation, the bacterial suspensions were irradiated to increasing fluences of 808-nm infrared light at 40 mW/cm², ranging from 12.5 J/cm² (5 minutes and 13 seconds) to 200 J/cm² (1 hour, 23 minutes and 20 seconds). The samples were diluted and plated immediately after irradiation, and incubated at 37 ºC for 18-24 h for the CFU count. All experiments were performed in triplicate and repeated on 3 separate occasions (n=9).

3.1.3 Cytotoxicity assays

J774A.1 murine macrophages (ATCC® TIB-67™, ATCC, USA) and L929 murine fibroblasts (ATCC® CCL-1™, ATCC, USA) were cultured in Dulbecco’s modified Eagle medium (DMEM) supplemented with 10% fetal bovine serum (FBS). A549 human lung epithelial cells (ATCC® CCL-185™, ATCC, USA) were cultured in Ham's F-12K (Kaighn's)

Medium, also supplemented with 10% FBS. For each experiment, 2-5 x 10^4 cells were seeded into each well of 96-well plates and incubated at 37 ºC and 5% CO2 for 18-24 hours before the treatment protocols. To observe the toxicity of ICG alone, samples were incubated with increasing concentrations of the photosensitizer in their respective culture media (ranging from 6.25 to 400 µM). For the light-only and photodynamic toxicity, the cells were incubated in media with or without ICG (10 µM) for 15 minutes and then irradiated under 808-nm infrared light at the same irradiance and exposure times as the bacterial suspensions. The cell cultures were then placed back at the incubator for another 18 hours. To assess cell viability, the CellTiter 96® reagent was used (Promega Corporation, USA). Briefly, the samples were incubated with the reagent for 3 hours then read for absorbance at 490 nm using an EnVision plate reader (Perkin Elmer, USA). Positive controls (with untreated cells) and negative controls (with only the medium and reagent) were used to determine what 100% and 0% viability would be. All experiments were performed in triplicate and repeated on three separate occasions (n=9).

3.1.4 Animal experiments

Female BALB/c mice, aged 6-8 weeks and weighting 15 to 21 grams were used for this experiment. They were obtained from Envigo RMS, LLC (USA) and allowed to acclimate for at least a week with a 12/12h light-dark cycle with food and water *ad libitum*. Before each intervention, the animals were put under anesthesia using an intraperitoneal injection of ketamine and xylazine (KX, 75 and 5 mg/kg weight, respectively). Euthanasia was performed using pentobarbital sodium (Fatal-Plus, Vortech Pharmaceuticals, USA). All animal experiments were approved and performed under the guidelines of the Texas A&M University Institutional Animal Care and Use Committee. Fluorescence imaging was performed using the IVIS Spectrum and the Living Image software (PerkinElmer, USA), with the excitation filter set for 745 nm and the emission filter at 840 ± 40 nm. The exposure time was adjusted for each sample using the “auto” setting, that is achieved by an initial test run by the equipment in order to optimize the detection and avoid overexposure. The total radiant efficiency (expressed in [p/s] / [µW/cm²]) was extracted from the manually defined regions of interested (ROI) and then transformed either into relative fluorescence (RF) or into relative increase in fluorescence, depending on the experiment. For the ICG delivery assay, 8 animals (2 per experimental group) were anesthetized using KX and given a solution of ICG at 100 µM in water for injection either through endotracheal instillation (50 µL, using a 20G

catheter), intranasal instillation (30 µL, 15 in each nostril) or nebulization (using the Omron NE-C801 jet nebulizer for 6 minutes, in the same way as previously described by Kassab *et al*[64]). Animals were imaged immediately after the drug delivery. The controls were not given any drug nor sham solution. After euthanasia, the lungs, liver, and stomach were removed and imaged. The organs were then homogenized in 1.0 mL of phosphate buffer solution (PBS) and three aliquots of each sample were placed in a black 96-well plate and imaged once more. For the ICG bleaching and treatment safety experiment 7 animals were imaged, given ICG via nebulization, then imaged again. Subsequently, 3 mice were randomly assigned to receive the light treatment (PDI), while the other 4 were kept in the dark (ICG). After every 5 minutes (36 J/cm²) of exposure, the mice were imaged again side-by-side (in their pre-set pair or trio), until the light-treated animals received 30 minutes (or 216 J/cm²) of irradiation. In this experiment, the ROI were selected according to the region of the animal that was exposed to the light treatment, i.e. the thorax. The control animals (n=3) did not receive any type of treatment, and were monitored for later comparison with the treated groups. The mice were monitored once a day for 7 days using a general health score based on the one proposed by Hetze *et al*.[93] Their behavior, posture, eyes, fur, breath, and gastrointestinal health were tracked, being given a score from 0 (normal) to 2 (clearly affected) for each condition, resulting in a total score per animal ranging from 0 to 12. After 7 days, they were euthanized and the organs of interest (lungs, liver and stomach) were harvested for further analysis.

3.1.5 Organ and tissue toxicity analysis

Upon the harvest, the lungs, liver and stomach were macroscopically compared for signs of necrosis or distension. Then, the organs were blocked into paraffin, sliced, stained with hematoxylin and eosin (HE) and mounted onto microscopy slides. Each slide received a code and was analyzed using the Axio Observer Z1 microscope (Zeiss, Germany), in search for signs of inflammation and tissue damage. In the lungs, such signs were: inflammatory infiltrates, fibrosis, and bronchiolar epithelial damage. Liver samples were searched for necrosis. In the stomach, the mucosal, submucosal and muscular layers were observed for signs of necrosis. Only after that, the codes were matched with the corresponding experimental groups and the results were compared. Representative images of each group were obtained with the Pannoramic Desk digital slide scanner and the Pannoramic Viewer software (3DHISTECH Limited, Hungary).

3.1.6 Statistical analysis

All data was processed using Prism (GraphPad software, USA). CFU counts from the MIC experiments were compared using the Kruskal-Wallis test. For the MBC experiment, since multiple groups were monitored over time, the Friedman test was used to compare the treatments as a whole, with a *post hoc* Dunn multiple comparisons test. The Kruskal-Wallis test was used to compare the different light fluences within the same group, using the *post hoc* Dunn test to compare each dose to the group's "no light" control. The cell viability and the fluorescence data from the ICG delivery experiment were compared using the one-way ANOVA and a *post hoc* Tukey test. For the ICG bleaching experiment, the two-way ANOVA was used. In all tests, results were considered significantly different using a p-value ≤ 0.05.

3.2 Results

3.2.1 Dark ICG toxicity on *S. aureus* and pulmonary host cells

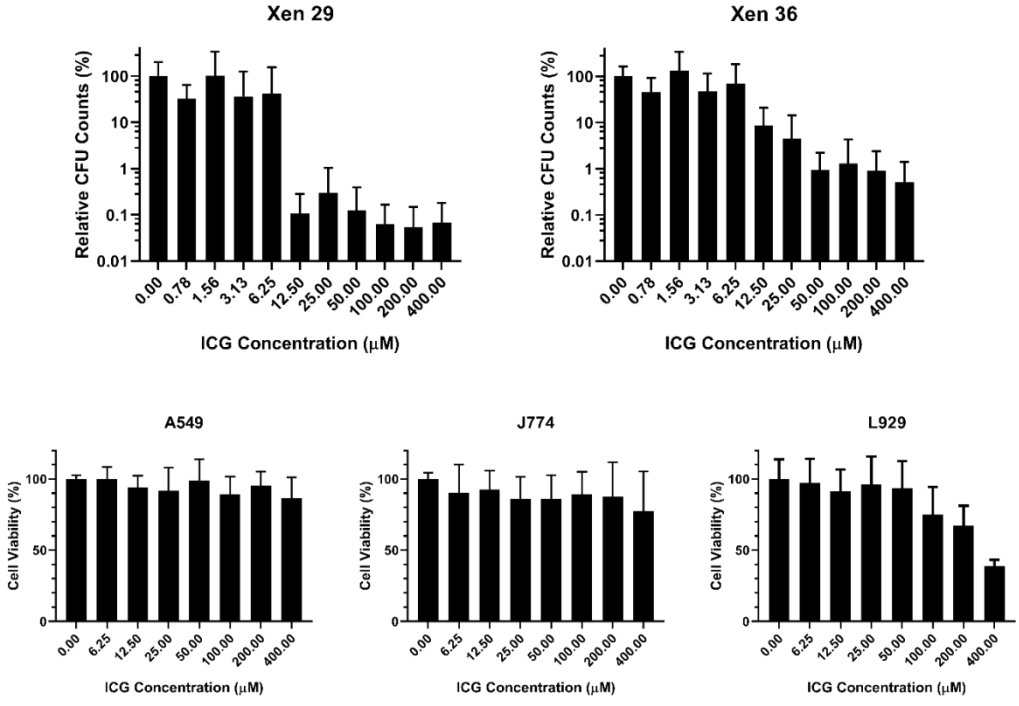

Figure 7 - Effect of increasing concentrations of ICG in the bacterial growth of S. aureus strains (Xen29 and Xen36) and viability of A549, J774 and L929 cell lines. For Xen29 and Xen36, the relative CFU counts are significantly different from the control starting from 12.5 μM of ICG. For L929, concentrations of 100 μM of higher result in a significantly lower cell viability. For A549 and J774, no concentration of ICG was different from the control. Given the different nature of the cell replication and the magnitude of the impact in the viability, the microorganism plots were expressed in mono-log scale, while the cells were expressed in linear scale. Experiment performed in triplicate on 3 different occasions (n = 9), mean value and standard deviation are shown.
Source: KASSAB *et al.*[92]

The effect of different concentrations of ICG on a variety of bacterial strains and mammalian cell lines is shown in Figure 7. The presence of ICG is able to hinder the growth of *S. aureus* starting from 12.5 µM, decreasing the final CFU count in about 3 logs for Xen29. In tissue cultures, the concentration required to cause an effect is much higher. For the L929 fibroblasts, an effect on cell viability was observed only starting at concentrations of 100 µM of ICG, where there was a loss of viability of about 20%. For A459 and J774, there were no significant effects of ICG treatment even at 400 µM.

3.2.2 Light and ICG-PDI toxicity on *S. aureus* and pulmonary host cells

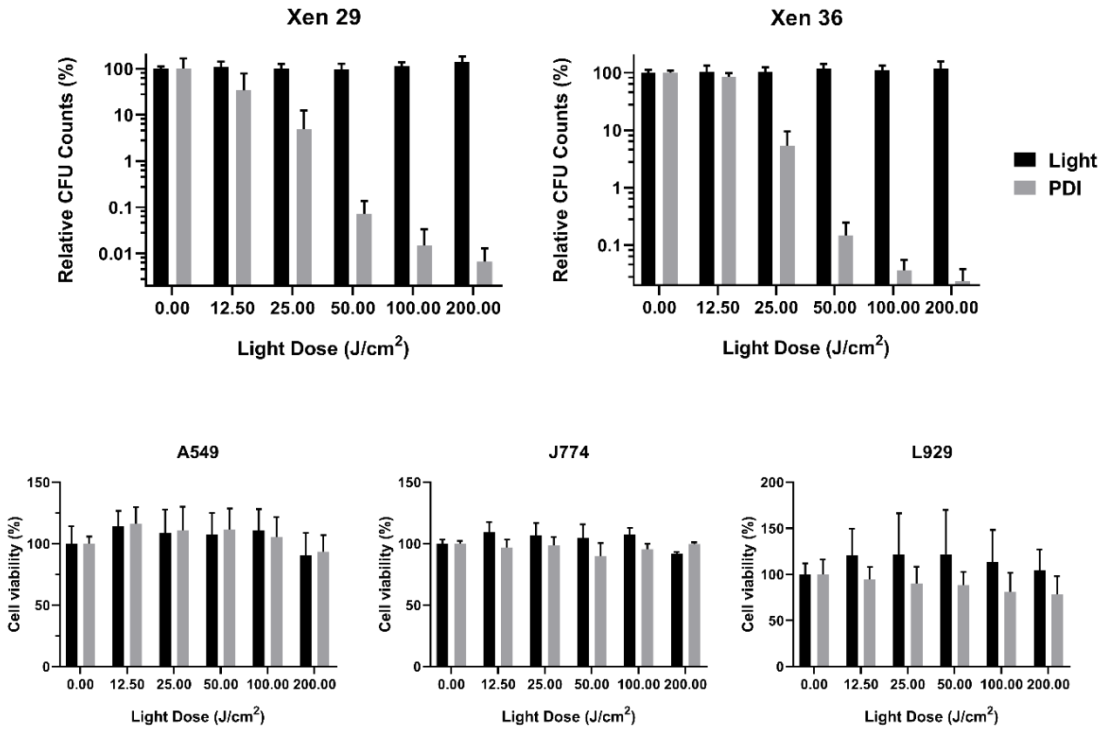

Figure 8 - Effect of increasing doses of 808 nm infrared light on of S. aureus strains and different cell lines in the presence (PDI) and absence (light) of ICG at 10 µM. For Xen29 and Xen36, the matched Friedman test showed that the two treatments are significantly different. And within the PDI group, the differences in relative CFU counts are significant starting from a fluence of 50 J/cm². For A549, J774, and L929, there was no difference from the controls. As in figure 1, the microorganism plots were expressed in mono-log scale, while the cells were expressed in linear scale. Experiment performed in triplicate on 3 different occasions (n = 9), mean value and standard deviation are shown.
Source: KASSAB *et al*.[92]

Exposure to 808 nm infrared light alone did not cause death or inhibition to *S. aureus* strains nor to the lung cells lines (Figure 8). There was no statistically significant difference between groups for the bacteria. However, when the infrared light is combined with ICG, the Friedman test showed that the PDI groups were different from the controls ($p<0.01$). Over

time, there is a clear reduction in CFU counts for both strains, starting from 50 J/cm² ($p<0.005$). In this condition, there is a reduction of about 3 logs. After 200 J/cm² of exposure, the reduction in CFU counts is of 4.18 logarithmic units for Xen29 and 3.62 logs for Xen36.

The viability of J774, L929 and A549 cells was not affected by light treatments at any of the conditions tested. In the case of L929, we observed a tendency towards loss of viability after PDI, reaching about 25% after the highest dose of light, but the statistical analysis showed no difference between this group and the control one. This suggests a large therapeutic window between the dose of light required to inactivate the bacteria and the one to induce relevant damage to the host cells.

3.2.3 Respiratory delivery of ICG

Fluorescent imaging techniques allowed us to monitor the drug's pathways as well as its accumulation/elimination points following inhalation in a mouse model. This is of extreme relevance for further analysis of the effects of the lighting action, particularly in terms of reaching locations of interest and protection of other regions. Furthermore, due to the connection of the respiratory tract and the digestive tract, the accumulation of ICG in both can be measured as well as its elimination. Since the excitation and emission of ICG fall within infrared wavelengths, is it relatively easy to detect through layers of biological tissue.

Thus, fluorescence imaging was used to compare three potential routes for respiratory delivery of ICG (Figure 9). Endotracheal instillation caused the largest increase in relative fluorescence for the whole animal, as well as each individual organ, and all of the results for this delivery method were significantly different from the controls. In contrast, intranasal delivery resulted in lower levels of fluorescence in all organs. Nebulization caused the second largest increase in the whole animal, but showed similar results as the intranasal instillation for the isolated organs. For all methods, the largest increase in fluorescence occurred in the lungs. In the stomach and liver, the increase in fluorescence was only statistically significant for the endotracheal group.

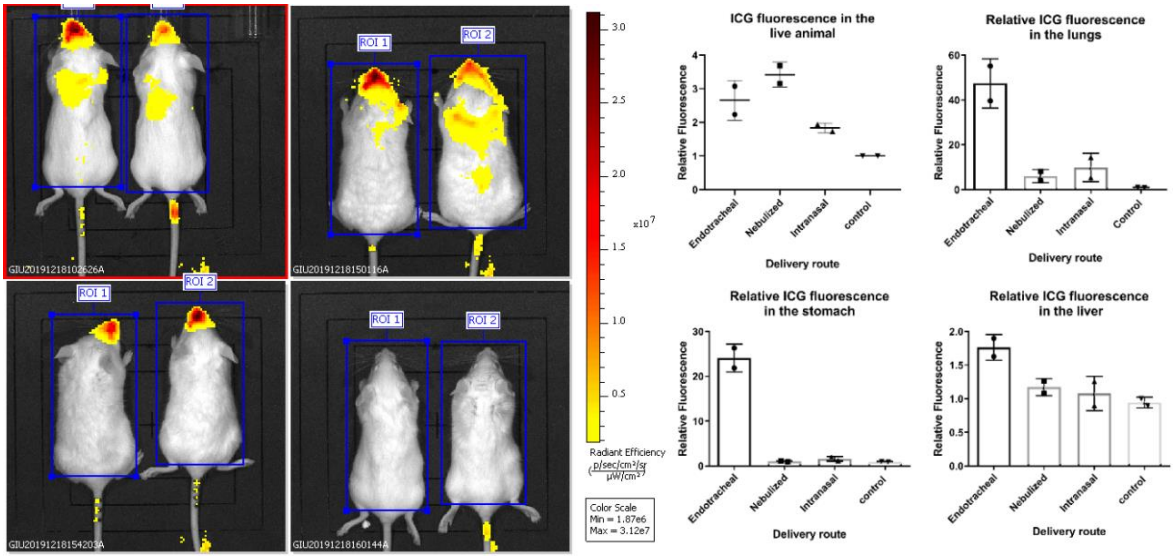

Figure 9 - Comparison of the respiratory delivery methods for ICG. The left panel shows a representative image of the quantification using the IVIS imaging system, in which each pair of animals had been given of one the treatments: endotracheal instillation (upper left); nebulization (upper right); intranasal instillation (bottom left); and control (bottom right). On the right panel, each of the graphs compares the RF obtained for each delivery route for the whole animal, and the homogenates of the lungs, liver and stomach. On the live animal, the RF detected after the endotracheal instillation and the nebulization are significantly different from the control. The RF detected in all three organs is only different for the endotracheal instillation method. Three aliquots were measured for each organ sample and their mean values were compared, so that the number of samples would correspond to the number of animals on each group (n = 2). The mean values and standard deviations for each group are shown, as well as the mean values of each animal (dots).

Source: KASSAB *et al.*[92]

3.2.4 Light dose, ICG bleaching, and photodynamic reaction

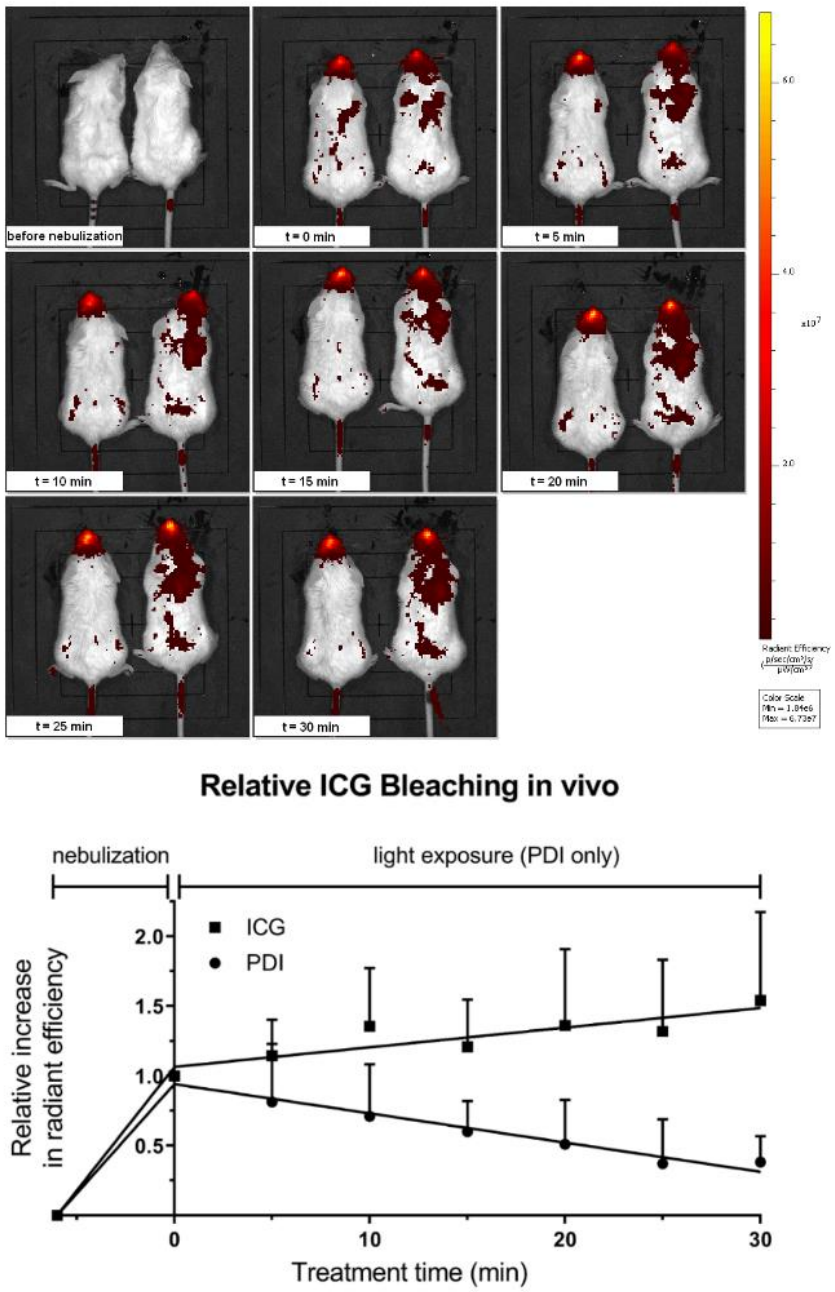

Figure 10 - ICG fluorescence and bleaching in the mice after incremental treatments with 808 nm light (100 µM using nebulization, 36 J/cm² at a time at 120 mW/cm²). The left panel shows a representative image of the fluorescence detection over time, of a mouse that was given the full PDI treatment (left) and one only exposed to the photosensitizer (right) at the times before nebulization (- 6 min); immediately after (0 min); and after each incremental light treatment (5 to 30 min). On the right, the graph shows the relative increase in fluorescence compared to the animal's baseline as a function of time for the animals that received the light treatment (PDI) and the ones that did not (ICG). The two-way ANOVA showed that the treatments are significantly different ($\boldsymbol{p < 0.05}$) and so are the times ($\boldsymbol{p < 0.001}$). The lines correspond to a segmental linear regression using a least square fit. Means and standard deviations are shown ($\boldsymbol{n = 3 - 4}$).
Source: KASSAB *et al.*[92]

Irradiation using the 808-nm light device successfully reduced the fluorescence of ICG in the upper body of the mice (Figure 10). After the end of the nebulization (t=0 min), the

fluorescence detected in the thorax of the animals that only received ICG continued to increase. In the animals that also received light treatment, the intensity of fluorescence started to decrease with the beginning of the irradiation (36 J), and two-way ANOVA showed that the ICG-only and PDI treatments were significantly different from each other.

3.2.5 *In vivo* treatment safety

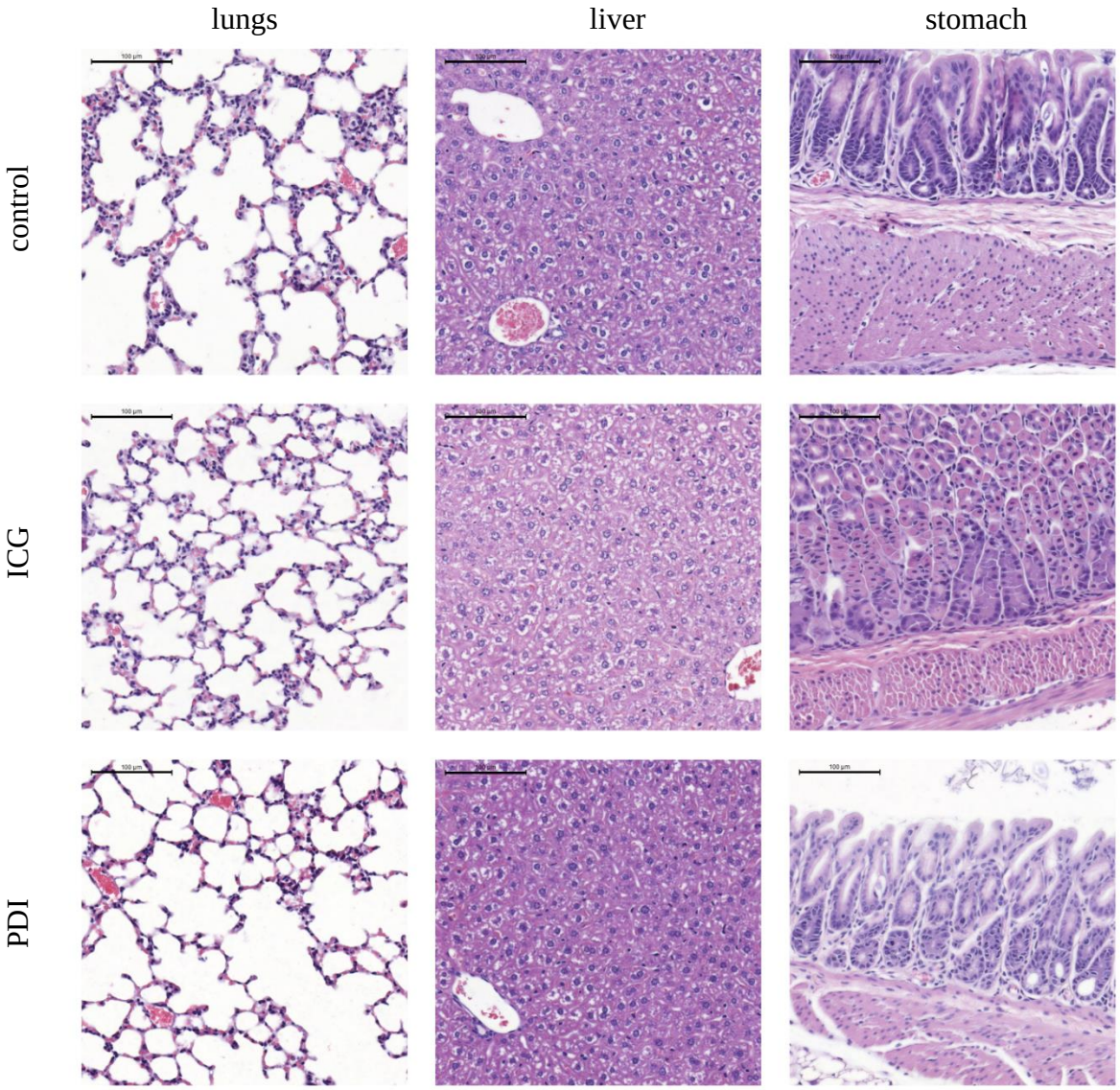

Figure 11 - Representative histological slides showing the target tissue integrity seven days after the pulmonary delivery of ICG (ICG) or the photodynamic treatment (PDI). There was no difference between the groups (n = 3-4). The scale bars indicate 100 µm. HE staining.
Source: KASSAB *et al.*[92]

All animals fully recovered after the ICG and the PDI treatments (Figure 11). On the first day after the treatment, all treated animals had ruffled fur, which gave them a score of 1

on the general health scale. Then, starting from day 2, they scored a 0 on the scale and their behavior and appearance was indistinguishable from controls. Macroscopic comparison of the organs showed no sign of enlargement nor necrosis. Histological analysis showed no difference between the groups. There was no sign of inflammatory infiltration, fibrosis nor bronchitis in the lungs of neither the ICG nor the PDI-treated animals. There was also no sign of necrosis in their livers or stomachs.

3.3 Discussion

The application of ICG and extracorporeal infrared light to inactivate bacteria has been found to be successful in a number of different applications, including the treatment of oral periodontitis and acne.[47,94–96] In the specific case of pneumonia-causing pathogens, ICG-PDI was effective against *S. pneumoniae* with concentrations of the photosensitizer as low as 5 μM when combined with a 780 nm laser device or 10 μM when using an 850 nm LED, and against *S. aureus* in a range of different regimens, ranging from 1 log of CFU reduction (using about 5 μM of ICG and 84 J/cm² of light at 809 nm) to over 5 logs of reduction (using 32 μM of ICG and 411 J/cm² of light at 808 ± 5 nm).[8,11-12,95] In several cases, higher concentrations failed to provide better results with PDI, likely due to aggregation and/or shielding from the light because of its high molecular concentration.

The effect of the ICG-PDI or PDT in healthy cells lines, however, is poorly described in the literature. None of the aforementioned protocols against pneumonia-causing bacteria were tested on host cells, with one exception from Leite *et al*., that tested it on RAW 264.7 macrophages. They found that not only was the treatment safe for the macrophages, but also enhanced their ability to fight the infection.[8] A few descriptions have been found for the cytotoxicity of ICG-PDI for other applications. Engel *et al*. observed a loss of viability in porcine retinal pigment epithelial (RPE) cells that were incubated with light-decomposed ICG.[97] Pourhajibagher *et al*. reported a PDI-induced cytotoxicity in HuGu gingival fibroblasts, but under conditions that differed greatly from the *in vitro* bacterial inactivation protocols.[98] Thus, to enable a proper comparison, the same protocol that was successful against the pneumonia pathogen was tested on 3 cells types that are part of the alveolar microenvironment: pulmonary epithelial cells, macrophages and fibroblasts.

The toxicity of a photosensitizer in the dark provides us with an important guide for possible complications and side effects in PDI treatments. Figure 7 shows a substantial difference in the response of bacteria and mammalian cells. Xen29 and Xen36, although

genetically different, are both inhibited from growing in the presence of high concentrations of ICG. While for Xen29 the transition from non-inhibition to inhibition is abrupt and clear, for Xen36 the transition is smoother, demonstrating the greater tolerance of Xen36 to the drug as compared to Xen29.

On the other hand, this susceptibility does not occur for any of the tested mammalian cell lines. The results of Figure 7 suggest a practical absence of toxicity in the dark for A549 and J774 cells within the range of tested concentrations. The L929 cells only begin to present toxicity in the dark in a concentration of ICG that is 10 times higher than the one proposed for the *in vivo* protocol. In the work of Engel *et al*. authors found a moderate toxicity for ICG in the dark for RPE cells, with a loss of viability of about 20%, but using a concentration of ICG of about 320 µM.[97] Pourhajibagher *et al*. only found toxicity for ICG without irradiation in HuGu cells with concentrations above 645 µM.[98] The absence of toxicity in the dark for the presented tissue cultures is an indicator of ICG selectivity.

Light toxicity in the absence of ICG is another important control. As indicated in the results of Figure 8, the light group showed no difference from the dark control on microorganisms and tissue cultures. It was possible that the infrared light would induce a photobiomodulation, or heat-related effects. However, if there is any, the effect of light alone in this protocol in negligible.

Based on the results of Figure 7, the ICG concentration of 10 µM was chosen for the *in vitro* PDI experiments. At this concentration, small toxicity in the dark and availability of a large photodynamic effect can be granted for the bacteria. Our PDI protocol had similar results for the presented strains, reaching a reduction of 4.18 logs for Xex29 and 3.62 for Xen36 using 10 µM of ICG and 200 J/cm² of light at 808 nm (Figure 8). The dependence of PDI with the dose of light shows a curve with marked growth of the elimination effect between 25 and 50 J/cm², suggesting that the median threshold dose is somewhere within this range. In photodynamic therapy, the threshold dose is the amount of light required to cause irreversible cell damage.[99] In a population, the variability between individuals leads to a distribution in the threshold values which could explain the behavior seen in Figure 8. On the other hand, the same protocol had no significant impact on the viability of any of the cell lines tested, thus not allowing a median threshold dose to be estimated. The other publications that used ICG and infrared light on cell lines found cytotoxicity but used concentrations of ICG that were much higher.[98-99] In the case of Engel *et al*., rather than measuring the photodynamic effect, they were interested in the toxicity of the products of the

photodegradation of ICG, which was significant for RPE cells. However, in our case, there is no evidence of that occurring.

The ROS generated by PDI are not selective for cell types, so the difference in susceptibility to the treatment depends on ICG's ability to penetrate membranes and the cell's resilience against oxidative stress. In bacteria, ICG uptake seems to be highly dependent on surface charges, while in mammalian cells it depends on endocytic activity and the presence or absence of tight junctions.[101-102] Small changes in these parameters help explain the variable response to PDI between strains of the same pathogen, as it happened for Xen29 and Xen36 in Figure 8, and for the strains studied by Wong *et al*.[12]

We took advantage of the fluorescent character of ICG to compare different routes of its respiratory delivery, using doses that would yield a concentration in the lungs high enough for the bacterial killing, but low enough to be safe for the host cells. In their successful protocol of ICG-PDI against pneumonia, Geralde *et al*. used intranasal instillation as a localized delivery method.[9] However, this would not be suitable for clinical applications, so air-jet nebulization was presented as an alternative.[64] The delivery of substances to the lungs of mice using aerosolization can be quite challenging because of their small tidal volume, specially using equipment that was designed for humans, and deposition in the upper respiratory tract seems inevitable.[102] Still, Figure 9 shows that instillation and nebulization were very similar in delivering ICG to the lungs of mice. The fluorescence detected in the whole animal is higher following nebulization, but in individual organ homogenates there is no difference between the two methods. Endotracheal instillation is a much more effective method for pulmonary delivery, as seen by the increased fluorescence in all of the organs in Figure 9, but it is more invasive and even less applicable as a translational delivery protocol.

ICG administered intravenously is rapidly cleared from the blood, taken up by the liver, and excreted in the bile.[104-105] In a previous attempt to track the distribution of ICG after nebulization, fluorescence was found in the liver an hour after administration and found to be distributed in multiple organs after 4 hours.[105] Considering that the light treatment is given over the thorax, ICG present in organs like the liver and the stomach could be activated and cause undesired effects. Therefore, understanding tissue distribution is key for the correct design of the PDI treatment. We observed that immediately after respiratory delivery, ICG was not present in the liver or stomach for neither the intranasal instillation nor the nebulization. However, the mice that received endotracheal instillation showed fluorescence in all three organs suggesting that this quicker, more efficient method could possibly have worsened side effects.

Then, we decided to study the toxicity of a simulated treatment. After irradiation, monitoring the sensitizer photobleaching is an indirect way to evaluate the singlet oxygen formation and cell death.[106] This fluorescence monitoring aids to estimate the required dose for a PDT or PDI treatment, and has been done successfully for other photosensitizers.[91] Thus, the bleaching of nebulization-delivered ICG using 808 nm was tested on the mice (Figure 10). We normalized the increase in fluorescence detected before and after the nebulization for each animal as being equal to 1. This consideration mitigates other effects such as the variability of the drug delivery via nebulization, and standardizes the bleaching to be measured. The initial t = 0 min timepoint is when the light treatment starts for the PDT group. In this instance, the animals of both groups are considered to be equivalent, making the error bar at t = 0 min zero. From this point, it is observed that the groups behave differently: without illumination (ICG) there is an accumulation of ICG fluorescence, while with illumination (PDT) it decays. This is similar to what has been previously described for ICG and 780 nm using other quantification methods.[64,105] The rate of accumulation, driven by a redistribution if the ICG that initially went to the upper respiratory tract, does not exceed the rate of bleaching initially. In terms of a basic rate equation, we could assume that:

$$\boldsymbol{dC/dt = L - BC - E} \quad (1)$$

Where t is time; C is ICG concentration at a given instant (proportional to the detected fluorescence); L is the accumulation rate at the observation site due to the drug transport; B is the intensity-dependent bleaching coefficient; and E represents the rate of natural elimination (tissue clearance).

The concentration C is time-dependent on both sides of the equation. In the case of B = 0 (absence of light), the variation in concentration depends only on the balance between the rate of accumulation and natural elimination. Figure 10 shows that for the ICG group there is a seemingly linear increase for t > 0, allowing to conclude that L > E for this time interval, in a way that makes it possible to disregard E. For this group, in arbitrary units, the natural accumulation rate is expressed as L ~ 1/60 units / min, corresponding to the slope of graph in the figure. With this consideration, the practical solution for equation $\boldsymbol{dC/dt = L - BC - E}$ (**1** is given by:

$$\boldsymbol{C(t) = L/B\,(1 - e^{-Bt}) + C_0 e^{-Bt}} \quad (2)$$

Where C_0 corresponds to the concentration at t = 0, and has the value of one unit. For long timepoints, looking at the behavior of the group with irradiation, we find that the concentration tends to reach the point of equilibrium when the accumulation is compensated by bleaching, remaining constant. In this case, an adjustment of the group curve with light by

the solution in equation 2, shows that the asymptote C is of the magnitude of L/B, in this case of the order of 0.25 units. With this, the bleaching rate can be estimated to be in the order of B = 1/15 per min. After 30 minutes, which corresponds to 216 J/cm², most of the fluorescence has been bleached. This value demonstrates a high photodynamic action occurring on the target organ, despite the layers of fur, skin, fat and bone between the light source and the lungs of the mice. If there were microorganism colonies there, this suggests there would be enough light to eliminate them without relevant collateral damage.

Subsequently to the photobleaching treatment, the animals were kept alive and monitored for 7 days. Considering the range of the health score scale (from 0 to 12), a score of 1 was not considered worrisome. They quickly recovered from the stress and seemed to be as healthy as controls from day 2 onwards. Still, damaging PDT treatments result in intense inflammation, which could potentially lead to macroscopic changes in the organs. Because there was evidence of ICG present in the liver and stomach after the nebulization (from Figure 9), there was a chance that there would already be some photosensitizer in these organs during the illumination, and subsequent activation could cause necrosis. This effect is observed (and intentional) in the PDT of hepatic cancers, but is not desired in our proposed protocol.[107] In 1996, Loh *et al* compared two protocols of pyloric PDT, and one of them resulted in a gross distension of the stomach. Histological analysis showed that that protocol had caused necrosis, edema, and interstitial hemorrhage of the stomach.[108] Moreover, not all substances are compatible with pulmonary delivery. In a study from 2017, for example, mice that received an anti-infective peptide via nebulization showed epithelial sloughing and bronchitis 4 hours after the treatment.[109] It had been previously shown that it was possible to deliver ICG using nebulization, but there was no demonstration that it would not trigger an inflammatory response. The histological analysis showed that neither type of damage was observed on the organs for ICG-PDI using 808 nm (Figure 11). This suggests that, at least in the presented conditions, PDI using ICG and light at 808 nm does not cause acute damage to the lungs, the stomach or the liver.

In summary, the photodynamic inactivation treatment using indocyanine green and infrared light at 808 nm has evidence of being safe *in vitro* and in a murine model. The protocol presented successfully inactivated two strains of *S. aureus*, while showing no cytotoxicity to three different mammalian cell lines. Moreover, mice that received the treatment recovered fully and seven days later showed no signs of tissue damage or inflammation. The light doses proposed in this protocol can be achieved with extracorporeal

illumination without limitations, in relatively short times and with complete safety with respect to damage to healthy host cells.

4 TRANSLATIONAL CHALLENGES AND A FIRST INSIGHT

Considering the initial proof-of-principle of the treatment of bacterial pneumonia in mice presented by Geralde and co-workers[9], and the successful expansion results described in the previous chapter, the natural following step would be to repeat the efficacy experiments in mice, as to see if the modifications in the treatment protocol (including delivery of ICG using nebulization and the new wavelength of 808 nm) would improve or hinder the bacterial killing and the host survival in the *in vivo* level. However, this study faced challenges that are intrinsic to animal research and its translation to clinical trials, such as attributing proper significance to the obtained results and interpreting them correctly in face of the high variability that is typical of living beings. Infections models are particularly complex because include both the intrinsic variability of the pathogens as well as of the hosts. Additionally, differences in the pathophysiology of the infection in the model compared to the human infection must be taken into account.

Thus, over the course of the project, new infection models had to be developed and the efficacy of aPDT was tested in each of them. Unfortunately, in these new models, obtaining successful results in the treatment of bacterial pneumonia was a challenge in itself. Multiple attempts were performed to both obtain adequate pneumonia models and improve the aPDT parameters, so this chapter describes only the most representative of these results. Eventually, we hypothesized that the importance of the alveolar microenvironment to the success of the treatment was being overlooked, and some experiments were proposed to investigate that.

Experiments involving the genetically-modified *S. aureus* strain were performed at the Health Science Center of Texas A&M University, under the co-supervision of Professor Jeffrey Cirillo. Experiments involving pigs were performed at the Faculty of Medicine of the University of São Paulo (FM-USP), under collaboration with Professors Paulo Pêgo Fernandes (InCor-USP) and Marcelo Amato (FM-USP).

4.1 Methodology

4.1.1 *S. aureus* infection and efficacy experiments in mice

The *S. aureus* infection model and the bioluminescence imaging were based on and adapted from McDowell and co-workers.[110] Female BALB/c mice were obtained and

handled as described in section 3.1.4, after approval and under the guidelines of the Texas A&M University Institutional Animal Care and Use Committee. The bioluminescent *Staphylococcus aureus* strain Xen29 was stocked and grown as described in section 3.1.2, and then resuspended in Hank's balanced salt solution (HBSS) in a concentration of 10^{10} CFU/mL. For the establishment of the infection model, 6 animals were anesthetized using isoflurane and then inoculated with 100 µL of bacterial suspension *via* endotracheal instillation, resulting in 10^9 CFU/mouse. Bioluminescence imaging was performed using the IVIS Spectrum and the Living Image software (PerkinElmer, USA) immediately after inoculation, and then three mice were euthanized and their lungs macerated and seeded for CFU counts. The remaining mice were imaged again at 24 h, underwent euthanasia and the organs were exposed for more imaging, then samples were processed for CFU counts.

For the aPDT efficacy experiment, 10 mice were inoculated in the same way and 16 hours later 5 of them were randomly selected to receive treatment. They were exposed to 6 minutes of nebulization of ICG 100 µM and 120 J/cm² of light at 808 nm, using the same equipment from section 3.1.4. The health and weight of the mice were monitored every 8 hours for 7 days, and then they were euthanized.

4.1.2 *S. pneumoniae* infection and efficacy experiments in mice

Female BALB/c mice, aged 6-7 weeks, were obtained from the animal research facility of the Ribeirão Preto Campus of the University of São Paulo (Brazil), after the approval and under the guidelines of the Animal Ethics Committee of the São Carlos Institute of Physics of the University of São Paulo (CEUA/IFSC-USP). They were immunosuppressed prior to the infection date using cyclophosphamide (150 mg/kg weight at $d(-4)$ and 100 mg/kg weight at $d(-1)$). The *Streptococcus pneumoniae* strain ATCC® 49619 (American Type Cell Culture, USA) was grown from frozen stocks in Brain-Heart Infusion (BHI) broth using a microaerophilic candle jar at 37 ºC until log-phase (4 – 5 hours). It was then resuspended in PBS in different concentrations.

For the establishment of the infection model, 9 mice were inoculated intranasally with 30 µL of the bacterial suspension, containing one of three possible doses: 10^5, 10^6, or 10^7 CFU/mouse. 24 hours later, they were euthanized and the lungs were processed for CFU counts using 2 different methods: first, the bronchoalveolar lavage fluid (BALF) was obtained by inserting 800 µL of PBS into the trachea and then pulled back; then, the lungs

were macerated in 1,0 mL of PBS. The BALF and macerates were diluted and seeded into blood agar plates, that were incubated at 37 ºC for 18-24 hours and then counted for CFUs.

For the *in vivo* bacterial inactivation experiment, 15 mice were immunosuppressed and then inoculated intranasally with 10^6 CFU/each. After 24 h, they were split into groups: ten mice were anesthetized with KX, nebulized with 6 minutes of ICG 100 µM, and exposed to 120 J/cm² of either 780 nm (n = 5) or 808 nm (n = 5). Five mice were kept untreated as controls. Then, 24 hours after treatment, they were euthanized and the BALF was collected for seeding and CFU counting.

For the survival curve, 20 mice were immunosuppressed and inoculated with 5,0 x 10^6 CFU each, then were split into groups of 5. Three hours after the infection, treatments started. Animals in the oxacillin group received 6 intraperitoneal injections containing 200 mg/kg weight, being 3 of them on day 0 and 3 on day 1. The aPDT group received 3 daily sessions of nebulized ICG at 100 µM and 120 J/cm² of 808 nm (on days 0 through 2), and the Sham group received the same sessions but with PBS instead of the ICG solution. The controls received no treatment. The health of the animals was monitored twice daily until day 2, and then once daily until day 7. At the end of the experiment, surviving animals were euthanized.

4.1.3 *S. aureus* proof-of-principle experiment in pigs

Pig experiments were performed after approval and in accordance to the guidelines of the Animal Ethics Committee of the São Carlos Institute of Physics of the University of São Paulo (CEUA/IFSC-USP), the Scientific Committee of the Heart Institute of the Clinics Hospital of the University of São Paulo (CP/InCor-USP), and the Animal Ethics Committee of the Faculty of Medicine of the University of São Paulo (CEUA/FM-USP).

A single female Landrace pig, weighting 35 kg, was obtained from Granja RG (Brazil) and brought into the animal intensive care unit of FM-USP. It was anesthetized using propofol (3 mg/kg), intubated orotracheally (100% O_2), and maintained with ketamine (5-15 mg/kg/h), midazolam (0,2-0,5 mg/kg/h), and fentanyl (0,02 mg/kg/h). Venous accesses and a urinary catheter were added to monitor vital signs. The *Staphylococcus aureus* strain ATCC® 25923 (American Type Cell Culture, USA) was grown from stock into a BHI agar plate (37 °C), then transferred into BHI broth for an overnight culture and then a log-phase culture (150 rpm, 37 ºC). It was resuspended in PBS and adjusted to a concentration of 10^6 CFU/mL. Two 15 mL aliquots of bacterial suspension were prepared, and ICG was

added to one of them to a final concentration of 10 µM, then each of them was sampled for CFU counts. After 15 minutes of incubation, the aliquots were instilled into specific portions of the porcine lung using a bronchoscope (the control in the lower left lobe, and the treated in the lower right lobe, based on the peak incidence of light). Then, the light treatment began, using two panels of 200 lasers each, with peak emission at 808 nm and an irradiance of 78 mW/cm², build specifically for this application by LAT (Brazil). The panels were on for 40 minutes, totaling an external dose of 187 J/cm². After that, the BALF was collected from each portion of the lung, by adding 20 mL of PBS through the bronchoscope and then pulling it back. The BALF was diluted and plated for CFUs, and the estimated bacterial burden of the recovered volume was calculated. Then, it was compared to the total *inoculum* estimated from the CFUs obtained for each suspension before being administered to the pig. Vital signs were monitored throughout the experiment, and once the samples were collected, the animal was euthanized using a lethal injection of KCl.

4.1.4 Bacterial inactivation in different media

The mice and the *S. pneumoniae* strain were the same from section 4.1.2, expect this time the culture was grown in a CO_2-controlled incubator (5% CO_2) instead of the microaerophilic jar. For the spiked group, the lung macerates were pooled from 5 healthy mice and then the bacteria were added afterwards, adjusting the final concentration to 5 x 10^6 CFU/mL. For the infected group, 5 mice were inoculated as described in the aforementioned section, and the lungs were harvested and pooled after 24 hours. The final concentration of bacterial in the infected macerate was of about 5 x 10^5 CFU/mL.

Then, a 96-well plate was set up containing 3 well of each of the groups: a bacterial suspension in PBS; the spiked macerate; the infected macerate; and a suspension with 5% Survanta®. Concentrated ICG was added to all groups, reaching a final concentration of 10 µM, and samples were diluted and plated for the 0 J/cm² condition. Then, the plate was placed under the 808 nm laser panel described in section 4.1.3, and given incremental doses of light. For the PBS and 5% Survanta groups, the experiment was repeated for two additional occasions (total: n=9) and thus these results were plotted separately.

4.1.5 Data analysis

All data was processed and plotted using GraphPad Prism 8. Health scores and weight were compared using two-way ANOVA and a *post hoc* Sidak's multiple comparison test to compare the groups within each time point. For the efficacy against *S. pneumoniae* in mice and against *S. aureus* in pigs, the one-way ANOVA was used on the log-transformed results. In the survival curve, the log-rank (Mantel-Cox) method was used. For the inactivation in different media, the two-way ANOVA was used on the log-transformed data, with a *post hoc* Dunnett's multiple comparison test. In all tests, results were considered significantly different using a p-value ≤ 0.05.

4.2 Results

4.2.1 *S. aureus* infection and treatment in mice

The results of the most successful protocol for *S. aureus* infection are shown in Figure 12. With an initial inoculum of about 10^9 CFU/mouse, 10^8 CFUs would remain viable in the lungs after the instillation and about 10^7 would still be viable after 24 h. However, it was not possible to detect the bioluminescence of the strain in any of the infection conditions, including this one (Figure 13).

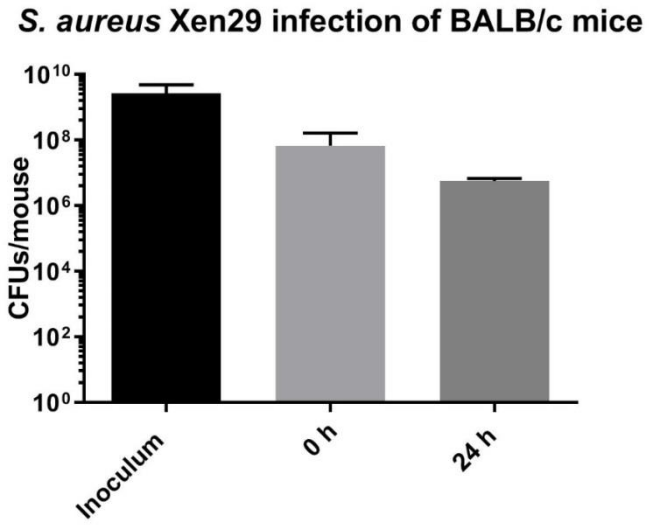

Figure 12 – Burden of infection of BALB/c mice immediately after endotracheal instillation of *S. aureus* Xen 29 and 24 hours later in comparison to the initial *inoculum* (n = 3). No statistical treatment.
Source: By the author.

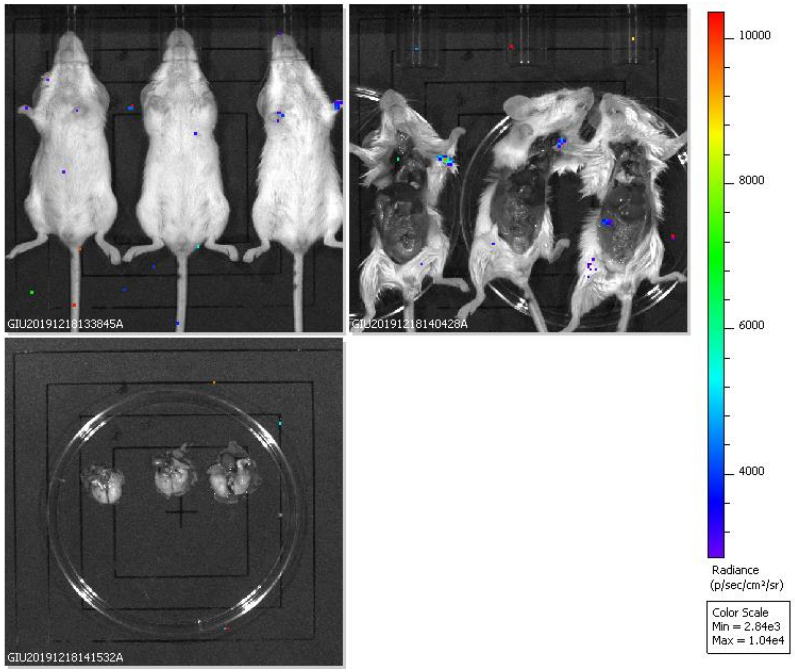

Figure 13 – Bioluminescence imaging of BALB/c mice 24 hours after inoculation with *S. aureus* Xen 29 (upper left), of the exposed organs after euthanasia (upper right), and specifically of the lungs (lower left). There was no significant detection of bioluminescence. N = 3.

Source: By the author.

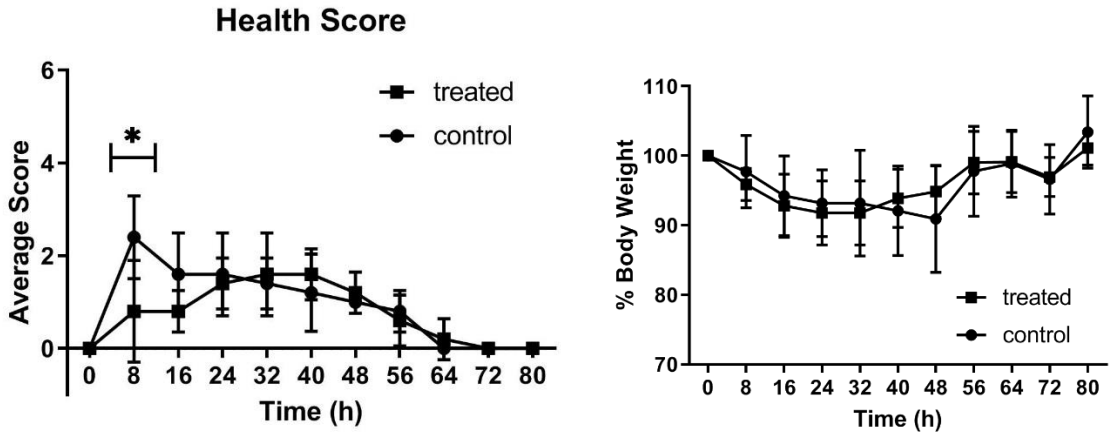

Figure 14 – Clinical monitoring of infected mice after ICG-aPDT treatment compared to untreated controls. Health scores were significantly different only at $\boldsymbol{t = 8\,h}$. There was no difference of weight between groups. N = 5.

Source: By the author.

Animals infected using this protocol were treated with aPDT and their health conditions were monitored for 7 days (Figure 14). None of the mice reached the criteria for euthanasia, so it was not possible to create a survival curve. The only difference between treated and control mice was in the health score 8 hours after the infection, which was quickly reversed.

4.2.2 *S. pneumoniae* infection and treatment in mice

The most successful *S. pneumoniae* infection required that the mice were previously immunosuppressed. Figure 15 shows that, in these conditions, the bacteria had either maintained its number or multiplied in the lungs 24 hours after the instillation. It was also observed that, for an initial inoculum of 10^6 CFU/mouse, the median survival time for untreated animals was 3 days (not shown).

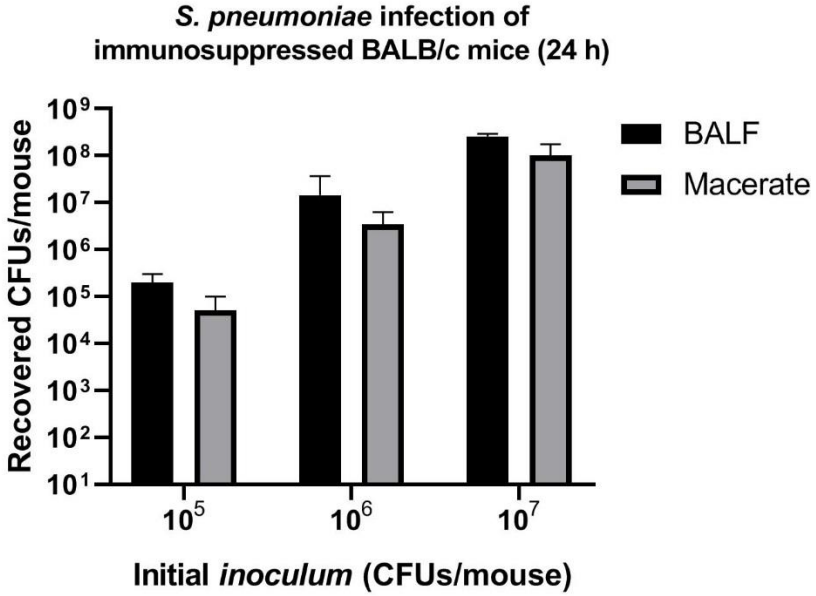

Figure 15 – Burden of infection of BALB/c mice 24 hours after nasal instillation of *S. pneumoniae*, as per initial *inoculum* and sample preparation method. No statistical treatment. N = 3.
Source: By the author.

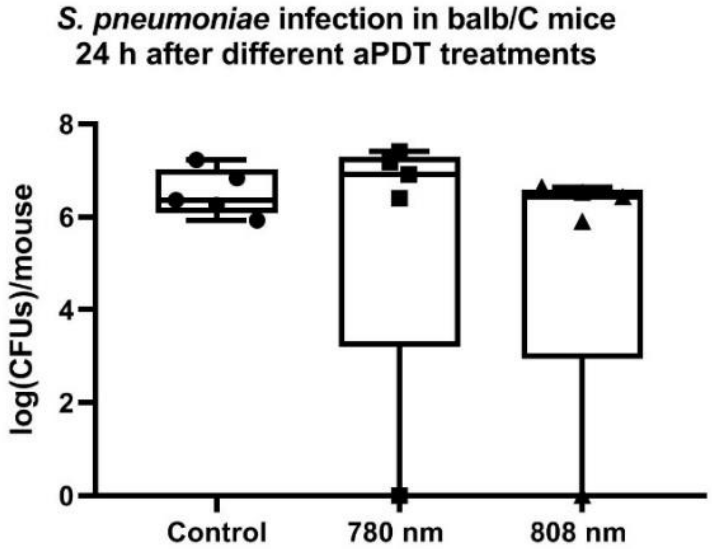

Figure 16 – Burden of *S. pneumoniae* infection of immunosuppressed BALB/c mice 48 hours after inoculation and 24 hours after aPDT treatment with nebulized ICG and either 780 nm or 808 nm (n = 5). There was no statistical difference between groups.
Source: By the author.

New mice were then infected with this protocol and treated with ICG-aPDT (Figure 16). A single mouse from each of the treated groups was completely cleared of the infection, but there was no reduction of the bacterial burden on the other mice. The Kruskal-Wallis test showed that there was no difference from the controls. Thus, using the same infection model, a multiple-session aPDT protocol was proposed, and a survival curve was built including sham and oxacillin (gold-standard) controls, as shown in Figure 17. Unfortunately, the aPDT was still unsuccessful, and no different from the sham and control. Only the oxacillin-treated animals were able to recover from the infection. Multiple similar experiments were performed with varying treatment frequencies, waiting times, and light and ICG doses, but there was no improvement in the infection treatment.

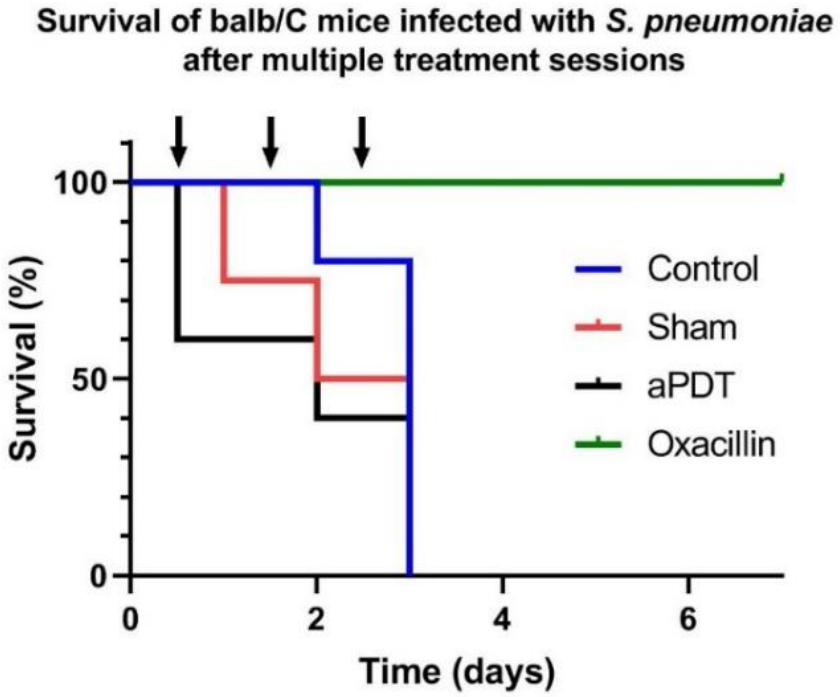

Figure 17 – Representative survival curve for experiments with *S. pneumoniae* infection in BALB/c mice and ICG-aPDT. Statistical analysis showed that only the oxacillin group is significantly different from the control. The arrows indicate the times for aPDT (and sham) treatments. N = 5.
Source: By the author.

4.2.3 ICG-aPDT proof-of-principle in pig

In the pig experiment, the ICG was combined with the bacterial suspension prior to the instillation. Still, the aPDT was not successful (Figure 18). The loss of viability seen in both the treated and control groups is likely due to a limitation in the sampling technique, combined with a direct effect of the defense mechanisms of a healthy lung.

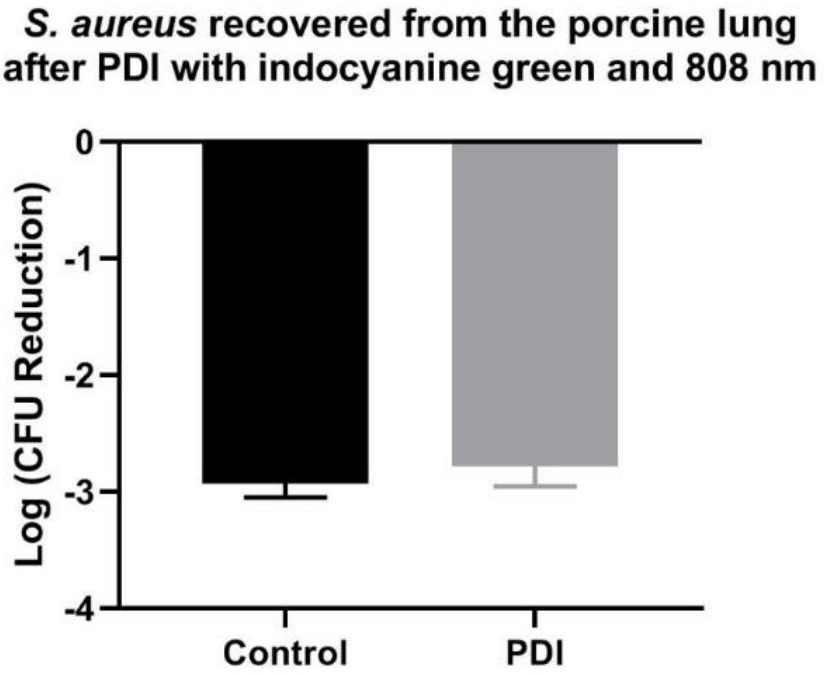

Figure 18 – Reduction of the *S. aureus* burden in the porcine lung after ICG-aPDT compared to the untreated control, in relation to the initial *inoculum*. Each group had a single sample, that was diluted and plated in triplicate. There was no statistical difference between groups.
Source: By the author.

4.2.4 Inhibition of the photodynamic inactivation effect by components of the alveolar microenvironment

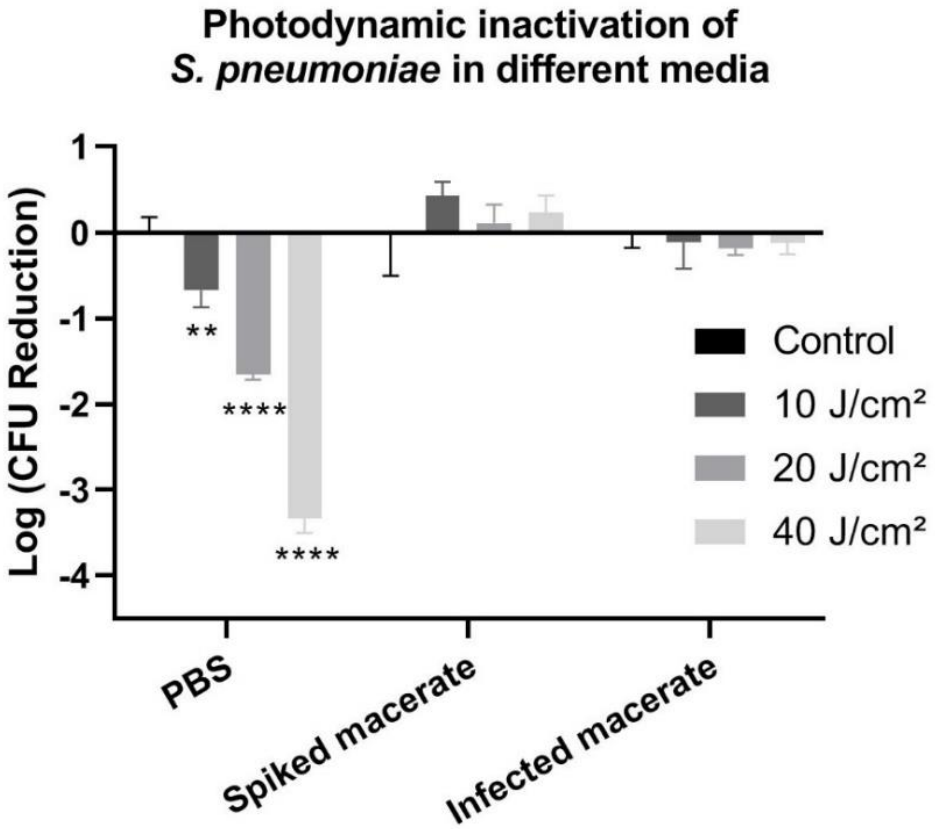

Figure 19 – Reduction of the *S. pneumoniae* burden after *in vitro* ICG-PDI in infected and spiked mouse macerates compared to PBS (n = 3). The stars indicate significant difference from the group's control (**: $p<0.01$; ****: $p<0.0001$).
Source: By the author.

The components of the lung macerate completely inhibit the photodynamic inactivation of *S. pneumoniae* (Figure 19). In PBS, there is a dose-response relationship between the light exposure and the reduction in the CFU counts. In the macerates, however, this does not occur. Even at the highest fluence delivered, there is no impact in the bacterial viability. This is true for both the infected and the spiked macerate.

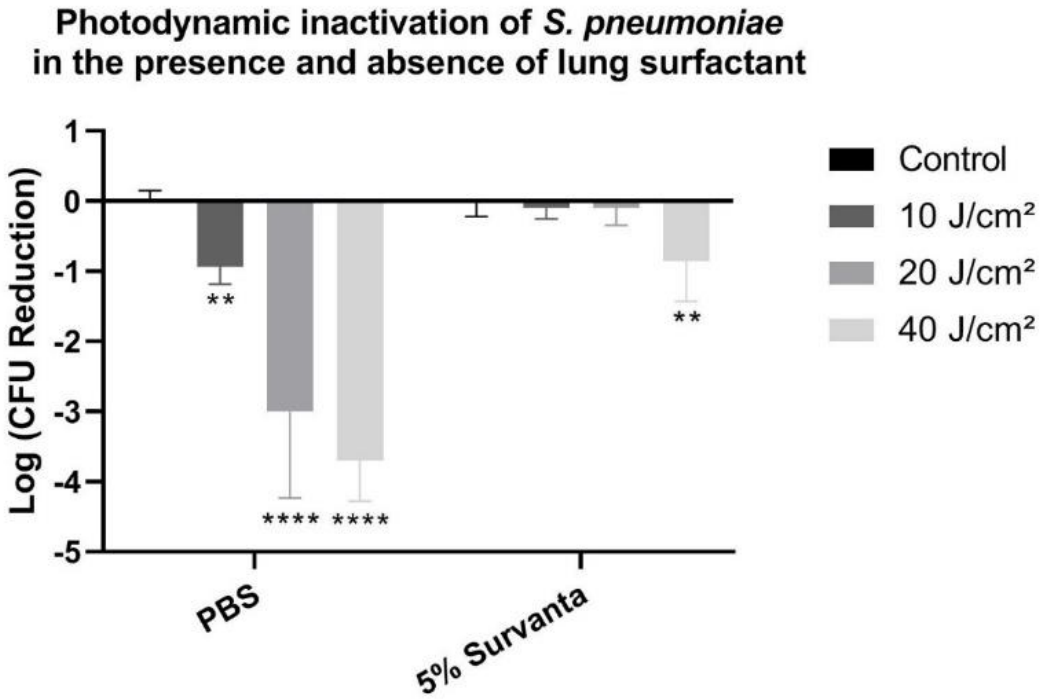

Figure 20 - Reduction of the *S. pneumoniae* burden after *in vitro* ICG-PDI in PBS with or without 5% of Survanta® (n = 9). The stars indicate significant difference from the group's control (**: $p<0.01$; ****: $p<0.0001$).
Source: By the author.

When the clinical lung surfactant Survanta® is added to the bacterial suspension, PDI is inhibited as well (Figure 20). However, as the light fluence increases, it is possible to see that there is some inactivation of *S. pneumoniae*.

4.3 Discussion

Geralde and co-workers presented an *in vivo* demonstration of the principle that ICG-aPDT could successfully treat bacterial pneumonia in 2017.[9] We have proposed to expand on this principle and presented improvements on the delivery aspects of the protocol, as discussed in chapter 3. We intended to use the same infection model presented in the 2017 study to investigate if the nebulization and the new wavelength would have any effect on the aPDT efficacy results in mice. However, the infection model proposed by Geralde *et al* proved to be limited and unreliable. In the original publication, control animals had a burden of roughly 10^4 CFUs of *S. pneumoniae* 7 days after its inoculation, and 60% of them died within 35 days of the infection. We, on the other hand, have found that many of the mice infected with that model would recover naturally from the infection, yielding a complete

absence of *S. pneumoniae* 7 days after instillation, and a complete survival of the control groups. Thus, alternative infection models were studied and investigated to be applied in this research.

As one of the goals of this study was to demonstrate the broad applicability of ICG-aPDT, and considering our interest in eventually performing pig experiments, a model was proposed using *Staphylococcus aureus* as the infectious agent. *S. aureus* is a major concern in pneumonia because it is often associated with resistance to multiple pathogens,[5] and it is often used as a model of ventilator-associated pneumonia in pigs.[112-113] Additionally, the strain Xen29 was chosen because of its bioluminescence, which allows for real-time monitoring of the infection.[110] After a few iterations of the protocol, it was possible to obtain an infection that would sustain for at least 24 hours (Figure 12), but it was not possible to detect any bioluminescence from it in the live mice nor of the exposed organs after euthanasia (Figure 13). We have confirmed that the genes responsible for the bioluminescence were being expressed in these conditions, and have increased the exposure time to up to 20 minutes, but found no success.

As it was not possible to monitor the infection in real time, the mice infected with *S. aureus* using this protocol were monitored using their weight and clinical symptoms. It was expected that, even if the infection was not strong enough to kill the mice, the difference between treated and untreated groups would be evident in how easily they recovered from it. However, this was not the case. Figure 14 shows that both groups had a very similar recovery, which seemed to be effortless. We concluded that this infection model was not strong enough to make evident the efficacy of the aPDT treatment, and decided to return to a *S. pneumoniae* model.

After reviewing the literature for similar efficacy studies using mouse models of pneumonia, we proposed to immunosuppress the mice prior to the infection. The innate immune response of mice is different than of humans, and thus poses a challenge for using them as model for human infections.[113] Immunosuppression is frequently used as a way to overcome that.[110,115-116] We have found that, after two administrations of cyclophosphamide, the infection profile of *S. pneumoniae* in our BALB/c mice improved significantly, and that the infection burden would even increase 24 hours after the inoculation (Figure 15). In the same experiment, we decided to compare different *inoculi* and different methods to determine the bacterial burden. There was a direct relationship between the dose instilled and the number of bacteria recovered from the lungs, in both methodologies. The BALF yielded slightly higher CFU counts than the lung macerate and there was less contamination present

in the BALF samples (not shown), thus it was chosen as the methodology of the following experiments.

Another indicator of the success of the immunosuppression prior to the *S. pneumoniae* infection was that all control mice reached the criteria for humane euthanasia within the first 3 days of the infection, while about 90% of the oxacillin-treated animals recovered fully (as seen in Figure 17, but also in other experiments). It meant that this infection model was a solid platform to investigate the efficacy of the aPDT. However, it was not possible to achieve the same results from Geralde *et al* using this model. Figure 16 shows the recovered CFUs from an experiment that meant to compare the use of 780 nm and 808 nm, but neither treatment had significant results. Many other experiments were performed to control and improve the treatment (including a return to instillation as the delivery method, and changes in light and photosensitizer dose), but they were equally unsuccessful. Likewise, Figure 17 shows the results from a typical survival-curve experiment. Oxacillin is an effective treatment for pneumonia, but even multiple sessions of aPDT were not able to yield any improvement in survival. Multiple trials were attempted, varying ICG dose and delivery route, wavelength, light fluence, incubation time, time between infection and treatment, frequency of treatment, anesthesia protocol, and hair removal protocol, but there was no improvement of the efficacy. Additional controls were included (like the sham from Figure 17) to test if the handling and interventions made for the treatment were injuring the animals in a way that would decrease their survival despite the aPDT being successful in inactivating the bacteria, but that did not seem to be the case.

In an attempt to try and determine what was the problem, a new proof-of-principle was proposed, this time using a pig. This experiment was done after another student, Johan S. D. Tovar, had measured the light attenuation of the 808 nm panel inside the lungs of the same pig and determined that there was enough light in the alveolar space to activate ICG. Tovar *et al* had previously demonstrated that PDI of bacteria was still effective if the light had to go through multiple layers of phantom, or a pig's carcass, and that complete inactivation was achieved at a similar fluence, even if the incident irradiance was much lower.[68] Thus, the proof-of-principle experiment consisted of ventilating the pig with 100% O_2 (to provide ample supply for the PDI), previously combining *S. aureus* and ICG (to ensure that they would incubate together), and delivering a light fluence calculated from the incident light inside of the specific location of the lung where the bacterial suspension was placed (so that there would be no doubt to whether it was sufficient or not). We determined that 15 minutes of exposure should be sufficient to see bacterial killing, and more-than-doubled that (to 40

minutes) for the proof-of-principle experiment. However, as it is evident in Figure 18, the aPDT was still unsuccessful. This led to the inevitable conclusion that the treatment was in fact not effective.

During the BALF recovery of the pig experiment, we noticed that foam was formed. This led to a discussion about the lung surfactant (that is responsible for the foam, and perfectly normal) and how it was possible that it could play a role in the inhibition of the PDI effect. It became evident that, in an *in vivo* setting, there was more to aPDT then combining photosensitizer, light and O_2 at the right place. In order to test if the pulmonary microenvironment was interfering in the efficacy results, an experiment was made using mouse lung macerates (Figure 19). A distinction was made between the healthy (spiked) and the infected macerates in case the expression of the inhibiting substances was different, but the PDI was completely inhibited in both of them. Lung macerates contain pulmonary, endothelial and immune cells, lung surfactant, extracellular matrix components, and blood (from which the albumin is already known to interact with ICG[117-118]). But considering how the alveoli are organized in the intact lung, and that ICG had been delivered through the airways, the lung surfactant was a likely candidate to be responsible for the *in vivo* effect. Survanta® is a clinical-grade lung surfactant extracted from bovine lungs used in premature newborns,[118] and as Figure 20 shows, its addition to the bacterial suspension also inhibits the PDI effect.

It is possible that other components of the macerate also contribute to the effect in the *in vitro* experiment, but the result in Survanta® brought a light to what was likely occurring in the animal experiments. Survanta contains 25 mg/mL of total phospholipids, and adding 5% of it to PBS yields about 1,25 mg/mL in the experimental conditions. In the human alveoli, a minimum of 30 mg/mL of lung surfactant is necessary to cover the air-water interface, and the actual concentration is estimated to be much higher than that, as it is stored in a dynamic reservoir of lamellar bodies and tubular myelin.[77,89] Therefore, despite seeing a moderate PDI effect with 5% Survanta® and the highest light dose *in vitro* (Figure 20), it is reasonable to assume that the lung surfactant could inhibit the aPDT completely in the *in vivo* experiments. We thus decided to stop pursuing the *in vivo* aPDT and to further investigate the interaction between photosensitizers and the lung surfactant.

5 UNDERSTANDING THE INHIBITION OF THE PHOTODYNAMIC INACTIVATION BY THE LUNG SURFACTANT

After many years invested in developing pneumonia models and improving aPDT parameters, it became clear that there was more to it than simply combining PS, light, and oxygen. Eventually, we hypothesized that the interaction between the photosensitizers and the lung surfactant could be inhibiting the expected phototoxicity. The lung surfactant is a mixture of phospholipids and proteins that is expressed by the lung epithelium and presents two main purposes: enabling the gas exchange by decreasing the surface tension of the air-water interface; and protecting the organism from contaminants in the air.[78,79] The decreased efficacy of antibiotics and other drugs in the presence of lung surfactant has been thoroughly reported in the literature.[82–84,86,119–121] To investigate this possibility, five photosensitizers with potential for aPDT applications in the lungs had their efficacy in killing the pneumonia-causing *Streptococcus pneumoniae* tested in the presence and absence of a medical grade lung surfactant. Then, optical measurements and a molecular dynamics simulation were used to further explain the observed results and potential mechanisms. The results of this chapter have been accepted for publishing at the Proceedings of the National Academy of Sciences.[122]

5.1 Methodology

5.1.1 Lung surfactant, photosensitizers, and light sources

Five photosensitizers were chosen to provide a wide range of chemical and photochemical characteristics (Table **2**Table **2**). Indocyanine Green (ICG, Ophthalmos, Brazil) was solubilized in water for injection on the same day of each experiment. Methylene Blue (MB, Sigma-Aldrich, USA) was prepared in PBS and stored at 4 ºC. Photodithazine (PDZ, Fotoditazin, Russia) was diluted from the commercialized solution as needed, and kept according to the manufacturer's instructions. Protoporphyrin IX (PpIX, Sigma-Aldrich, USA) and Bacteriochlorin-Trizma (BC-t, provided by the Microbiology and Parasitology Laboratory and the Bio-organic Chemistry Laboratory of UFSCar, Brazil) were diluted in DMSO on the same day of each experiment. From the stock solutions, each photosensitizer was further diluted in PBS to the appropriate concentration before each experiment. The lung

surfactant (Survanta®, AbbVie, USA) was diluted in experiment solutions to achieve a final concentration of 5%, which was sufficient to observe inhibition effects in a similar study.[82]

Table 2 - Photosensitizers used in this study and their key characteristics.

Photosensitizer	*Class*	*Molar Mass (g/mol)*	*Absorption Peak (nm)*	*ε ($M^{-1}cm^{-1}$)*	*$\phi_{^1O_2}$*	*Net charge***	*LogP**
Indocyanine Green (ICG)	Cyanine	775.0	780	205000[123]	not detectable [97]	-	4.17; 6.05
Methylene Blue (MB)	Phenothiazine	319.9	670	71089	0.49[124]	+	3.61; 2.61
Protoporphyrin IX (PpIX)	Porphyrin	562.7	365, 532, 557, 589, 641	47433[125]	0.56[124]	2-	5.9
Photodithazine (PDZ)	Chlorin	596.7	660	38200[126,127]	***	3-	4.6
Bacterionchlorin-trizma (BC-t)	Bacteriochlorin	711.8	755[128]	***	***	+	4.4; 6.78

ε: molecular absorption coefficient; $\phi_{^1O_2}$: quantum yield of singlet oxygen formation; *XLogP3-AA, ALogPS, ChemAxom; **of the main microspecies at pH 7, ChemAxom; *** Not reported in the literature.

Source: KASSAB *et al.*[122]

The light exposure was performed using custom-made devices developed by LAT (Laboratório de Suporte Técnico, IFSC-USP, Brazil). For ICG, laser devices were used, with peak emission at 808 nm (80 mW/cm² for the PDI experiment and 60 mW/cm² for the photobleaching assay). For all other photosensitizers, the light sources were LED-based devices, with peak emission at and 780 nm for BC-t (30 mW/cm² for the PDI, 60 mW/cm² for the photobleaching assay), and 660 nm for MB, PDZ and PpIX (50 mW/cm² for both experiments).

5.1.2 Bacterial Inactivation Assay

The gram-positive *Streptococcus pneumoniae* strain ATCC® 49619 (American Type Cell Culture, USA) was thawed from frozen stocks and grown in Brain-Heart Infusion (BHI) broth for 4-5 hours (37 ºC, 5% CO_2) until log-phase. It was then centrifuged and resuspended in phosphate-buffered saline (PBS) and the concentration was adjusted to 5.5 x 10^6 CFU/mL. The bacterial suspension was distributed into 96- or 24-well plates and either Survanta® or more PBS was added to the wells. The plates were placed in a shaker (150 rpm, 37 ºC) for 30 minutes so that any surface adsorption phenomena or interaction between lung surfactant and bacteria would take place and stabilize before inserting the photosensitizer. Then, the photosensitizers were added and the plates were incubated in the dark (37 ºC, no agitation) for

20 minutes. The final concentrations for each component during the aPDT treatment were: 5.0 x 10^6 CFU/mL of *S. pneumoniae*; 5% of Survanta® (when present); and either 10 µM of ICG, 1 µM of PpIX, MB or BC-t, or 100 nM of PDZ. Samples were taken prior to the illumination, and again after fluences of 10 and 20 J/cm². The samples were diluted, seeded onto blood agar, and incubated at 37 ºC. After 18-24 h, the colonies were counted. Experiments were performed in triplicate, on three separate occasions, totaling $n = 9$.

The data was processed using GraphPad Prism 8. The colony count units were transformed into $\log_{10}$ so that a two-way repeated measure ANOVA could be used for statistical comparison. A *post hoc* Sidak's multiple comparisons test was used to compare the effect of the presence of Survanta® in each of the light doses. Results were considered to be significantly different with $p < 0.05$.

5.1.3 Optical Properties Measurements

The absorbance and fluorescence spectra were collected for the five photosensitizers using a Cary 50-Varian Bio UV-Vis spectrophotometer and a Cary Eclipse Fluorescence Spectrophotometer, respectively. Four-sided clear plastic cuvettes of 1 cm path length were prepared with either 950 µL PBS or 900 µL + 50 µL Survanta® and were left under agitation (150 rpm, 37 ºC) for 30 minutes. Then, 50 µL of concentrated photosensitizer solutions (prepared as described previously) were added to the cuvettes, achieving a final concentration of 10 µM for each photosensitizer and 5% of Survanta®, when present. Absorbance was recorded at room temperature in the 300 - 900 nm range. The fluorescence spectra were collected for every photosensitizer at a specific wavelength, as listed in Table 3. For the photobleaching measurements, a total fluence of 20 J/cm² was fractionated in 5 J/cm² increments, and then the absorbance spectra were recorded. The absorbance at the wavelength of highest intensity was recorded and compared.

Table 3 – Optical parameters for the fluorescence spectra measurements.

Photosensitizer	$\lambda_{excitation}$ *(nm)*	$\lambda_{detection}$ *(nm)*
ICG	780	800 – 900
MB	660	680 – 800
PDZ	660	680 – 800
BC-t	780	800 – 900
PpIX	405	425 – 750

Source: KASSAB *et al.*[122]

All optical properties measurements were performed in triplicate, from independent photosensitizer solutions. Data was initially processed using Origin 2018, in which a smoothing processing was applied to the spectra in order to remove the noise. The Savitzky-Golay method was used since it preserves the original shapes of the signal peaks (points of window: 50, polynomial order: 2, no boundary condition). Then, the data was plotted using GraphPad Prism 8. Absorbance and fluorescence spectra are plotted as the mean for each triplicate. The photobleaching data was compared using a two-way ANOVA, with a *post hoc* Sidak's test to compare the effect of Survanta®.

5.2 Results

5.2.1 Photodynamic Inactivation of *S. pneumoniae*

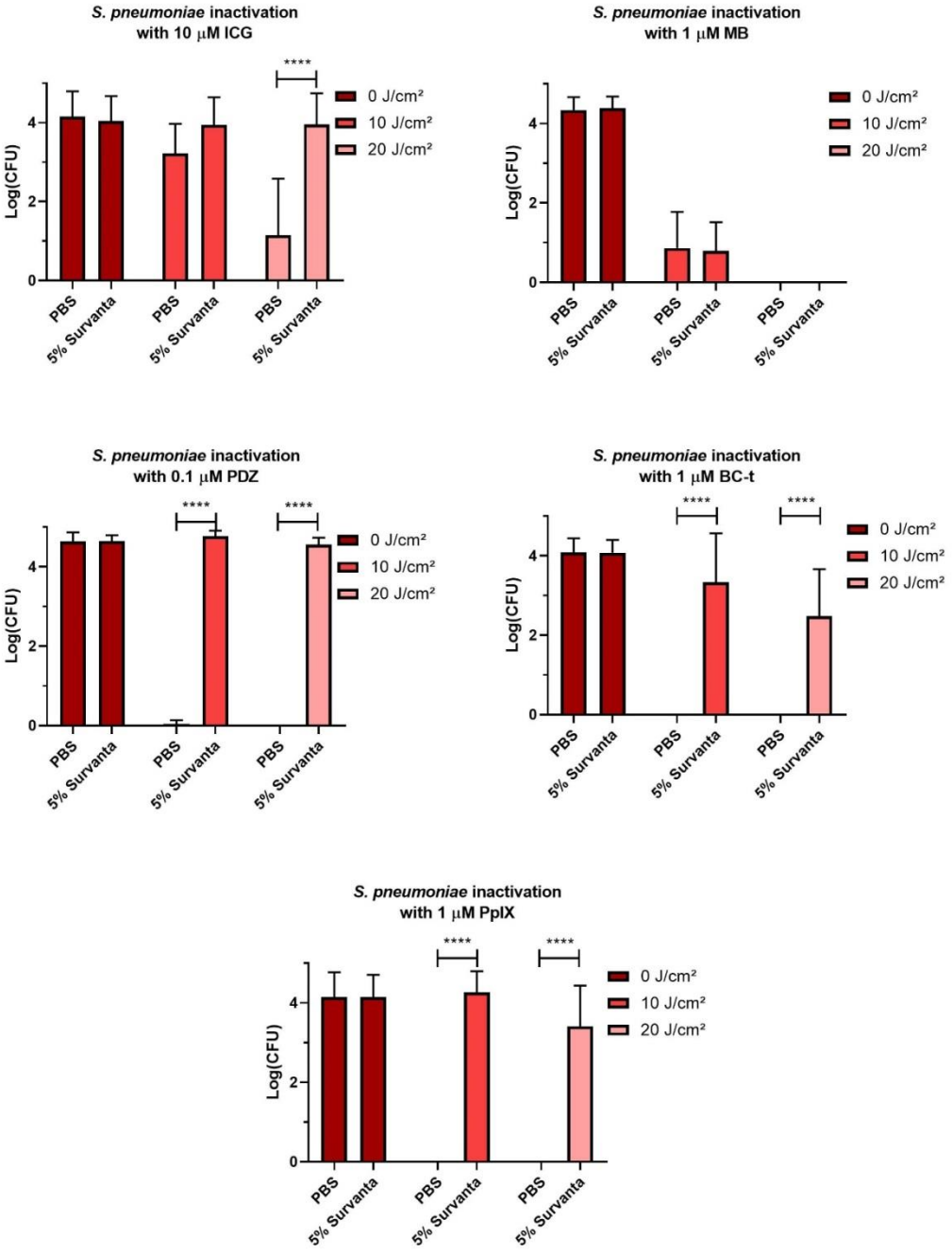

Figure 21 - Photodynamic inactivation of S. pneumoniae using different photosensitizers and wavelengths (808 nm for ICG, 660 nm for all others) in PBS with or without 5% of the medical-grade lung surfactant Survanta®. (****: $p<0.001$)

Source: KASSAB *et al.*[122]

All of the tested photosensitizers are effective against *S. pneumoniae*. However, as it is evident in Figure 21, most of them have their phototoxicity significantly suppressed in the presence of Survanta®. ICG has a moderate PDI effect in the presented concentration that is completely inhibited when the lung surfactant is present. PDZ achieves complete inactivation of the bacteria at a low concentration (100 nm) in PBS, but this effect also completely disappears with 5% Survanta®. For BC-t and PpIX, there is mild bacterial inactivation in the presence of Survanta®, but it is much lower than the complete inactivation achieved in PBS. The only exception to the suppression of the inactivation seems to be methylene blue, for which there is no difference between the PBS and the 5% Survanta groups. The PDI with 1 µM MB has a partial response with a fluence of 10 J/cm², but reaches complete inactivation with 20 J/cm². The presence of the lung surfactant has no effect on the photodynamic effect of MB.

5.2.2 Optical Properties

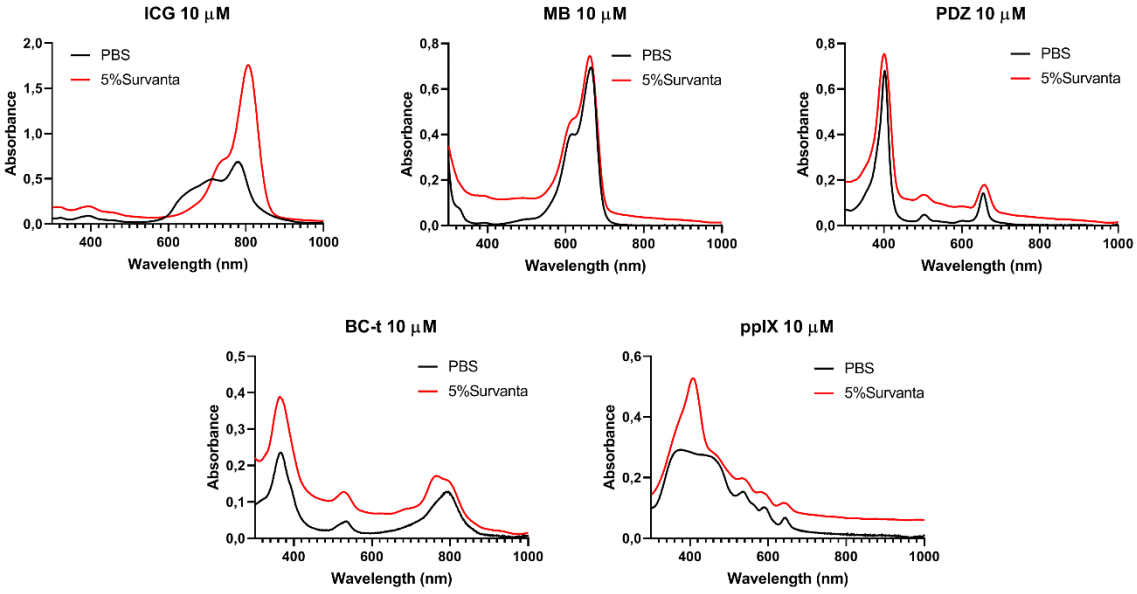

Figure 22 - Absorbance spectra of the five photosensitizers in PBS with and without 5% Survanta®.
Source: KASSAB *et al.*[122]

Changes in absorbance and fluorescence spectra are indicative of changes in the local field of interaction of a molecule, that directly changes the energy required for the electrons to be promoted to excited states. The absorbance spectra for the five photosensitizers in PBS with and without 5% Survanta® in the spectral range of 300 – 1000 nm are presented in Figure 22. The presence of the lung surfactant consistently increases the absorbance of the

photosensitizers, which suggests an interaction between them. For MB and PDZ no dislocations are observed in the spectra with and without Survanta®. In the case of BC-t, the characteristic peak at 793 nm is slightly shifted to 762 nm.

For ICG and PpIX, the spectra in PBS are indicative of the presence of aggregates. The addition of 5% Survanta® shows spectral evidence of a decrease in aggregation and increase of the higher-absorbing monomer forms. It is known that, in ionized solutions, the tendency to form aggregates is highly probable.[129] For ICG in PBS, that is seen in the absorbance in the 600 - 705 nm range, where there is a band associated with H-aggregates. In this solvent, the maximum absorbance of the ICG monomer peaks in 780 nm. ICG in 5% Survanta® shows a red-shift of the maximum absorption peak (to 806 nm), and lower absorption in the 600 – 705 nm band suggests a decrease in the concentration of H-aggregates. In the case of PpIX, the Soret band peaks at 379 nm in PBS, while in 5% Survanta® it shifts to 406 nm and has a drastic increase, which can also be associated with a reduced concentration of aggregates.

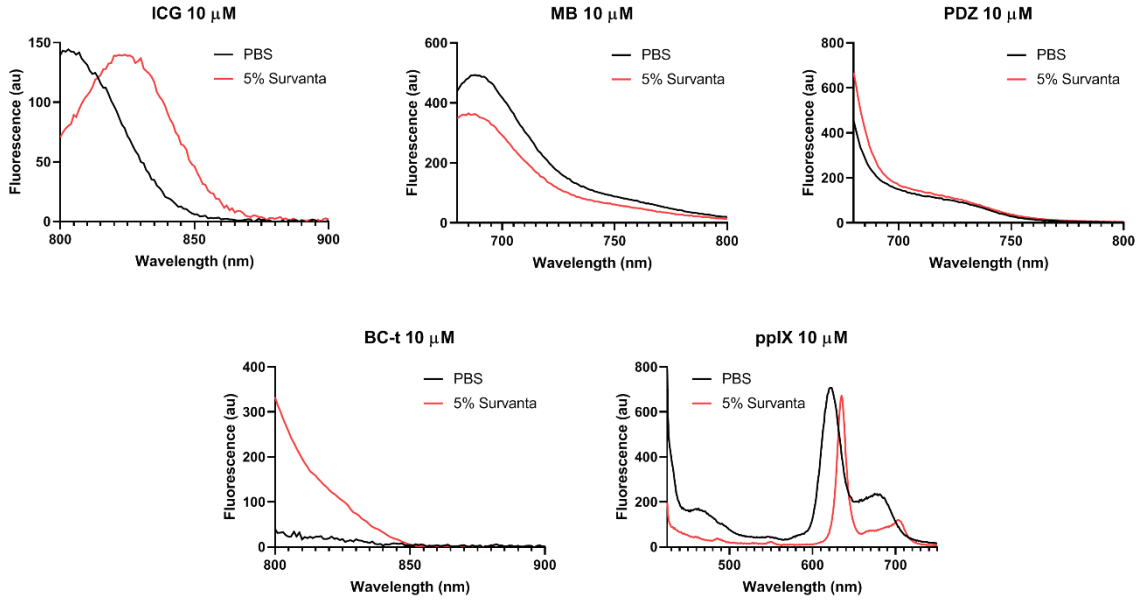

Figure 23 - Fluorescence spectra of five photosensitizers in PBS with and without 5% Survanta®.
Source: KASSAB *et al.*[122]

The fluorescence emission spectra presented in Figure 23 were recorded in PBS with and without 5% Survanta® at room temperature. The emission of the photosensitizers can be affected by the presence of lung surfactant in different ways: for ICG and PpIX, the most affected in terms of absorbance, there is a shift in the emission peak towards higher wavelengths, but without significant change in intensity; the fluorescence intensity of MB

decreases slightly, and the one of PDZ increases slightly; and for BC-t, the fluorescence signal is enhanced dramatically.

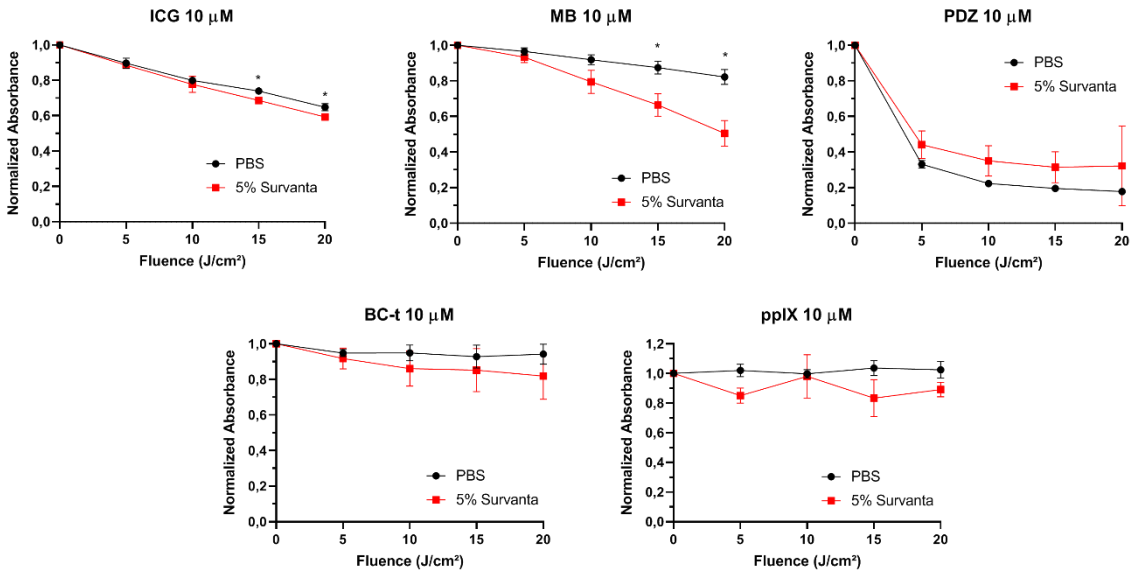

Figure 24 - Photobleaching profile of the five photosensitizers in the presence or absence of 5% Survanta®. (*: $p<0.05$)

Source: KASSAB *et al.*[122]

Despite the modifications seen in the absorbance and fluorescence spectra, the impact of Survanta® in the photobleaching rate of the photosensitizers is either small or not significant (Figure 24). This rate is an indirect measure of the photodynamic effect, since the ROS generated will eventually destroy the photosensitizer and decrease the sample's absorbance. For ICG and MB, the statistical analysis showed that the normalized absorbance is significantly smaller after 15 and 20 J/cm² of light treatment when Survanta® is present, indicating a higher photobleaching rate. For PDZ, BC-t, and PpIX, the addition of 5% Survanta® does not affect this phenomenon. This suggests that the interaction between the photosensitizers and the lung surfactant does not decrease the probability of encounter with the O_2, nor the formation of reactive species.

5.3 Discussion

The interaction with the lung surfactant negatively impacts the efficacy of many pulmonary medications, and the results of this research have shown this is also the case for multiple photosensitizers. The molecules selected for this study presented different chemical properties (Table **2**), including molar mass, net electric charge and polarity, as well as different photochemical properties, with varying molecular absorption coefficients and singlet oxygen

formation quantum yields. All of them had potential for the photodynamic inactivation of bacteria, as became evident in Figure 21 since they all significantly reduced the viability of *S. pneumoniae* in PBS. However, because of their chemical and photochemical differences, the concentration of each photosensitizer required for this effect varied in over 100-fold. Namely, PDZ completely eliminated the bacteria at 100 nM, while ICG only had a partial response at 10 µM. Yet, in the presence of the lung surfactant Survanta®, the inactivation effect of PDZ was completely suppressed and it showed no antimicrobial response. The same occurred for the less potent ICG. In the case of PpIX and BC-t, that were both completely effective at 1 µM in PBS, only a partial response was obtained in the presence of 5% Survanta®. Despite the different properties of these four photosensitizers, Survanta® consistently inhibited the PDI effect for all of them. On the other hand, methylene blue seemed to be an exception to this rule, and at 1 µM showed a partial killing of *S. pneumoniae* with 10 J/cm² and a complete killing with 20 J/cm² in both the presence and absence of the lung surfactant.

The aPDT effect of ICG had been previously reported to be inhibited in the presence of horse plasma and two mechanisms were proposed to explain it: quenching of the singlet oxygen produced, or inhibition of the uptake by the target organisms.[94] So, we proposed to test if either of these mechanisms played a role in the inhibition of the PDI by 5% Survanta®. The spectral modifications shown in Figure 22 and Figure 23 suggest a change in the environment surrounding the photosensitizer molecules, which indicate that there is a strong chemical interaction between them and the molecules present in the lung surfactant. But Figure 24 shows that this interaction does not inhibit the formation of reactive oxygen species, nor quenches their activity. If there was a direct quenching effect, say, by the presence of a molecule much more likely to be targeted by them than others, there would be a reduction of the photobleaching of the photosensitizer, because it would be less likely to be destroyed by the oxidative stress. Instead, what occurs is either an increase or maintenance of the photobleaching rate.

Thus, we propose that the interaction between the photosensitizer and the phospholipid components of the lung surfactant could hinder the molecular attachment to the bacterial wall, similarly to what happens to antimicrobial peptides.[83] The interaction with the bacterial wall seems to be fundamental for the mechanism of action of antimicrobial photosensitizers.[100] Thus, a collaboration was formed to investigate the interaction using molecular dynamics simulations, in particular to bring more information regarding the mobility of the photosensitizer in the presence of the lung surfactant, that correlates to its availability to interact with the target (in this case, the bacteria). The results of such simulation have been

published by Kassab *et al*.[122] Overall, the simulation shows that all photosensitizers interact with the phospholipid mixture. Each molecule preferably interacts with specific phospholipids in the surfactant layer. ICG interacts mostly with DPPC, the most abundant component of Survanta®. BC-t either also interacts with DPPC, or the second most frequent component, POPC. The Chlorin e_6 portion of PDZ mostly interacts with POPC. As for PpIX, the molecule is close to a DPPG rich region, but there is also proximity to DPPC. MB is closer to DPPG and palmitic acid molecules, which make up a smaller portion of the composition of the surfactant.

Besides the specific interaction with less abundant phospholipids, another result that separates MB from the other photosensitizers is the Z-profile (see Kassab *et al*[122]). MB interacts and is released from the surfactant multiple times over the course of the simulation, and even interacts with both the upper and lower layers. MB is the most water-soluble of the five photosensitizers (as seen on logP values of Table **2**), which is a likely explanation for this behavior. Moreover, MB has one positive charge distributed along the molecule, which might result in a strong interaction with the DPPG (or other negatively charged phospholipids such as DPPE or DPPI) polar heads. The other molecules, despite having positive or negative net charges, have more than one charged group, which might also result in a strong interaction with both positive and negative charges present in the polar heads. Thus, despite our Survanta® lung surfactant model having a negative net charge, free energy analyses might be necessary to evaluate the strength of the interaction with the polar heads. The estimated diffusion coefficient and radius of gyration (from Kassab *et al*) are probably more significant for the overall effect.[122] The radius of gyration of each photosensitizer molecule is similar in magnitude to the hydrodynamic radius. The mobility of non-spherical particles may be described by the hydrodynamic radius that is related to the frictional force of particle with the solvent. MB molecules present the smallest radius of gyration compared to the other photosensitizers, meaning that MB has the largest mobility.

Thus, there seems to be a correlation between the loss of mobility of a photosensitizer in the presence of Survanta® and its loss in efficacy against bacteria. As expected, the lung surfactant is a barrier to be transposed for the success of the photodynamic treatment of pneumonia. Still, different approaches can be taken to make this possible. On one hand, MB might seem to be the obvious candidate for pulmonary aPDT since it retained its PDI efficacy despite the presence of Survanta®. However, some of MB's photochemical characteristics are not ideal for this application. Because of the pathology and infectious nature of pneumonia, the best treatment for it needs to be as little invasive as possible, and in the case of aPDT that

relies on using an external light source, with a wavelength able to penetrate through multiple layers of biological tissue. We have gathered enough evidence to believe that would be possible using 808 nm and ICG, but it would be not able to activate MB with this wavelength.[68,130]

On the other hand, it might be possible to still use the photosensitizers that strongly interact with the lung surfactant. In studies where a similar problem was identified for other drugs, formulations were proposed as a solution: either using the lung surfactant itself as a vehicle[84,131]; encapsulating the active principles into nanoparticles or optimizing nanoparticle design[67,78,85,120-121,132]; or even using perfluorocarbons, which are pulmonary liquid ventilation agents[133,134]. Also, it is important to consider that the reduced mobility will decrease the local concentration of photosensitizer available to interact with the target, but it will not be zero. The bactericidal effect of aPDT of a given context depends of a relationship between the photosensitizer concentration and the light dose, in which the larger one of them is, the smaller the other one is required to be (for a complete description of the mathematical model, see Willis *et al*, 2021[135]). In other words, if there is a lower availability of PS, an increase in light dose might be enough to yield the same effect. An increase in the delivered dose of photosensitizer will also increase its locally available concentration, facilitating the killing of bacteria. This was seen for PDZ in the micromolar range, where there was complete inactivation of *S. pneumoniae* both in the absence and presence of Survanta® (data not shown). However, there would be a need to consider the safety of the pulmonary epithelium in this case, as well as the integrity of the lung surfactant itself, that is essential for the survival of the patient.

In summary, the presence of the clinical surfactant Survanta® decreases the PDI effect of indocyanine green, Photodithazine®, bacteriochlorin-trizma and protoporphyrin IX against *S. pneumoniae*. This is not due to quenching or other light-related effect, but more likely due to a physical distance between photosensitizer and target. Methylene blue is the only photosensitizer tested that did not lose efficacy when the lung surfactant was added, probably because of its higher water-solubility and positive charge, that provide further mobility when interacting with the lung surfactant. However, since other properties may deem other photosensitizers more appropriate for the treatment of pneumonia, there are formulation strategies that can be used to overcome the lung surfactant interaction. Nonetheless, with all the accumulated evidence that pulmonary aPDT could work, overcoming the lung surfactant barrier might be the main obstacle to its success.

6 SURFACE ACTIVITY OF PHOTOSENSITIZERS AND THEIR INTERACTION WITH OTHER SURFACE-ACTIVE COMPOUNDS

We have been able to show that molecular photosensitizers in fact interact with the lung surfactant, and that this interaction does not inhibit the generation of ROS, but instead separates them from the bacterial target and this leads to a loss of activity. Nevertheless, there was still a need to understand what drives the selectivity between the interaction with the surfactant over the interaction with the bacterial cell wall. Understanding these interactions and selecting photosensitizers that will overcome the surfactant barrier without disrupting its functionality is fundamental for the progress of this research. Thus, we proposed to investigate the interactions between photosensitizers, lung surfactant and a simulated bacterial membrane model using surface tension measurement techniques and the formation of mono- and bilayers as appropriate. We chose the previously discussed ICG, that was completely inhibited by Survanta, and MB, that was not, and have also added a MB nanoemulsion (neMB), a pyro-salt nanoemulsion (nePS), and a nanoemulsion blank, as a control. We investigated the interaction between each photosensitizer and the clinical-grade lung surfactant Survanta® and the lipopolysaccharides (LPS), characteristic from gram-negative bacterial membranes. The most relevant results from the investigation are presented in this chapter. All experiments in this section were performed at the Institut Galien of Université Paris-Saclay, under the supervision of Professor Véronique Rosilio and Doctor Jean-Philippe Michel.

6.1 Methodology

6.1.1 Materials

Indocyanine Green (ICG) was obtained from Ophthalmos (Brazil) and aliquoted into small solid samples that were solubilized in deionized water and then diluted in phosphate buffered saline (PBS) prior to each experiment, then discarded at the end of the day. Methylene Blue (MB) was obtained from Sigma-Aldrich (USA) and stocked in a concentrated solution in PBS at 4 °C. The methylene blue nanoemulsion (neMB), pyro-salt nanoemulsion (nePS) and a nanoemulsion blank (neBl, containing the components of the other nanoemulsion, but without photosensitizer) were produced in Gang Zheng’s laboratory

(UHN, Canada) and stored in PBS at 4 °C. To investigate their interaction with lung surfactant, the medical-grade Survanta® (AbbVie, USA) was used. Rough-strain lipopolysaccharides (LPS mutant Re 595) extracted from *Salmonella* (Sigma-Aldrich, USA) were chosen to study the interaction with gram-negative bacterial walls.

6.1.2 Surface tension measurements

The surface-activity of the photosensitizers and their ability to interact with other surface-active substances was investigated by the Wilhelmy plate method, using K10 tensiometers (Krüss, Germany). Before starting each experimental run, the temperature was set to 22 °C and cuvettes were filled with 20 mL of PBS. Then, concentrated solutions of the photosensitizers were injected through the side-arm of the cuvettes into the subphase of the PBS, resulting in final PS concentrations corresponding to the effective *in vitro* killing of bacteria (10 µM for ICG, 1 µM for all others).

The initial ICG and MB adsorption experiments had no deposition of any other material on the surface, and were allowed to run overnight at least once, to investigate the kinetics of the surface interaction of each PS. Afterwards, new experiments were run where 1 µL of Survanta was spread at the surface, resulting in a decrease in surface tension of about 25 mN/m, and then a PS was injected in the subphase. Finally, a similar experiment was done with LPS. LPS was dissolved in a chloroform-methanol mixture (9:1), and combined in a 4:1 molar ratio with the phospholipid POPC (1-palmitoyl-2-oleoyl-sn-glycero-3-phosphocholine). POPC was necessary for stabilizing the LPS monolayer at the interface. The LPS-POPC mixture (4-5 µL) was spread at the surface of PBS, in order to decrease the surface tension by about 35 mN/m, before the photosensitizers were injected. The experiments with Survanta and LPS were only run until the surface tension was stabilized, which took 20-60 minutes depending on the sample. Each combination was run in triplicate. The changes in surface tension were extracted from the runs and the means were compared using the one-way ANOVA and plotted in GraphPad Prism. Results were considered significantly different with $p < 0.05$.

6.1.3 Surface pressure measurements

The interaction between Survanta and the photosensitizers ICG and MB was further investigated using a Langmuir film balance (Biolin Scientific, Finland). The trough was set to 22°C and filled with PBS, then the surface pressure was zeroed. Samples were distributed

evenly on the surface in small aliquots. Then, isotherms were obtained by compressing the monolayer, starting from 775 cm² until collapse, at a rate of 39 cm/min.

Isotherms were first obtained from Survanta® alone, then it was combined with either ICG or MB at a 4:1 mass ratio, and new isotherms were obtained. Since ICG had to be solubilized in distilled water instead of PBS, a control was performed in which distilled water was added to Survanta in the same ratio, to account for possible structural changes that water could cause. Isotherms were also obtained for ICG and MB alone. All runs were performed in triplicate. The data was processed and plotted using Origin 9 (OriginLab, USA).

The surface compressibility modulus (C_s^{-1}) was calculated according to the equation:

$$\boldsymbol{C_s^{-1} = -A(\frac{d\pi}{dA})_T} \quad (3)$$

where A is the area, π is the surface pressure, and T is a constant temperature.

6.1.4 Quartz-crystal microbalance with dissipation (QCM-D) experiments

QCM-D experiments were performed using a quartz crystal microbalance with Dissipation monitoring (Q-sense, Finland), and processed in the software Qsoft401, from the same supplier. Two SiO_2 sensors were thoroughly cleaned using 100 μM SDS, dried in a N_2 flow, exposed to UV-Ozone for 30 minutes, then mounted onto parallel cells in the equipment. Resonant frequencies 3 through 11 and their corresponding dissipation factors were found and monitored during the experiments. At first, a baseline in air was obtained, and then PBS was circulated through the cell at 50 μL/min. Survanta was added (5% V/V in PBS), allowed to interact for a few minutes, then the excess was rinsed with PBS before the addition of each photosensitizer (ICG at 10 μM, MB, neMB and neBl at 1 μM). A few minutes were given to settle the interaction between PS and Survanta, then the cell was rinsed with PBS again. Later, SDS was flushed through the system (at 950 μL/min for a few seconds) and then ultrapure water was added, to remove the Survanta layer and restore the sensor to the initial conditions.

6.2 Results

6.2.1 Surface-activity of the photosensitizers and interactions with surface-active mixtures

Figure **25** shows the effect of the introduction of different photosensitizers to the subphase of PBS. ICG immediately reaches the surface and induces about 20 mN/m surface

tension decrease, indicating its strong surface activity. The nanoemulsion neMB and nePS adsorb more slowly, but eventually reach a similar $\Delta\sigma$. MB and the dissembled nanoemulsion components (neBl) do not show any surface activity in PBS.

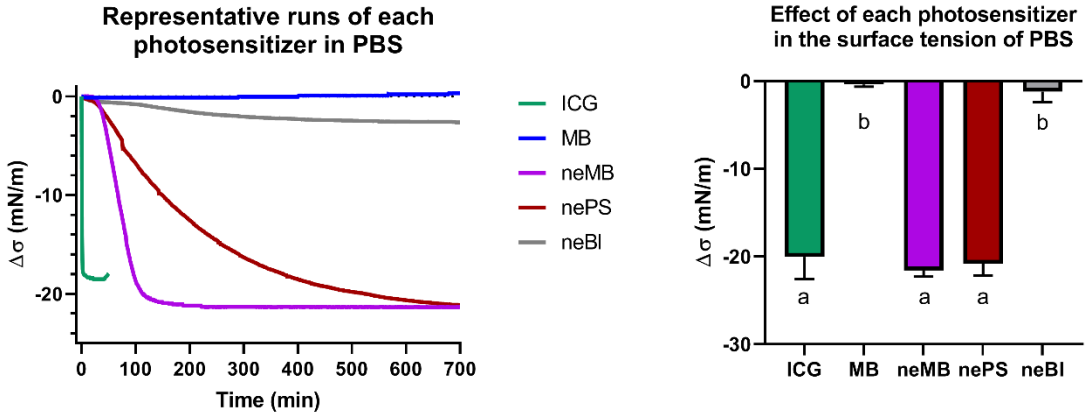

Figure 25 - Representative tensiometer runs and average surface tension change ($\Delta\boldsymbol{\sigma}$) for each of the photosensitizers when added to the subphase of PBS (10 µM for ICG, 1 µM for all others). Groups indicated with the same letter (a or b) are not significantly different from each other in the one-way ANOVA ($\boldsymbol{p > 0.05}$).

Source: By the author.

The effect of injecting the photosensitizers in the subphase of PBS while the surface is already saturated with Survanta® is shown on Figure **26**. When added to the subphase of PBS containing Survanta on the surface, ICG quickly interacts with the surface and the surfactant and decreases the tension by about 11 mN/m. The nanoemulsion neMB seems to also interact with Survanta on the surface, but more slowly and not as strongly. MB does not show any interaction, and nePS and neBl show ambiguous results of little to no interaction.

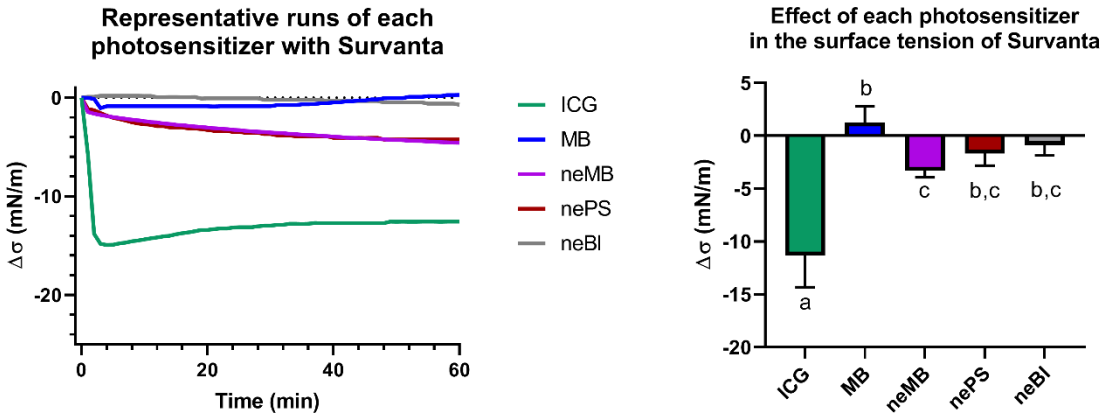

Figure 26 - Representative tensiometer runs and average surface tension change ($\Delta\boldsymbol{\sigma}$) for each of the photosensitizers when added to the subphase of PBS after the deposition of 1 µL of Survanta on the surface ($\boldsymbol{\pi \sim 25 \frac{mN}{m}}$). Groups indicated with the same letter (a, b or c) are not significantly different from each other in the one-way ANOVA ($\boldsymbol{p > 0.05}$).

Source: By the author.

In order to observe an interaction between the photosensitizers and the LPS, it was decided then to add enough of the latter to saturate the interface. This was achieved with a decrease the surface tension of PBS by about 35-37 mN/m. Figure **27** shows what further decrease was achieved when, after that, the photosensitizers were injected into the subphase. Once again, ICG led to a quick, significant Δσ, indicating an interaction with the surface and/or the LPS. All other samples showed a slight or no decrease in surface tension.

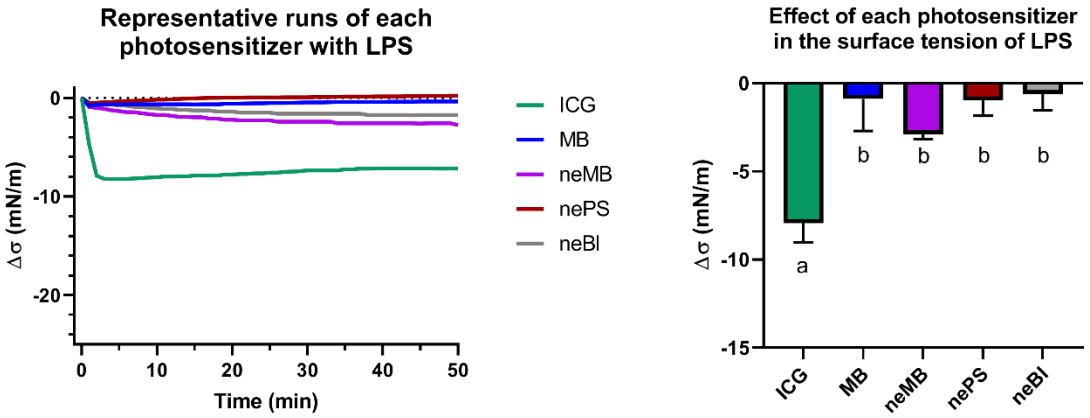

Figure 27 - Representative tensiometer runs and average surface tension change ($\Delta\boldsymbol{\sigma}$) for each of the photosensitizers when added to the subphase of PBS after the deposition of the LPS-POPC mixture on the surface ($\boldsymbol{\pi \sim 35 \frac{mN}{m}}$). Groups indicated with the same letter (a or b) are not significantly different from each other in the one-way ANOVA ($\boldsymbol{p > 0.05}$).
Source: By the author.

6.2.2 Effect of ICG and MB on Survanta's Langmuir isotherms

When deposited on the surface of PBS, Survanta presents an interesting Langmuir isotherm profile (Figure **28**). As expected, the surface pressure increases as the area decreases. However, there are two area intervals in which the surface pressure remains roughly constant, at around 50 mN/m and 70 mN/m. The first transition, at 50 mN/m, also occurs with Curosurf® and is described to be a monolayer-to-multilayer transition.[86] The second transition corresponds to the collapse.

When Survanta is mixed with ultrapure water before being added to the surface of PBS, the π/A isotherm shifts to larger areas, indicating monolayer expansion. When mixed with ICG or MB, the opposite occurs. However, the effect of the presence of ICG is much more pronounced than with MB, shifting the isotherm to a point that it was not even possible to see the end of the first transition. ICG on its own is surface active and produces a π/A isotherm with increased pressure at larger areas when compared to Survanta®, but that does not reach high pressures when further compressed. MB is not surface active on its own.

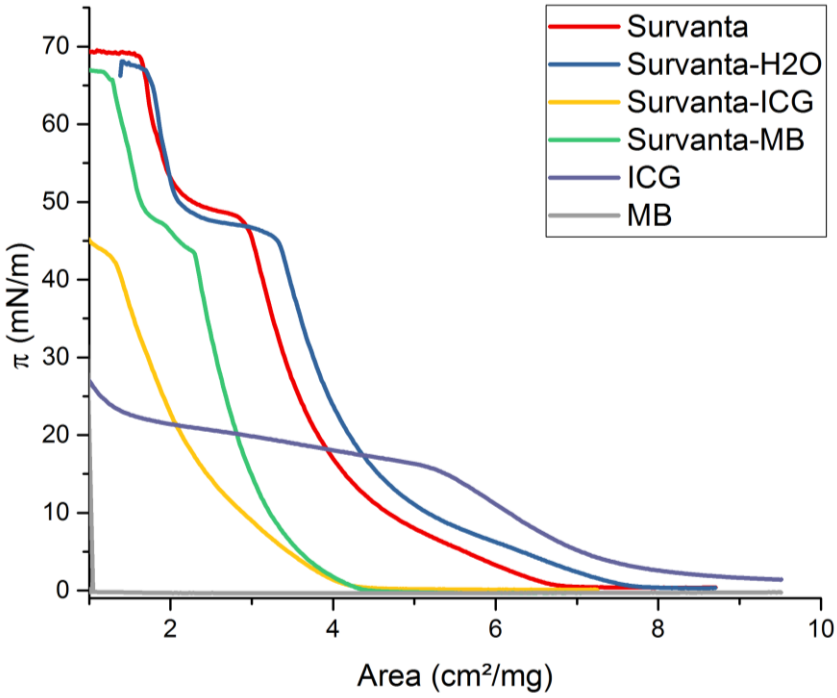

Figure 28 - Representative Langmuir isotherms of Survanta and selected photosensitizers when added to the surface of PBS.

Source: By the author.

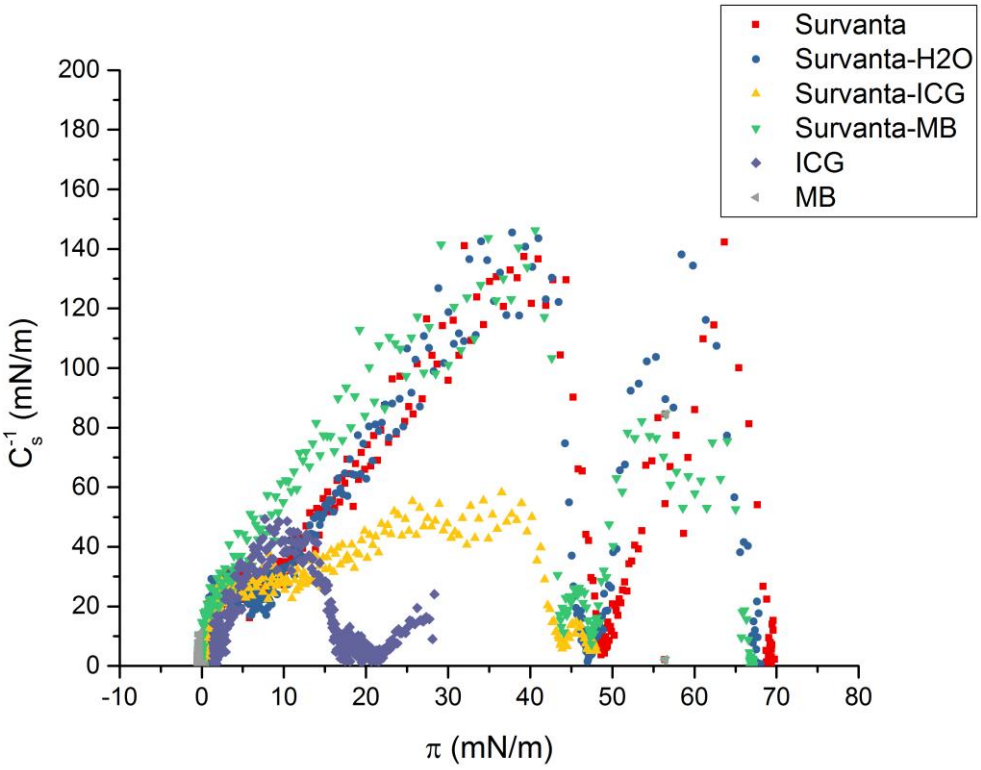

Figure 29 - Surface compressibility moduli of the Langmuir isotherms from Survanta and selected photosensitizers when added to the surface of PBS.

Source: By the author.

The compressibility results shown in Figure **29** further highlight the difference between ICG and MB. Despite the shifts in the π/A isotherms, the C_s^{-1} of pure Survanta and its mixture with water and MB are quite similar, reaching about 130 mN/m before the first transition. The only difference is after that, where the C_s^{-1} goes back to about the same value except when MB is present, stopping at about 80 mN/m. Survanta and ICG, on the other hand, only reach up to about 50 mN/m, similarly to ICG alone.

6.2.3 Photosensitizer interactions in bilayer models

Figure 30 through Figure **33** show representative QCM-D runs for the interaction between different photosensitizers and Survanta. No description of QCM-D experiments using Survanta was found in the literature, so it was not initially possible to confirm if there was a bilayer being formed or other arrangement, but the frequency deviation results were consistent between experiments and seemed to be stable upon rinsing with PBS and reversible after adding SDS. The changes in dissipation provide information on the viscoelastic properties of the adsorbed layers.

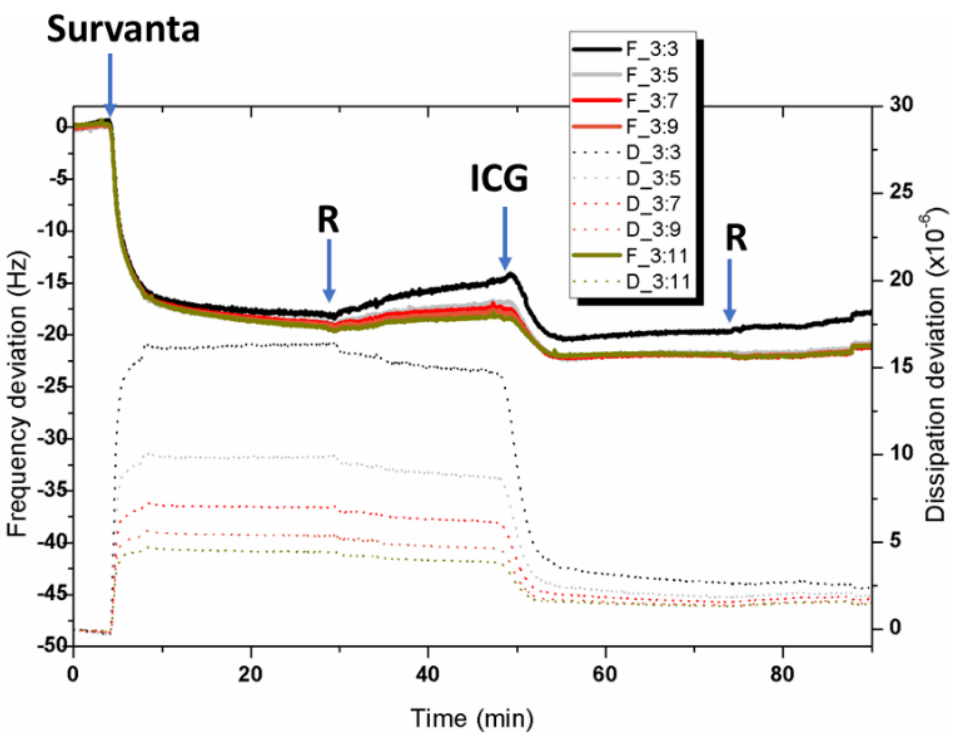

Figure 30 - Representative QCM-D run for Survanta and ICG 10 µM. R: rinsing with PBS.

Source: By the author.

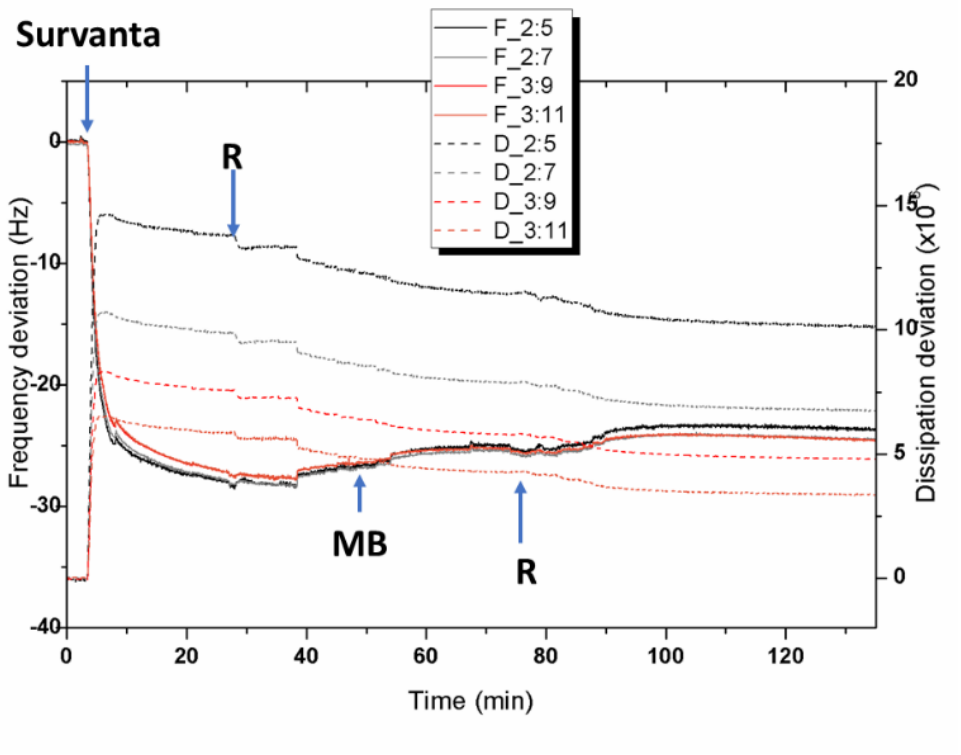

Figure 31 - Representative QCM-D run for Survanta and MB 1 µM. R: rinsing with PBS.
Source: By the author.

As expected from the other experiments, Figure 30 shows that ICG interacts with Survanta. When added to the sensor, ICG decreases the resonance frequencies by about 7 Hz, and rinsing it with PBS does not restore them, suggesting that binding is stable. Additionally, the dissipation that had initially increased when Survanta was added is lowered in the presence of ICG, indicating that it reduces the viscous behavior of the Survanta layer, making it more rigid. MB, on the other hand, does not cause a significant change in frequency nor dissipation, which suggests that there is no interaction, also corroborating with the other experiments (Figure 31). Figure **32** and Figure **33** show that when neMB or the blank nanoemulsion are added, the resonance frequencies increase instead of decreasing, suggesting that something is being taken away from the sensor instead of being deposited onto it. Also, the dissipation decreases, suggesting the same thing.

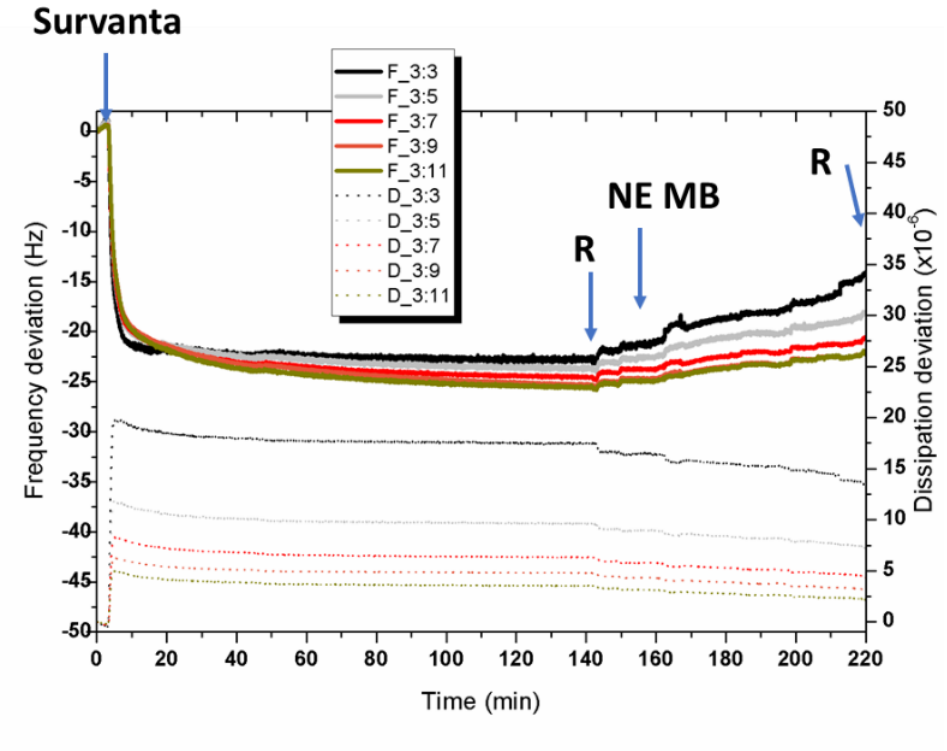

Figure 32 - Representative QCM-D run for Survanta and neMB 1 µM. R: rinsing with PBS.
Source: By the author.

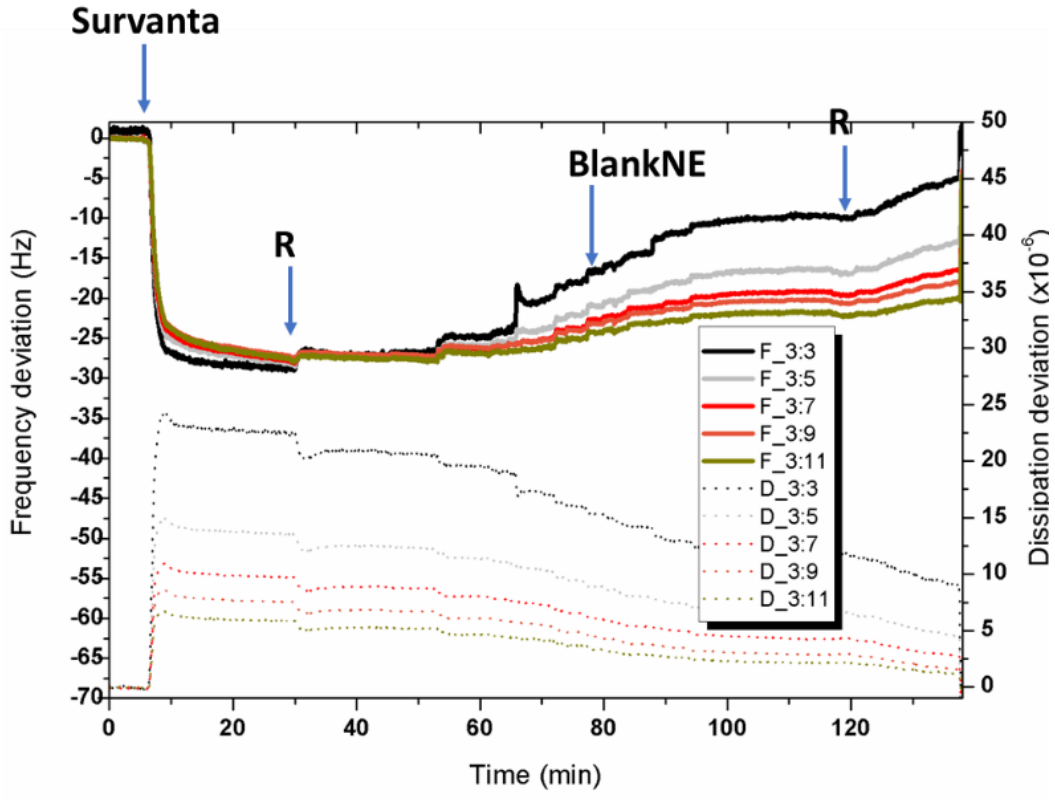

Figure 33 - Representative QCM-D run for Survanta and neBlank (equivalent to neMB 1 µM). R: rinsing with PBS.

Source: By the author.

6.3 Discussion

The surface tension (γ) of PBS at room temperature is about 72.8 mN/m, similar to water. When a surfactant is added, it interacts with the surface and decreases the surface tension. The stronger a surfactant is, the more it decreases the surface tension of water, and therefore the higher is the surface pressure at the surface. The Langmuir isotherms results are usually presented in terms of this surface pressure (π), which is the difference in surface tension of water or an aqueous solution after a certain amount of a certain surfactant is added to it, or in other words:

$$\pi = -\Delta\sigma \tag{4}$$

As the area of the surface is compressed, there is a local increase in the concentration and organization of the surfactant on the surface, thus increasing its surface pressure even further.

The LPS-POPC (4:1) mixture strongly decreases the surface tension of PBS, and there is a somewhat linear relationship between deposited mass and Δσ (not shown). Survanta® is very surface active, as expected, and adding 1 µL of it to the surface of PBS decreases the surface tension by about 25 mN/m. Interestingly, adding a larger volume of the lung surfactant does not decrease the surface tension any further, suggesting a saturation of the surface, even with this small amount. Since some of the components of Survanta® are soluble in water, it is possible that they are pushed into the subphase as more mass is deposited on the surface.

Still, a molecule that interacts strongly with Survanta is able to further decrease the surface tension when added to it, as seen for ICG in Figure 26. ICG shows a strong surface activity when injected into the subphase of PBS (Figure **25**) and it persists even when the surface is covered with the LPS-POPC mixture (Figure **27**). But its interaction with Survanta® is particularly interesting because the saturated lung surfactant layer should behave like a polymer barrier, decreasing the access of molecules on the subphase to the air-liquid interface, but ICG's kinetics are unchanged by its presence, meaning there is no barrier effect. ICG decreased surface tension in less than one minute in all 3 experimental conditions. This has two possible explanations: either ICG has such a strong affinity to the surface that it competes with Survanta® and penetrates through the barrier, pushing some of the phospholipids or proteins back into the subphase; or ICG interacts directly with the components of the lung surfactant, changing its organization and allowing for a further decrease in surface tension.

The results from Figure **28** and Figure **29** seem to indicate that both of these phenomena happen simultaneously. On one hand, Survanta's isotherm is shifted to the left in the presence of ICG, which means that more compression is required to yield the same surface pressure with the same mass deposited. In other words, this suggests that a part of the mass is being solubilized into the subphase, losing its ability to change the properties of the surface. On the other hand, the compressibility modulus of Survanta® is dramatically reduced in the presence of ICG, even at low surface pressures. This implies a change of organization and loss of elasticity, that can be attributed to an interaction that decreases rigidity.

Another evidence of this can be seen in Figure **30**. ICG has such a strong interaction with Survanta® that, despite it being a small molecule, it noticeably decreases the resonance frequencies in the QCM-D experiment. But more importantly, it dramatically changes the dissipation factor of the Survanta® layers. This is a different phenomenon from the one observed with the surface pressure measurements. In those, ICG is able to penetrate the single surfactant monolayer (spread at the interface), and disorganize it (Figure 26). With QCM-D experiments, a multilayer is formed. Survanta® increases the dissipation of the SiO_2 sensor in all frequencies, but especially in the smaller harmonics, that are related to the layers further away from the sensor. This probably means that a viscous, multilayer system is present, in which there is water in between bilayers of phospholipids, consistent to what has been described from microscopies of the lung surfactant layer *in vivo*.[89] Thus, the further away from the sensor, the more dissipation occurs.

When ICG is added to this system, the dissipation factor decreases on all frequencies, almost to the point of returning to the baseline prior to the addition of Survanta®. That is indicative of an increase in viscosity, that could be achieved by the formation of ICG "bridges" between the bilayers. Considering ICG's symmetrical chemical structure (Figure 2), and its predicted interaction with abundant phospholipids DPPC and POPC (described in section 5.3), we hypothesize that the PS interacts with the surfactant probably both by hydrophobic and electrostatic interactions, and does so in more than one layer. It seems reasonable to assume that it could thus having a bridging mechanism that rigidifies the system.

MB, on the other hand, does not seem to be surface-active. Figure **25**Figure **27** show that MB does not disturb the surface tension of PBS, regardless of the presence of Survanta® or LPS on the air-liquid interface. Figure 31 also does not show any mass deposition of change in viscosity when it is added to the Survanta® multilayer system. MB only seems to interact with Survanta® if it is mixed with it prior to the deposition on the surface, as it occurs in

Figure **28**. Figure **29** shows that the compressibility modulus of Survanta® is only slightly modified by MB at high surface pressures (above the first transition), meaning that, for the most part, MB does not modify the organization of the lung surfactant at the interface. This also corroborates with the predictions made from the molecular simulation in section 5.3.

It was not possible to predict the behavior of the nanoemulsions using molecular dynamics simulation, due to their large size and complexity when compared to single molecules. Nonetheless, they present an interesting behavior that is consistent with their properties as emulsions. Both neMB and nePS show strong surface activity, but have a slow-paced kinetic profile (Figure **25**). It is likely that, as nanoemulsions, they are stable in the subphase of PBS, with the hydrophilic moieties exposed to the solvent and the hydrophobic portions protected from it and interacting with the oil core. However, as these nanostructures reach the air-liquid interface, they eventually break into single molecules, some of which are surface-active. Thus, it takes multiple hours for the system to stabilize. Chang *et al* have measured the surface properties of a pyro-lipid nanoemulsion (similar to nePS), and have found that, 2 and 8 weeks after its preparation, it presented a surface tension of about 42 mN/m.[136] That corresponds to a $\Delta\sigma$ of about 30 mN/m, comparable to what neMB and nePS seem to be trending towards. In the cases where a surfactant is already deposited on the surface (Figure **26** andFigure **27**), neMB and nePS are unable to reach the interface and break, likely due to the previously mentioned barrier effect (longer experimental times have been tested, but are not shown).

The "nanoemulsion blank" neBl consists of the same components of the PS nanoemulsions, but without any photosensitizer. However, as the PSs are essential for the stability of the nanostructure, neBl is not in fact a nanoemulsion, but rather a simple mixture of immiscible components. When it is injected into the subphase of PBS (Figure **25**), its aqueous phase immediately solubilizes, but is not surface-active; and its oil phase, that would probably decrease the γ if added directly to the surface, has no mobility in the PBS. Therefore, neBl does not significantly decrease the surface tension of PBS in the experimental time. But it is understood that, had the oil in it reached the surface, it would probably have resulted in a similar effect to neMB and nePS.

In the QCM-D Survanta® multilayer model, neMB and neBl have similar results (Figure 32 andFigure **33**). It was expected that any interaction with Survanta would be more evident for the nanoemulsions compared to single molecules, because they have a much larger mass. Nonetheless, the larger structures are dragged by the constant flow of liquid, so instead of detecting an increase in deposited mass as it is seen for ICG, the interaction between

Survanta® and the neMB nanoparticles or the microdroplets of oil from neBl is made evident by a removal of mass from the detector. In other words, as neMB or neBl flow through the Survanta multilayers in the QCM-D cell, they interact with and partially solubilize it, dragging it away from the sensor. This increases the resonance frequencies and decreases the dissipation deviation, and the effect is more pronounced on the third harmonic, that is related to the layers further away from the sensor (and thus closer to the sample flow).

In summary, ICG is a strongly surface-active photosensitizer, and it interacts strongly with the clinical lung surfactant Survanta®, decreasing the elasticity of its monolayer at the air-liquid interface and the viscosity of its multi-bilayer system. ICG also interacts with LPS at the air-liquid interface. MB, on the other hand, it not surface-active and does not show great interaction with neither Survanta® nor the LPS. The nanoemulsions neMB and nePS seem to only exhibit surface-activity as they slowly break into single molecules on the unchanged surface of PBS, but not when it is already covered by other surface-active compounds. neMB and the oil component from the nanoemulsions (neBl) interact with the multilayered Survanta® and seem to partially dissolve or at least destabilize it.

7 OVERCOMING THE SURFACTANT BARRIER

The results from chapter 5 established the importance of the lung surfactant for the success of aPDT against pneumonia, and the results from chapter 6 shed a light on the nature of its interaction with photosensitizers ICG and MB. Then, new efforts were put into finding ways to overcome the surfactant barrier. ICG has the strongest interaction with the lung surfactant, but it remains the most promising candidate for pulmonary PDT because of its safety and excitation range. Therefore, new ICG formulations and combinations with other treatments were proposed and tested *in vitro* for the killing of *S. pneumoniae* in the presence of Survanta™. The most promising strategy was the formulation with perfluorooctyl bromide (PFOB), and its preliminary results are presented in this chapter.

Additionally, we decided to pursue the investigation with MB. MB interacts the least with Survanta®, but does not have the ideal profile for pulmonary PDT. Nonetheless, learning more about how MB works in the pulmonary microenvironment may aid the development of new pulmonary photosensitizers in the future. We also proposed that neMB could serve as a model for understanding how the nanoemulsion formulations would affect the aPDT efficacy. Preliminary results with MB and neMB are also shown in this chapter.

Finally, another lesson learned from previous experiments was that animal experiments are incredibly complex and it is best to investigate new strategies in more controllable systems beforehand. With that in mind, a new setup was developed for these new experiments, the *in vitro* alveolar infection model. It consists of a more complex *in vitro* setup, that includes surfactant-expressing pneumocytes in an air-liquid interface, endothelial cells simulating the blood vessel barrier, and the infectious bacteria. Both the PFOB and the MB/neMB strategies were tested in this new model.

7.1 Methodology

7.1.1 Photosensitizer formulations and light sources

Perfluorooctyl bromide (PFOB) was purchased from Oakwood Chemical (USA). It was combined with a concentrated solution of ICG *in loco*, since it is not miscible with water. For the initial *in vitro* experiments, a laser-based device was used, with peak emission at 808 nm and irradiance of 78 mW/cm². For the *in vitro* alveolar model experiments, a 780 nm LED-

based Biotable compatible with 24-well plates and with an irradiance of 30 mW/cm² was used. The methylene blue nanoemulsion (neMB) was kindly provided by the Zheng Lab (University Health Network, Canada). Photodynamic activation of neMB was performed using a 660 nm Biotable with an irradiance of 50 mW/cm² (the same described in section 5.1.1).

7.1.2 *In vitro* bacterial inactivation

For the PFOB experiments, *S. pneumoniae* ATCC 49619 was grown as described previously (5.1.2) and resuspended in PBS at 1 x 10^8 CFU/mL. Then, 5 µL of the suspension were placed in wells of a 96-well plate and combined with either 5 µL of ICG at 200 µM or PBS. Finally, the wells were filled with 90 µL of either PFOB or more PBS, yielding in the PDI groups a concentration of 5 x 10^6 CFU/mL of *S. pneumoniae* and 10 µM of ICG, as used in previous ICG-PDI experiments. The experimental groups were the control (no ICG, no PFOB), PFOB only, ICG only, and ICG+PFOB (n = 3). All groups were exposed simultaneously to 20 J/cm² of light treatment, then samples were diluted and plated into blood agar Petri dishes and incubated overnight for CFU counts. No statistical treatment was performed.

The neMB stock solution was kept at 4 °C and diluted in PBS to an appropriate concentration prior to each use. Inactivation experiments were performed exactly as described for MB in section 5.1.2, but only on a single occasion (n = 3). There was no statistical treatment.

7.1.3 *In vitro* alveolar infection model

This model was based on the methods described by Huh *et al* and Hermanns *et al*[137,138]. Briefly, sterile PET Thincert® cell culture inserts with pore size of 0,4 µm, were purchased from Greiner Bio-one (Brazil) and placed on a 24-well plate. Human endothelial cell line EA.hy926 (CRL-2922, ATCC, USA) was attached to the underside (day 0) of the insert membrane and grown in antibiotic-free DMEM at 37°C and 5% CO_2 until confluence (day 3). Then, human lung epithelial cells A549 (CCL-185, ATCC, USA) were added to the upper side and grown in antibiotic-free F-12K (Kaighn's) nutrient. After they reached confluence (day 4), dexamethasone 1 µM was added to the F-12K to induce tight-junction formation. On day 7, all media was removed from the upper side (so that the lung epithelium would have an

air interface) and the media on the underside was replaced with a 1:1 mixture of DMEM and F-12K. The media were replaced again on day 11. On day 14, *S. pneumoniae* was grown as previously described and 10 µL containing 10^5 CFUs in PBS were added to the upper side of each insert. That resulted in the complete *in vitro* alveolar infection model, represented in Figure 34. The media mixture was replaced with PBS as soon as *S. pneumoniae* was introduced to the inserts, and they were incubated for 30 minutes prior to any of the PDI experiments.

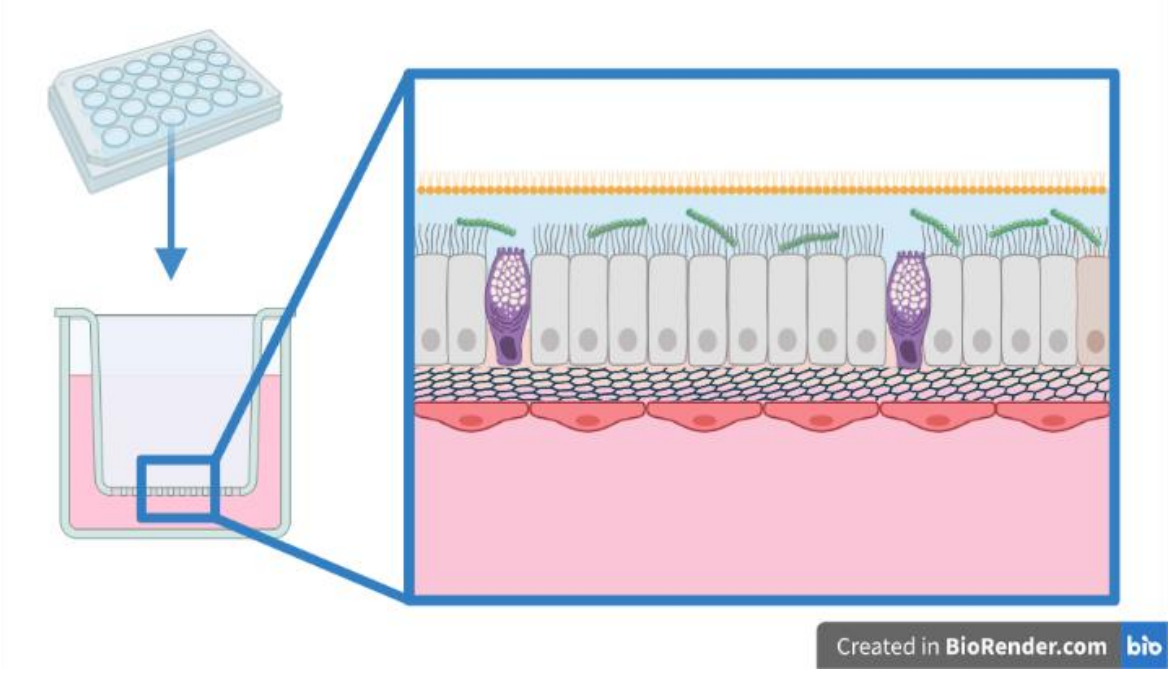

Figure 34 – The *in vitro* alveolar infection model. PET-membrane inserts are added to 24-well plates and endothelial cells (red) are grown on the underside, while pulmonary epithelial cells are grown on the upper side, with an air interface. In these conditions, A549 cells differentiate into type I (gray) and type II (purple) pneumocytes, that express the lung surfactant (yellow). Later, *S. pneumoniae* (green) is added to the upper side, to simulate pneumonia.
Source: By the author, made using biorender.com.

For the PFOB experiments, ICG was added in different ways to represent different delivery methods: first, for the "intravenous" delivery, 500 µL of ICG 100 µM were added instead of the PBS on the underside of the insert, and it was incubated for one hour; then, for the "pulmonary" delivery, 100 µL of ICG 10 µM were added to the upper side of the insert, and for the "PFOB" delivery, 10 µL of ICG 100 µL were added to the upper side in combination with 90 µL of PFOB, and they were incubated for 10 minutes. The control group received 100 µL of PBS on the upper side. Then, the whole 24-well plate was treated with 20 J/cm² of infrared light (780 nm). Following that, samples were diluted and plated in blood agar for CFU counts. Each insert was diluted and counted three times, and the median value was used to plot the result. Each group consisted of three inserts, and the experiment was

performed on two separate occasions (n = 6). Groups were compared using the Kruskal-Wallis and the *post hoc* Dunn tests, and considered significantly different with $p<0.05$.

For the neMB experiment, its PDI efficacy was compared to the one of MB. Both photosensitizers were diluted in PBS to either 1 or 10 μM and added to the upper side of the insert (the control received only PBS). After 20 minutes of incubation in the dark, the entire 24-well plate was treated with 20J/cm² of 660 nm light. Following that, samples were diluted and plated in blood agar for CFU counts. Each group consisted of 3 inserts (n = 3). Each insert was diluted and counted 3 times, and the mean log-transformed value was used to plot the result. Groups were compared using two-way ANOVA and the *post hoc* Dunnett tests, and considered significantly different with $p<0.05$.

7.2 Results

7.2.1 Perfluorooctyl bromide (PFOB) ICG formulation

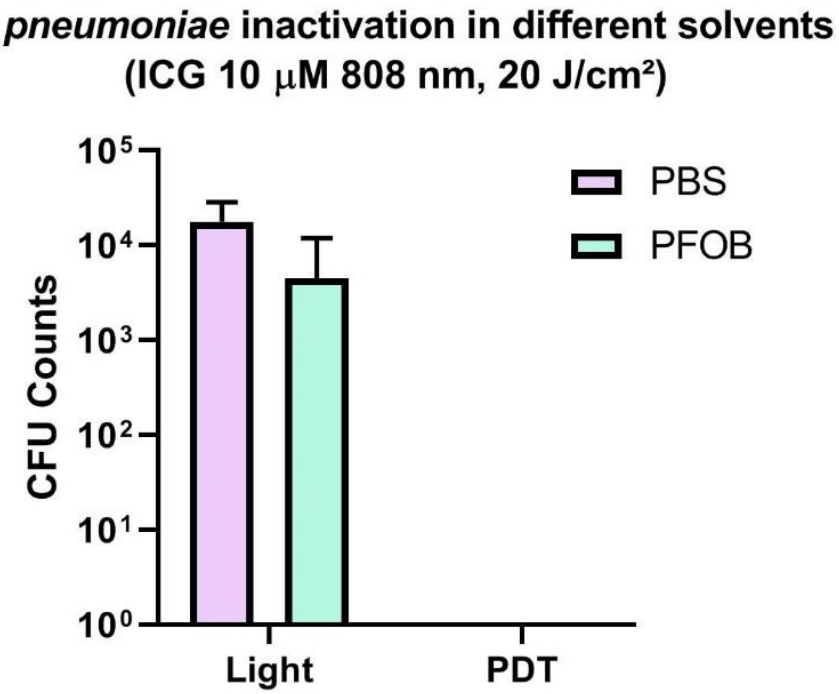

Figure 35 – Photodynamic inactivation of *S. pneumoniae* with indocyanine green in combination with different solvents. N = 3. No statistical treatment.
Source: By the author.

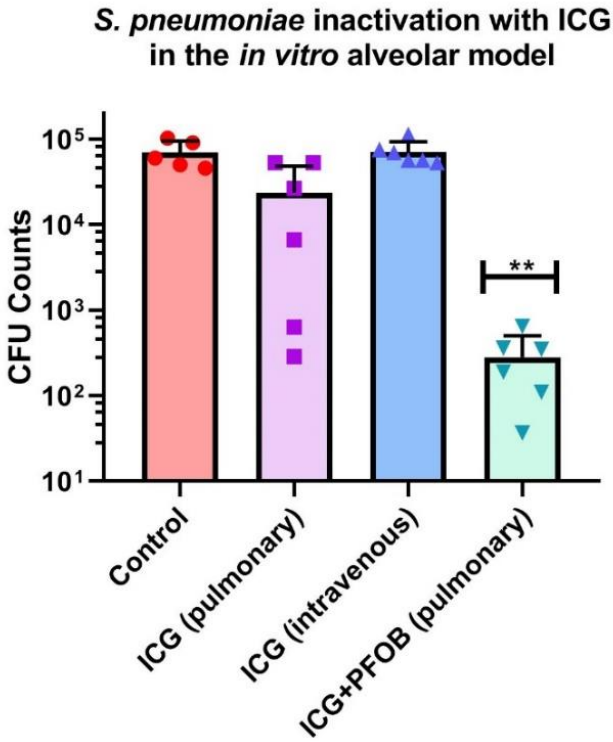

Figure 36 – Photodynamic inactivation of *S. pneumoniae* with ICG using different delivery methods in the *in vitro* alveolar model, using illumination with 780 nm (20 J/cm²). N = 5-6. **: $p<0.01$.
Source: By the author.

The addition of PFOB to the *in vitro* system does not impact the PDI of *S. pneumoniae* with ICG. Figure 35 shows that, when combined with ICG, PFOB does not inhibit the inactivation of the bacteria, yield complete elimination as in the PBS control. At the same time, PFOB does not inactivate the bacteria directly, given that there is a small difference between the PBS and the PFOB controls. Nonetheless, in the *in vitro* infection model, the combination of ICG and PFOB yielded a significant decrease in bacterial viability (Figure 36). In this model, the “pulmonary” ICG-PDI is not effective, likely due to the presence of the lung surfactant. The “intravenous” delivery, that had a longer incubation time and higher concentration of ICG, was also not effective.

7.2.2 Methylene blue (MB) and its nanoemulsion formulation (neMB)

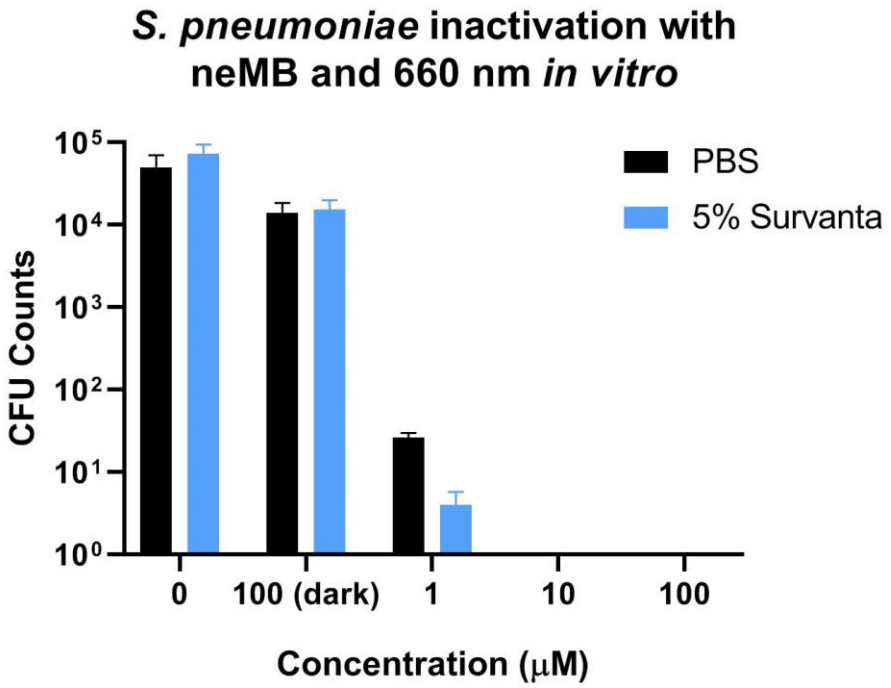

Figure 37 – Photodynamic inactivation of *S. pneumoniae* with methylene blue nanoemulsion, in the presence and absence of Survanta®. N = 3. No statistical treatment.
Source: By the author.

Figure 37 shows that neMB successfully inhibits *S. pneumoniae in vitro*, even in the presence of Survanta®. It shows complete elimination of the bacteria after light exposure starting at 10 µM, with partial killing at 1 µM, while it only shows a slight response in the dark, even at 100 µM. These results are similar to what has been found for the single-molecule MB in section 5.2.1.

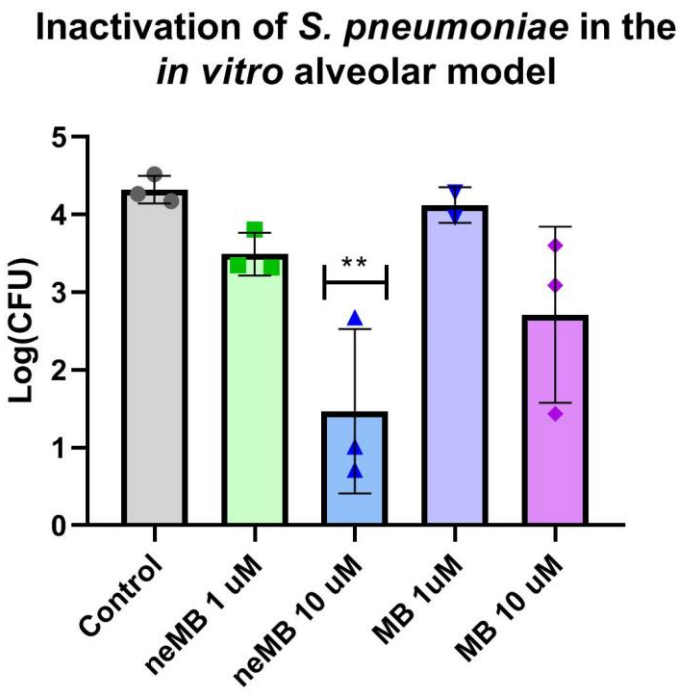

Figure 38 – Photodynamic inactivation of *S. pneumoniae* with MB and neMB using the *in vitro* alveolar model, using illumination with 660 nm (20 J/cm²). N = 2-3. **: $\boldsymbol{p < 0.01}$.
Source: By the author.

In the *in vitro* alveoli, neMB shows a better PDI response than MB. Figure 38 shows that, at 10 µM, neMB significantly decreases the infection burden in the system, while MB does not. At 1 µM, neither drug produces significant results in this preliminary analysis, but there is about 1 log of difference between neMB 1 µM and the control.

7.3 Discussion

Many strategies were tested to improve ICG's photodynamic inactivation in the presence of Survanta®, including: formulations with different types of surfactants (BRIJ-98, Pluronic F-127, sodium dodecyl-sulphate, Tween 80 and BRIJ-L4); formulations with polyethylene glycol in different sizes (PEG E 400, PEG 500, PEG 2000 and PEG 5000); formulations with polyelectrolytic compounds (chitosan, mucin, dextran sulphate, carboxymethyl dextran and hyaluronic acid); formulations with perfluorocarbons (perfluorohexane and perfluorooctyl bromide); an ICG calcium salt; combination with ultrasound therapy (40 kHz, 1 MHz and 3 MHz); and combination with antibiotics (amoxicillin, erythromycin, gentamicin and oxacillin). However, most of these were unsuccessful. Some of the added elements, on their own, had an ability to reduce bacterial

viability (specially ultrasound and antibiotics), but were not able to synergistically improve the PDI results (not shown).

The one exception was the use of perfluorocarbons (PFCs), which are not active against *S. pneumoniae* on their own, but significantly improved the photodynamic inactivation with ICG (Figure 35 andFigure **36**). PFCs are similar to hydrocarbons, but in which all hydrogens have been replaced with fluorine, and they are typically liquid at ambient temperature.[139] They present specific characteristics such as biocompatibility, great solubilization of gases, and low surface tension, that make them ideal for a number of clinical applications, including the replacement of blood in intravascular transport of oxygen, and the treatment of lung collapse and acute lung injury[133]. PFCs have been investigated as vehicles for the pulmonary delivery of antibiotics, using fluorosurfactants to form emulsions, which showed promising results.[135,140-141]

PFOB is one of the most commonly used PFCs for pulmonary application. It has a surface tension of 18 mN/m and is able to dissolve up to 530 mL of O_2 per liter (water can only dissolve 30 mL/L)[134]. It is radiopaque, which allows for an easy monitoring of the lung perfusion, and it has a quicker excretion rate than other PFCs[141]. *In vitro*, PFOB has a slight impact in the viability of *S. pneumoniae*, and does not inhibit the effect of the ICG-PDI (Figure 35). In the alveolar model, ICG does not have a photodynamic inactivation effect on its own, likely due to the presence of lung surfactant, but is effective when combined with PFOB (Figure 36). When delivered through the underlayer of the alveolar model, simulating the intravenous delivery, ICG does not interact directly with the lung surfactant, but probably also does not penetrate through the endothelium, membrane and epithelium to reach the bacteria, despite the longer incubation time and higher concentration when compared to the other groups. On the other hand, PFOB interacts with the endogenous lung surfactant, changing its interfacial dynamic behavior.[142] We believe that PFOB solubilizes the lung surfactant, disrupting its organization, which enables the aqueous phase containing ICG to reach the bacterial targets. In this experiment, it was not possible to use fluorosurfactants to form the emulsion, so the PFOB and the ICG phases were immiscible, but the results were successful nonetheless. Using the emulsion will likely improve stability, reproducibility, and perhaps even the efficacy of these results. Unfortunately, in a clinical application setting, the PFOB-based strategy would require the patient to be hospitalized, and likely completely intubated, so that the lungs could be filled with the solvent. Thus, as promising as this alternative is, it is also interesting to investigate strategies that would be easier and accessible to more patients.

In the typical *in vitro* experiment, neMB inactivates *S. pneumoniae* regardless of the presence of Survanta® (Figure 37), and yields similar inactivation results to MB when using the same concentration, incubation time and light fluence (see Figure 21). However, in the alveolar model, PDI using neMB is significantly better than using MB (Figure 38). *S. pneumoniae* is harder to kill in this model, for both photosensitizers. While both of them showed about 3 logs of reduction with 1 µM in 5% Survanta, neither achieve even 1 log in this concentration on the alveolar model. However, at 10 µM, PDI with neMB reduces CFU counts in about 3 logs, resulting in a statistically significant difference from the control. At this concentration, MB reduces the bacterial burden in about 1,5 logs, which is not significant. The findings from chapters 5 and 6 suggested that MB should be mobile, and have little interaction with Survanta®, thus being free to interact with the bacteria; while neMB, that has some interaction with the lung surfactant, should be less available and thus yield poorer results at the same concentration. But neMB also interacts slightly better with bacterial membrane components (Figure 27), and despite *S. pneumoniae* not having any LPS, it serves to show that the result in a complex biological system is a combination of multiple factors and simultaneous interactions.

One possible hypothesis is that the nanoemulsion formulation could improve the efficacy of multiple photosensitizers for this application, not necessarily due to their surface activity, but rather to other nanotechnology-based properties. So, to test that, a natural next step would be to prepare a nanoemulsion formulation of ICG, combining the improved efficacy seen in neMB and the ideal photodynamic characteristics of ICG. Unfortunately, ICG is unstable in solution, producing a dimer that has no photodynamic activity, and leading to a loss of efficacy as soon as 6 hours after solubilization[143]. The nanoemulsion formulation does not shield ICG from this degradation mechanism, thus it would not be viable to use neICG as a photosensitizer. Yet, the same rational can be applied to develop other photosensitizers or even ICG-based formulations and nanostructures that could potentially be applied in the treatment of pulmonary infections.

8 CONCLUSION

As previous research had already placed aPDT as a highly promising technique for the treatment of bacterial pneumonia, the initial objective of this study was to demonstrate the efficacy of ICG-aPDT against multiple pathogens and safety in different models. Initially, this was done by investigating the selectivity of ICG-PDI using *in vitro* bacterial and mammalian cell cultures. The protocol presented successfully inactivated two strains of *S. aureus*, while showing no cytotoxicity to three different mammalian cell lines. Moreover, mice that received the treatment recovered fully and seven days later showed no signs of tissue damage or inflammation.

However, despite having excellent *in vitro* results, a good pharmacokinetics profile, and strong evidence of safety, the *in vivo* treatment of bacterial pneumonia was unsuccessful. Over the course of the project, new infection models were developed, using different pathogens in either mice or pigs. Unfortunately, in all of these new models, the aPDT treatment failed to reduce bacterial burden or aid recovery. Eventually, we hypothesized that the importance of the alveolar microenvironment to the success of the treatment was being overlooked, and discovered that molecular photosensitizers interact with the lung surfactant, inhibiting the photodynamic inactivation of bacteria.

To investigate this possibility, five photosensitizers with potential for aPDT applications in the lungs had their efficacy in killing the pneumonia-causing *Streptococcus pneumoniae* tested in the presence and absence of a medical grade lung surfactant. It became evident that it was not a matter of inhibiting the generation of ROS, but rather a special separation between the photosensitizers and the bacterial target that lead to a loss of activity. This was true for all of the photosensitizers tested. Even methylene blue, that seemed to be an exception in the Survanta® experiment, is negatively affected in the *in vitro* alveolar model experiment. The nature of this interaction was further investigated using surface-based experiments, and it was discovered that ICG had a great affinity for surfaces and interacts with the lung surfactant, altering some of its properties. MB, on the other hand, did not show surface-activity in its molecular form, but showed some interesting behavior in nanoemulsion form.

Finally, some strategies were proposed to overcome the barrier imposed by the lung surfactant. A complex in vitro system was developed so that the presence of the LS could be taken into account in preliminary experiments, without the immediate need for animal testing. ICG remained as the most promising candidate for pulmonary PDT because of its safety and

excitation range, and preliminary results in such a system indicated that combining it with the perfluorocarbon PFOB might be a viable alternative for the treatment of in-hospital patients. Additionally, despite MB not having the ideal characteristics for pulmonary aPDT, initial results with the MB nanoemulsion have been promising and might aid the development of new pulmonary photosensitizers in the future.

Overall, this piece of research highlights the challenges of developing a truly innovative therapy. The need for new approaches in treating pneumonia is evident, and aPDT remains as a promising alternative for it, with many advantages when compared to traditional antibiotics. However, during the pre-clinical stages of research, it is fundamental that biological systems are considered in their full complexity. Understanding the mechanisms through which a proposed treatment fails brings scientist closer to findings treatments that will eventually be successful.

REFERENCES

1 WORLD HEALTH ORGANIZATION (WHO) **The top 10 causes of death**. 2020. Available from: https://www.who.int/news-room/fact-sheets/detail/the-top-10-causes-of-death. Accessible at: 23 Jan. 2021.

2 LOZANO, R. *et al*. Global and regional mortality from 235 causes of death for 20 age groups in 1990 and 2010: a systematic analysis for the Global Burden of disease study 2010. **Lancet**, v. 380, n. 9859, p. 2095–2128, 2012.

3 MAISCH, T. Anti-microbial photodynamic therapy: useful in the future? **Lasers in Medical Science**, v. 22, n. 2, p. 83–91, 2007.

4 RUSSELL, C. J. *et al*. The use of inhaled antibiotic therapy in the treatment of ventilator-associated pneumonia and tracheobronchitis: a systematic review. **BMC Pulmonary Medicine**, v. 16, n. 1, p. 10–16, 2016.

5 TORRES, A. Antibiotic treatment against methicillin-resistant *staphylococcus* aureus hospital-and ventilator-acquired Pneumonia: a step forward but the battle continues. **Clinical Infectious Diseases**, v. 54, n. 5, p. 630–632, 2012.

6 KASHEF, N.; HAMBLIN, M. R. Can microbial cells develop resistance to oxidative stress in antimicrobial photodynamic inactivation? **Drug Resistance Updates**, v. 31, p. 31–42, 2017. DOI: 10.1016/j.drup.2017.07.003.

7 DAI, T. *et al.* Photodynamic therapy for localized infections-State of the art. **Photodiagnosis and Photodynamic Therapy**, v. 6, n. 3–4, p. 170–188, 2009.

8 LEITE, I. S. *et al*. Near-infrared photodynamic inactivation of S. pneumoniae and its interaction with RAW 264.7 macrophages. **Journal of Biophotonics**, v. 11, n. 1, p. 1–10, 2018. DOI: 10.1002/jbio.201600283

9 GERALDE, M.C. *et al*. Pneumonia treatment by photodynamic therapy with extracorporeal illumination - an experimental model. **Physiological Reports**, v. 5, n. 5, p. e13190, 2017.

10 KASSAB, G.; *et al*. Nebulization as a tool for photosensitizer delivery to the respiratory tract. **Journal of Biophotonics**, v. 12, n. 4, p. e201800189, 2019.

11 TOPALOGLU, N. *et al*. Antimicrobial photodynamic therapy of resistant bacterial strains by indocyanine green and 809-nm diode laser. **Photomedicine and Laser Surgery**, v. 31, n. 4, p. 155–162, 2013.

12 WONG, T. *et al*. Indocyanine Green—mediated photodynamic therapy reduces methicillin-resistant *staphylococcus* aureus drug resistance. **Journal of Clinical Medicine**, v. 8, n. 3, p. 411, 2019.

13 Acute lower respiratory infections. *In*: GIBSON, G. J. *et al*. (ed.). **European lung white book**. European Respiratory Society, 2013, p. 210–223.

14 WALLIHAN, R.; RAMILO, O. Community-acquired pneumonia in children: current

challenges and future directions. **Journal of Infection**, v. 69, n. S1, p. S87–S90, 2014.

15 CORRÊA, R.D.A. *et al*. Brazilian guidelines for community-acquired pneumonia in immunocompetent adults - 2009. **Jornal Brasileiro de Pneumologia:** publicacao oficial da sociedade brasileira de pneumologia e tisilogia, v. 35, n. 6, p. 574–601, 2009.

16 FERREIRA-COIMBRA, J. *et al*. Burden of community-acquired pneumonia and Unmet Clinical Needs. **Advances in Therapy**, v. 37, n. 4, p. 1302–1318, 2020.

17 SHOAR, S.; MUSHER, D.M. Etiology of community-acquired pneumonia in adults: a systematic review. **Pneumonia**, v. 12, n. 1, 2020. DOI: 10.1186/s41479-020-00074-3

18 CILLÓNIZ, C. *et al*. Microbial aetiology of community-acquired pneumonia and its relation to severity. **Thorax**, v. 66, n. 4, p. 340–346, 2011.

19 ISTURIZ, R. E. *et al*. Clinical and economic burden of pneumonia among adults in Latin America. **International Journal of Infectious Diseases**, v. 14, n. 10, p. e852–e856, 2010.

20 GUPTA, R. K. *et al*. Bacterial pneumonia and pandemic influenza planning. **Emerging Infectious Diseases**, v. 14, n. 8, p. 1187–1192, 2008.

21 NAIR, G. B.; NIEDERMAN, M.S. Nosocomial pneumonia. lessons learned. **Critical Care Clinics**, v. 29, n. 3, p. 521–546, 2013.

22 JONES, R.N. Microbial etiologies of Hospital-acquired bacterial pneumonia and ventilator-associated bacterial pneumonia. **Clinical Infectious Diseases**, v. 51, n. S1, p. S81–S87, 2010.

23 METLAY, J. P.; WATERER, G.W. Treatment of community-acquired pneumonia during the Coronavirus disease 2019 (COVID-19) pandemic. **Annals of Internal Medicine**, v. 173, n. 4, p. 304–305, 2020.

24 OSUCHOWSKI, M. F. *et al*. The COVID-19 puzzle: deciphering pathophysiology and phenotypes of a new disease entity. **Lancet Respiratory Medicine**, v. 9, n. 6, p. 622–642, 2021.

25 RAWSON, T. M. *et al*. Bacterial and Fungal Coinfection in Individuals With Coronavirus: a rapid review to support COVID-19 antimicrobial prescribing. **Clinical Infectious Diseases**, 2020.

26 BASSETTI, M. *et al*. Antiviral treatment selection for SARS-CoV-2 pneumonia. **Expert Review of Respiratory Medicine**, v. 15, n. 8, p. 985–992, 2021.

27 PICKENS, C.O. *et al*. Bacterial superinfection pneumonia in patients mechanically ventilated for COVID-19 pneumonia. **American Journal of Respiratory and Critical Care Medicine**, v. 204, n. 8, p. 921–932, 2021.

28 SIESWERDA, E. *et al.* Recommendations for antibacterial therapy in adults with COVID-19 – an evidence based guideline. **Clinical Microbiology and Infection**, v. 27, n. 1, p. 61–66, 2021.

29 GOULD, I. M. *et al*. New insights into meticillin-resistant *staphylococcus* aureus (MRSA) pathogenesis, treatment and resistance. **International Journal of Antimicrobial Agents**, v. 39, n. 2, p. 96–104, 2012.

30 MENDES, R.E. *et al.* Linezolid update: stable in vitro activity following more than a decade of clinical use and summary of associated resistance mechanisms. **Drug Resistance Updates**, v. 17, n. 1–2, p. 1–12, 2014.

31 FELDMAN, C.; ANDERSON, R. Review: current and new generation pneumococcal vaccines. **Journal of Infection**, v. 69, n. 4, p. 309–325, 2014.

32 GIBSON, G. J. *et al*. Immunisation against respiratory diseases. *In:* GIBSON, G. J. *et al*. (ed.); **European Lung White Book**. European Cystic Fibrosis Society, 2013. chapter 18, p. 306–315.

33 AGOR, J. K.; ÖZALTIN, O. Y. Models for predicting the evolution of influenza to inform vaccine strain selection. **Human Vaccines and Immunotherapeutics**, v. 14, n. 3, p. 678–683, 2018.

34 FORMAN, R. *et al*. COVID-19 vaccine challenges: what have we learned so far and what remains to be done? **Health Policy**, v. 125, n. 5, p. 553–567, 2021.

35 RAAB, O. Über die Wirkung fluorescirender Stoffe auf Infusorien. **Zeitschrift für Biologie**, v. 1, n. 39, p. 524, 1900.

36 KHARKWAL, G.B. *et al*. Photodynamic therapy for infections: clinical applications. **Lasers in Surgery and Medicine**, v. 43, n. 7, p. 755–767, 2012.

37 WAINWRIGHT, M.; BAPTISTA, M. S. The application of photosensitisers to tropical pathogens in the blood supply. **Photodiagnosis and Photodynamic Therapy**, v. 8, n. 3, p. 240–248, 2011.

38 AGOSTINIS, P. *et al*. Photodynamic therapy of cancer: an update. **CA:** a cancer jounal for clinicians, v. 61, n. 4, p. 250–281, 2011.

39 BALDEA, I.; FILIP, A. Photodynamic therapy in melanoma-an update. **Journal of Physiology and Pharmacology**, v. 63, n. 2, p. 109–118, 2012.

40 GORMAN, A. *et al*. In vitro demonstration of the heavy-atom effect for photodynamic therapy. **Journal of the American Chemical Society**, v. 126, n. 34, p. 10619–10631, 2004.

41 KASSAB, G. **Nebulization as a tool for the delivery of photosensitizers in the photodynamic inactivation of respiratory diseases**. 2018. Dissertation (Master in Science) - Instituto de Física de São carlos, Universidade de São Paulo, São Carlos, 2018.

42 LIM, C. *et al*. Indocyanine green fluorescence imaging in the surgical management of liver cancers: current facts and future implications. **Journal of Visceral Surgery**, v. 151, n. 2, p. 117–124, 2014.

43 FICKWEILER, S. *et al*. Indocyanine green: intracellular uptake and phototherapeutic

effects in vitro. **Journal of Photochemistry and Photobiology B:** biology, v. 38, n. 2-3, p. 178–183, 1997.

44 PANSARE, V. J. *et al*. Formulation of long-wavelength indocyanine green nanocarriers. **Journal of Biomedical Optics**, v. 22, n. 9, p. 1, 2017.

45 SHEMESH, C. S.*et al*. Indocyanine green loaded liposome nanocarriers for photodynamic therapy using human triple negative breast cancer cells. **Photodiagnosis and Photodynamic Therapy**, v. 11, n. 2, p. 193–203, 2014.

46 BOEHM, T.K.; CIANCIO, S.G. Diode laser activated indocyanine green selectively kills bacteria. **Journal of the International Academy of Periodontology**, v. 13, n. 2, p. 58–63, 2011.

47 MONZAVI, A. *et al*. Antimicrobial photodynamic therapy using diode laser activated indocyanine green as an adjunct in the treatment of chronic periodontitis: A randomized clinical trial. **Photodiagnosis and Photodynamic Therapy**, v. 14, p. 93–97, 2016. DOI: 10.1016/j.pdpdt.2016.02.007

48 TOPALOGLU, N. *et al*. The role of reactive oxygen species in the antibacterial photodynamic treatment: Photoinactivation vs proliferation. **Letters in Applied Microbiology**, v. 62, n. 3, p. 230–236, 2016.

49 INTERNATIONAL AGENCY FOR RESEARCH ON CANCER. Methylene Blue. *In:* **IARC Working Group on the Evaluation of Carcinogenic:** risks to humans. 2016. chapter 108, p. 155.

50 PROVAYBLUE™ (methylene blue) injection, for intravenous use. **Food and Drug Administration**, 2016. Available from: https://www.accessdata.fda.gov/drugsatfda_docs/label/2017/204630s005lbl.pdf . Accessible at: 30/04/2022.

51 TARDIVO, J. P. *et al*. Methylene blue in photodynamic therapy: from basic mechanisms to clinical applications. **Photodiagnosis and Photodynamic Therapy**, v. 2, n. 3, p. 175–191, 2005.

52 ORTH, K. *et al*. Methylene blue mediated photodynamic therapy in experimental colorectal tumors in mice. **Journal of Photochemistry and Photobiology B:** biology, v. 57, n. 2–3, p. 186–192, 2000.

53 BOLTES CECATTO, R. *et al*. Methylene blue mediated antimicrobial photodynamic therapy in clinical human studies: the state of the art. **Photodiagnosis and Photodynamic Therapy,** v. 31, p. 101828, Sept. 2020. DOI: 10.1016/j.pdpdt.2020.101828.

54 DERIKVAND, N. *et al*. Antimicrobial photodynamic therapy with diode laser and methylene blue as an adjunct to scaling and root planning: a clinical trial. **Photodiagnosis and Photodynamic Therapy**, v. 31, n. l, p.101818, April 2020. DOI: 10.1016/j.pdpdt.2020.101818

55 SADAKSHARAM, J. *et al*. Treatment of oral lichen planus with methylene blue mediated

photodynamic therapy - a clinical study. **Photodermatology Photoimmunology and Photomedicine**, v. 28, n. 2, p. 97–101, 2012.

56 SHEN, X. *et al*. Treatment of infected wounds with methylene blue photodynamic therapy: An effective and safe treatment method. **Photodiagnosis and Photodynamic Therapy**, v. 32, p. 102051, 2020. DOI: 10.1016/j.pdpdt.2020.102051.

57 HUANG, Y. *et al*. Low-level laser therapy: an emerging clinical paradigm. **SPIE Newsroom**, n. 9, p. 1–3, 2009. DOI:10.1117/2.1200906.1669

58 LIM, H. J.; OH, C. H. Indocyanine green-based photodynamic therapy with 785nm light emitting diode for oral squamous cancer cells. **Photodiagnosis and Photodynamic Therapy**, v. 8, n. 4, p. 337–342, 2011.

59 CHATTERJEE, D.K. *et al.* Nanoparticles in photodynamic therapy: an emerging paradigm. **Advanced Drug Delivery Reviews**, v. 60, n. 15, p. 1627–37, 2008.

60 MONTAZERABADI, A.R. *et al.* The effects of combined treatment with ionizing radiation and indocyanine green-mediated photodynamic therapy on breast cancer cells. **Journal of Photochemistry and Photobiology B:** biology, v. 109, p. 42–49, 2012.

61 KASSAB, G. *et al.* Supporting information - lung surfactant negatively affects the photodynamic inactivation of bacteria - in vitro and molecular dynamic simulation analyses. **Proceedings of the National Academy of Sciences**, v. 119, p. e2123564119, 2022. DOI: 10.1073/pnas.2123564119

62 GERALDE, M.C. *et al*. **Pulmonary decontamination for photodynamic inactivation with extracorporeal illumination**. 2014. Available from: https://www.spiedigitallibrary.org/conference-proceedings-of-spie/8927/89271B/Pulmonary-decontamination-for-photodynamic-inactivation-with-extracorporeal-illumination/10.1117/12.2039366.pdf. Accessible at: 23 Jan. 2021.

63 LEITE, I. S. *et al*. **Photodynamic inactivation of microorganisms which cause pulmonary diseases with infrared light**: an in vitro study. 2014. Available from: https://www.spiedigitallibrary.org/conference-proceedings-of-spie/8927/89271A/Photodynamic-inactivation-of-microorganisms-which-cause-pulmonary-diseases-with-infrared/10.1117/12.2039300.pdf. Accessible at: 23 Jan. 2021.

64 KASSAB, G. *et al*. Nebulization as a tool for photosensitizer delivery to the respiratory tract. **Journal of Biophotonics**, v. 12, n. 4, p. e201800189, 2019.

65 CASSIDY, C. M. *et al*. Drug and light delivery strategies for photodynamic antimicrobial chemotherapy (PACT) of pulmonary pathogens: A pilot study. **Photodiagnosis and Photodynamic Therapy**, v. 8, n. 1, p. 1–6, 2011.

66 LEHMANN, J. *et al*. Improvement of pulmonary photodynamic therapy: nebulisation of curcumin-loaded tetraether liposomes. **Pharmaceutics**, v. 13, n. 8, p. 1243, 2021.

67 BAGHDAN, E. *et al*. Development of inhalable curcumin loaded nano-in-microparticles for bronchoscopic photodynamic therapy. **European Journal of Pharmaceutical Sciences**,

v. 132, p. 63–71, 2019. DOI: 10.1016/j.ejps.2019.02.025.

68 TOVAR, J. S. D. *et al*. Photodynamic inactivation of S. pneumoniae with external illumination at 808 nm through the ex vivo porcine thoracic cage. **Journal of Biophotonics**, v. 15, n. 2, p. e202100189, 2021.

69 SVYATCHENKO, V. A. *et al*. Antiviral photodynamic therapy: inactivation and inhibition of SARS-CoV-2 in vitro using methylene blue and Radachlorin. **Photodiagnosis and Photodynamic Therapy**, v. 33, p. 102112, 2021.

70 POURHAJIBAGHER, M. *et al*. Robust antimicrobial photodynamic therapy with curcumin-poly (lactic-co-glycolic acid) nanoparticles against COVID-19: A preliminary in vitro study in Vero cell line as a model. **Photodiagnosis and Photodynamic Therapy**, v. 34, p. 102286, 2021. DOI: 10.1016/j.pdpdt.2021.102286.

71 ARENTZ, J.; HEIDE, H. J. Evaluation of methylene blue based photodynamic inactivation (PDI) against intracellular B-CoV and SARS-CoV2 viruses under different light sources in vitro as a basis for new local treatment strategies in the early phase of a Covid19 infection. **Photodiagnosis and Photodynamic Therapy**, v. 37, p. 102642, 2022. DOI: 10.1016/j.pdpdt.2021.102642.

72 SHARSHOV, K. *et al*. The photosensitizer octakis(Cholinyl)zinc phthalocyanine with ability to bind to a model spike protein leads to a loss of sars-cov-2 infectivity in vitro when exposed to far-red led. **Viruses**, v. 13, n. 4, p. 643, 2021.

73 WEBER, H. M. *et al*. Successful reduction of SARS-CoV-2 viral load by photodynamic therapy (PDT) verified by QPCR – a novel approach in treating patients in early infection stages. **Medical and Clinical Research**, v. 5, n. 11, p. 311, 2020.

74 POURHAJIBAGHER, M.; BAHADOR, A. Computational biology analysis of COVID-19 receptor-binding domains: a target Site for indocyanine green through antimicrobial photodynamic therapy. **Journal of Lasers in Medical Sciences**, v. 11, n. 4, p. 433–441, 2020.

75 PERLIN, M. *et al*. Photodynamic inactivation of influenza and herpes viruses by hematoporphyrin. **Antiviral Research**, v. 7, n. 1, p. 43–51, 1987.

76 AROSO, R.T. *et al*. Photodynamic inactivation of influenza virus as a potential alternative for the control of respiratory tract infections. **Journal of Photochemistry and Photobiology**, v. 7, p. 100043, 2021. DOI: 10.1016/j.jpap.2021.100043.

77 NOTTER, R.H. **Lung surfactants:** basic science and clinical applications. New York: Marcel Dekker, 2000.

78 GARCIA-MOUTON, C. *et al*. The lord of the lungs: the essential role of pulmonary surfactant upon inhalation of nanoparticles. **European Journal of Pharmaceutics and Biopharmaceutics**, v. 144, p. 230–243, 2019. DOI: 10.1016/j.ejpb.2019.09.020.

79 OSELIERO FILHO, P. L. *et al*. Structure and thermotropic behavior of bovine- and porcine-derived exogenous lung surfactants. **Langmuir**, v. 36, n. 48, p. 14514–14529, 2020.

80 KLENZ, U. *et al*. Influence of lipid saturation grade and headgroup charge: a refined lung surfactant adsorption model. **Biophysical Journal**, v. 95, n. 2, p. 699–709, 2008.

81 HICKMAN-DAVIS, J. M. *et al*. Lung surfactant and reactive oxygen-nitrogen species: antimicrobial activity and host-pathogen interactions. **American Journal of Physiology:** lung cellular and molecular physiology, v. 281, p. 517–523, 2001. DOI: 10.1152/ajplung.2001.281.3.L517.

82 SILVERMAN, J.A. *et al*. Inhibition of daptomycin by pulmonary surfactant: in vitro modeling and clinical impact. **Journal of Infectious Diseases**, v. 191, n. 12, p. 2149–2152, 2005.

83 SOUZA, L.M.P. *et al*. Penetration of antimicrobial peptides in a lung surfactant model. **Colloids and Surfaces B:** biointerfaces, v. 167, p. 345–353, 2018. DOI: 10.1016/j.colsurfb.2018.04.030

84 BANASCHEWSKI, B. J. H. *et al*. Antimicrobial and biophysical properties of surfactant supplemented with an antimicrobial peptide for treatment of bacterial pneumonia. **Antimicrobial Agents and Chemotherapy**, v. 59, n. 6, p. 3075–3083, 2015.

85 MOUSSEAU, F. The role of surface charge in the interaction of nanoparticles with model pulmonary surfactants. **Soft Matter**, v. 14, n. 28, p. 5764–5774, 2018.

86 ORTIZ-COLLAZOS, S. *et al*. Interaction of levofloxacin with lung surfactant at the air-water interface. **Colloids and Surfaces B:** biointerfaces, v. 158, p. 689–696, 2017. DOI: 10.1016/j.colsurfb.2017.07.066.

87 PHAM, S.; WIEDMANN, T.S. Note: dissolution of aerosol particles of budesonide in Survanta™, a model lung surfactant. **Journal of Pharmaceutical Sciences**, v. 90, n. 1, p. 98–104, 2001.

88 VEEN, A. *et al*. Exogenous pulmonary surfactant as a drug delivering agent: influence of antibiotics on surfactant activity. **British Journal of Pharmacology**, v. 118, n. 3, p. 593–598, 1996.

89 ROBERTSON, B.; HALLIDAY, H. L. Principles of surfactant replacement. **Biochimica et Biophysica Acta:** molecular basis of disease, v. 1408, n. 2–3, p. 346–361, 1998.

90 MIRASTSCHIJSKI, U. *et al*. Lung surfactant for pulmonary barrier restoration in patients with COVID-19 pneumonia. **Frontiers in Medicine**, v. 7, p. 1–4, 2020. DOI: 10.3389/fmed.2020.00254.

91 JAMES, N.S. *et al*. Measurement of cyanine dye photobleaching in photosensitizer cyanine dye conjugates could help in optimizing light dosimetry for improved photodynamic therapy of cancer. **Molecules**, v. 23, n. 8, p. 1842, 2018.

92 KASSAB, G. *et al*. Safety and delivery efficiency of a photodynamic treatment of the lungs using indocyanine green and extracorporeal near infrared illumination. **Journal of Biophotonics**, v. 13 n. 10, p. e202000176, 2020.

93 HETZE, S. *et al*. Superiority of preventive antibiotic treatment compared with standard treatment of poststroke pneumonia in experimental stroke: a bed to bench approach. **Journal of Cerebral Blood Flow and Metabolism**, v. 33, n. 6, p. 846–854, 2013.

94 OMAR, G. S. *et al*. Lethal photosensitization of wound-associated microbes using indocyanine green and near-infrared light. **BMC Microbiology**, v. 8, n. 1, p. 111, 2008.

95 TUCHIN, V. V. *et al*. A pilot study of ICG laser therapy of acne vulgaris: photodynamic and photothermolysis treatment. **Lasers in Surgery and Medicine**, v. 33, n. 5, p. 296–310, 2003.

96 PARK, K. Y. *et al*. 1,213 cases of treatment of facial acne using indocyanine green and intense pulsed light in Asian skin. **BioMed Research International**, v. 2015, 2015. DOI: 10.1155/2015/596161

97 ENGEL, E. *et al*. Light-induced decomposition of indocyanine green. **Investigative Ophthalmology and Visual Science**, v. 49, n. 5, p. 1777–1783, 2008.

98 POURHAJIBAGHER, M. *et al*. Evaluation of antimicrobial photodynamic therapy with indocyanine green and curcumin on human gingival fibroblast cells: an in vitro photocytotoxicity investigation. **Photodiagnosis and Photodynamic Therapy**, v. 15, p. 13–18, 2016. DOI: 10.1016/j.pdpdt.2016.05.003.

99 FARIA, C.M.G. *et al.* Determination of the threshold dose distribution in photodynamic action from in vitro experiments. **Journal of Photochemistry and Photobiology B:** biology, v. 162, p. 168–175, 2016. DOI: 10.1016/j.jphotobiol.2016.06.041.

100 GEORGE, S. *et al*. Uptake pathways of anionic and cationic photosensitizers into bacteria. **Photochemical & Photobiological Sciences**, v. 8, n. 6, p. 788, 2009.

101 ONDA, N. *et al*. Preferential tumor cellular uptake and retention of indocyanine green for in vivo tumor imaging. **International Journal of Cancer**, v. 139, n. 3, p. 673–682, 2016.

102 NADITHE, V. *et al*. Evaluation of nose-only aerosol inhalation chamber and comparison of experimental results with mathematical simulation of aerosol deposition in mouse lungs. **Journal of Pharmaceutical Sciences**, v. 92, n. 5, p. 1066–1076, 2003.

103 YASEEN, M. A. *et al*. Biodistribution of encapsulated indocyanine green in healthy mice. **Molecular Pharmaceutics**, v. 6, n. 5, p. 1321–1332, 2009.

104 CHEN, C.Y. *et al*. A liquid chromatography tandem mass spectrometry method for the quantification of indocyanine green in dog plasma and bile. **Journal of Pharmaceutical and Biomedical Analysis**, v. 47, n. 2, p. 351–359, 2008.

105 KASSAB, G. *et al*. Fluorescence assessment of the delivery and distribution of nebulized indocyanine green in a murine model. **Proceedings of SPIE**, v. 10475, 2018. DOI: 10.1117/12.2293013

106 JARVI, M. T. *et al*. Insights into photodynamic therapy dosimetry : simultaneous singlet

oxygen luminescence and photosensitizer photobleaching measurements. **Biophysical Journal**, v. 102, n. 3, p. 661–671, 2012.

107 KASUYA, K. *et al*. Novel photodynamic therapy against biliary tract carcinoma using mono-L-aspartyl chlorine e6: basic evaluation for its feasibility and efficacy. **Journal of Hepato-Biliary-Pancreatic Sciences**, v. 17, n. 3, p. 313–321, 2010.

108 LOH, C.S. *et al*. Mucosal ablation using photodynamic therapy for the treatment of dysplasia: an experimental study in the normal rat stomach. **Gut**, v. 38, n. 1, p. 71–78, 1996.

109 KWON, E. J. *et al*. Porous silicon nanoparticle delivery of tandem peptide anti-infectives for the treatment of *pseudomonas aeruginosa* lung infections. **Advanced Materials**, v. 29, n. 35, p. 1701527, 2017. DOI: 10.1002/adma.201701527.

110 MCDOWELL, S. A. *et al*. Simvastatin is protective during *staphylococcus* aureus pneumonia. **Current Pharmaceutical Biotechnology**, v. 12, n. 9, p. 1455–1462, 2011.

111 LUNA, C. M. *et al*. Effect of linezolid compared with glycopeptides in methicillin-resistant Staphylococcus aureus severe pneumonia in piglets. **Chest**, v. 135, n. 6, p. 1564–1571, 2009.

112 MARTÍNEZ-OLONDRIS, P. *et al.* An experimental model of pneumonia induced by methicillin-resistant Staphylococcus aureus in ventilated piglets. **European Respiratory Journal**, v. 36, n. 4, p. 901–906, 2010.

113 MATUTE-BELLO, G. *et al*. Animal models of acute lung injury. **American Journal of Physiology**, p. 379–399, 2008. DOI: 10.1152/ajplung.00010.2008.

114 WICHA, W.W. *et al*. Pharmacokinetics / pharmacodynamics of lefamulin in a neutropenic murine pneumonia model with Staphylococcus aureus and Streptococcus pneumoniae. **Journal of Antimicrobial Chemotherapy**, v. 74, suppl. 3, p. 11–18, 2019.

115 ANDES, D.; CRAIG, W.A. In vivo activities of amoxicillin and amoxicillin-clavulanate against Streptococcus pneumoniae: Application to breakpoint determinations. **Antimicrobial Agents and Chemotherapy**, v. 42, n. 9, p. 2375–2379, 1998.

116 MOODY, E. D. *et al*. Non-covalent labeling of human serum albumin with indocyanine green: a study by capillary electrophoresis with diode laser-induced fluorescence detection. **Journal of Chromatography B:** biomedical sciences and applications, v. 729, n. 1–2, p. 55–64, 1999.

117 AN, F. *et al*. Rationally assembled albumin/indocyanine green nanocomplex for enhanced tumor imaging to guide photothermal therapy. **Journal of Nanobiotechnology**, v. 18, n. 1, p. 1–11, 2020.

118 ZHANG, H. *et al*. Comparative study of clinical pulmonary surfactants using atomic force microscopy. **Biochimica et Biophysica Acta -** biomembranes, v. 1808, n. 7, p. 1832–1842, 2011.

119 ESTRADA-LÓPEZ, E. D. *et al.* Prednisolone adsorption on lung surfactant models:

insights on the formation of nanoaggregates, monolayer collapse and prednisolone spreading. **RSC Advances**, v. 7, n. 9, p. 5272–5281, 2017.

120 SOUZA, F. R. *et al*. Permeation of beta-defensin-3 encapsulated with polyethylene glycol in lung surfactant models at air-water interface. **Colloids and Surfaces B:** biointerfaces, v. 182, p. 110357, 2019. DOI: 10.1016/j.colsurfb.2019.110357

121 SOUZA, F. R. *et al*. Polymer-coated gold nanoparticles and polymeric nanoparticles as nanocarrier of the BP100 antimicrobial peptide through a lung surfactant model. **Journal of Molecular Liquids**, v. 314, p. 113661, 2020. DOI: 10.1016/j.molliq.2020.113661

122 KASSAB, G. *et al*. Lung surfactant negatively affects the photodynamic inactivation of bacteria - in vitro and molecular dynamic simulation analyses. **Proceedings of the National Academy of Sciences**, v. 119, p. e2123564119, 2022. DOI: 10.1073/pnas.2123564119

123 LEE, S. K.; BARD, A. J. Near-IR electrogenerated chemiluminescence of tricarbocyanine dyes in micellar systems. **Analytical Letters**, v. 31, n. 13, p. 2209–2229, 1998.

124 FERNANDEZ, J. M. J. *et al*. Singlet oxygen generation by photodynamic agents. **Journal of Photochemistry and Photobiology B:** biology, v. 344, n. 96, p. 131–140, 1997.

125 MYRZAKHMETOV, B. *et al*. Photophysical properties of protoporphyrin IX, pyropheophorbide-a and photofrin® in different conditions. **Pharmaceuticals**, v. 14, n. 2, p. 1–21, 2021.

126 SILVA, R. C. **Avaliação da eficiência fotodinâmica de fotossensibilizadores com aplicação em terapia fotodinâmica**. 2007. Dissertação (Mestrado em Ciências) - Instituto de Química de São Carlos, Universidade de São Paulo, São Carlos, 2007.

127 CORRÊA, J. C. **Fotodegradação do photoditazine e citotoxicidade dos fotoprodutos formados após irradiação com laser**. 2006.114p.Dissertaçao(Mestrado) - Instituto de Quimica de Sao Calos, Universidade de São Paulo,2006.

128 PRATAVIEIRA, S. *et al*. Photodynamic therapy with a new bacteriochlorin derivative: Characterization and in vitro studies. **Photodiagnosis and Photodynamic Therapy**, v. 34, p. 1–8, 2021. DOI: 10.1016/j.pdpdt.2021.102251

129 DIAZ TOVAR, J. S. *et al.* Photodegradation in the infrared region of indocyanine green in aqueous solution. *In:* 2019 SBFOTON INTERNATIONAL OPTICS AND PHOTONICS CONFERENCE**,**2019.**SBFoton IOPC,** IEEE,2019. **DOI:** 10.1109/SBFoton-IOPC.2019.8910207

130 KASSAB, G. *et al*. Non-invasive activation of photosensitizers in the lungs: achievable goal or impossible dream? *In*: CONGRESS OF THE EUROPEAN SOCIETY FOR PHOTOBIOLOGY,19th,. Eigenverlag, 2021.**Book Abstracts,**Salsburg: World Wide Web, 2021.

131 VAN'T VEEN, A. *et al*. Pulmonary surfactant as vehicle for intratracheally instilled tobramycin in mice infected with Klebsiella pneumoniae. **British Journal of Pharmacology**,

v. 119, n. 6, p. 1145–1148, 1996.

132 CAÑADAS, O. *et al*. Polyhydroxyalkanoate nanoparticles for pulmonary drug delivery: Interaction with lung surfactant. **Nanomaterials**, v. 11, n. 6, p. 1–17, 2021.

133 KRAFFT, M. P. Perfluorocarbons and perfluorocarbon emulsions for pulmonary indications. *In*: SEPPELT, K. (ed.). **The curious world of fluorinated molecules**: molecules containing fluorine. Berlin: Elsevier, 2021.

134 LEHMLER, H. J. Perfluorocarbon compounds as vehicles for pulmonary drug delivery. **Expert Opinion on Drug Delivery**, v. 4, n. 3, p. 247–262, 2007.

135 WILLIS, J. A. *et al*. Photodynamic viral inactivation: recent advances and potential applications. **Applied Physics Reviews**, v. 8 n. 2, p. 021315, 2021.

136 CHANG, E. *et al*. Porphyrin-lipid stabilized paclitaxel nanoemulsion for combined photodynamic therapy and chemotherapy. **Journal of Nanobiotechnology**, v. 19, n. 1, p. 1–15, 2021.

137 HUH, D. *et al.* A human disease model of drug toxicity-induced pulmonary edema in a lung-on-a-chip microdevice. **Science Translational Medicine**, v. 4, n. 159, 2012. DOI: 10.1126/scitranslmed.3004249.

138 HERMANNS, M. I. *et al*. Lung epithelial cell lines in coculture with human pulmonary microvascular endothelial cells: development of an alveolo-capillary barrier in vitro. **Laboratory Investigation**, v. 84, n. 6, p. 736–752, 2004.

139 NELSON, D. L. **Pulmonary drug delivery via reverse perfluorocarbon emulsions**: a novel method for bacterial respiratory infections and acute respiratory failure. 2018. 177 p. Thesis (Doctor of Philosophy) - Department of Biomedical Engineering, Carnegie Mellon University, Pittsburgh, 2018.

140 ORIZONDO, R.A. *et al*. Effects of fluorosurfactant structure and concentration on drug availability and biocompatibility in water-in-perfluorocarbon emulsions for pulmonary drug delivery. **Colloid and Polymer Science**, v. 295, n. 12, p. 2413–2422, 2017.

141 RIESS, J.G. *et al*. Advanced fluorocarbon-based systems for oxygen and drug delivery, and diagnosis. **Artificial Cells, Blood Substitutes, and Biotechnology**, v. 25, n. 1–2, p. 43–52, 1997.

142 ECKMANN, D.M. *et al*. Influence of intravenous perfluorocarbon administration on the dynamic behavior of lung surfactant. **Artificial Cells, Blood Substitutes, and Immobilization Biotechnology**, v. 26, n. 4, p. 359–366, 1998.

143 LI, D.H.; SMITH, B.D. Deuterated indocyanine green (ICG) with extended aqueousstorage shelf-life: chemical and clinical implications. **Chemistry**, v. 27, n. 58, p. 14535-14542, 2021.

ANNEX A – Research Ethics Committee approval documents

UNIVERSIDADE DE SÃO PAULO
Instituto de Física de São Carlos

COMISSÃO DE ÉTICA NO USO DE ANIMAIS

CERTIFICADO

Certificamos que a proposta intitulada "Inativação fotodinâmica da pneumonia bacteriana utilizando nebulização do fotossensibilizador e iluminação extracorpórea", protocolada sob o CEUA nº 3620051018, sob a responsabilidade de **Giulia Kassab** *e equipe; Vanderlei Salvador Bagnato* - que envolve a produção, manutenção e/ou utilização de animais pertencentes ao filo Chordata, subfilo Vertebrata (exceto o homem), para fins de pesquisa científica ou ensino - está de acordo com os preceitos da Lei 11.794 de 8 de outubro de 2008, com o Decreto 6.899 de 15 de julho de 2009, bem como com as normas editadas pelo Conselho Nacional de Controle da Experimentação Animal (CONCEA), e foi **aprovada** pela Comissão de Ética no Uso de Animais da Instituto de Física de São Carlos - Universidade de São Paulo (CEUA/IFSC) na reunião de 22/10/2018.

We certify that the proposal "Photodynamic Inactivation of Bacterial Pneumonia with nebulization of the photosensitizer and extracorporeal illumination", utilizing 110 Isogenics mice (110 males), protocol number CEUA 3620051018, under the responsibility of **Giulia Kassab** *and team; Vanderlei Salvador Bagnato* - which involves the production, maintenance and/or use of animals belonging to the phylum Chordata, subphylum Vertebrata (except human beings), for scientific research purposes or teaching - is in accordance with Law 11.794 of October 8, 2008, Decree 6899 of July 15, 2009, as well as with the rules issued by the National Council for Control of Animal Experimentation (CONCEA), and was **approved** by the Ethic Committee on Animal Use of the Physics Institute of São Carlos - São Paulo University (CEUA/IFSC) in the meeting of 10/22/2018.

Finalidade da Proposta: Pesquisa (Acadêmica)

Vigência da Proposta: de 11/2018 a 11/2020 Área: Grupo de Óptica / Fcm

Origem:	Não aplicável biotério						
Espécie:	Camundongos isogênicos	sexo:	Machos	idade:	8 a 10 semanas	N:	110
Linhagem:	BALB/c AnUnib			Peso:	20 a 25 g		

Local do experimento: Laboratórios do Grupo de Óptica do Instituto de Física de São Carlos IFSC/USP

São Carlos, 22 de outubro de 2018

Prof. Dr. Fernando Fernandes Paiva
Coordenador da Comissão de Ética no Uso de Animais
Instituto de Física de São Carlos - Universidade de São Paulo

Profa. Dra. Ana Paula Ulian de Araújo
Vice-Coordenadora da Comissão de Ética no Uso de Animais
Instituto de Física de São Carlos - Universidade de São Paulo

Av. Trabalhador São-Carlense, 400 - Pq. Arnold Schimdt, CEP: 13566-590 - São Carlos/SP. - tel: 55 (16) 3373-6673 / fax: ---
Horário de atendimento: 2ª a 6ª das 08h às 12h e 13h30 às 17h30 : e-mail: ceua@ifsc.usp.br
CEUA N 3620051018

DIVISION OF RESEARCH

Research Compliance and Biosafety

November 13, 2019

MEMORANDUM

TO: Dr. Jeffrey Cirillo
TAMHSC - MPI - Microbial Pathogenesis and Immunology

FROM: Dr. Mark Westhusin, Chair
Institutional Animal Care and Use Committee

SUBJECT: **Approval of Personnel Change Request**
AUP: IACUC 2018-0282
Title: CAREER: Optical sensing and imaging of bacterial infection to improve global health
Reference Number: 097923
Funding Source: National Science Foundation(NSF), William Marsh Rice University
AUP Approval Date: 09/13/2018
Expiration Date: 09/12/2021
Species: Guinea Pigs, Hartley, Mice

This is to inform you that the IACUC has approved the above-referenced amendment as follows:

- Ciceron Ayala-Orozco and Giulia Kassab have been added as study personnel.

The Committee thanks you for your efforts to keep the IACUC informed of any changes to your protocol. If we can be of any further assistance, please contact the IACUC office at 979.845.1828.

Best of success in your research endeavors.

Pc: Comparative Medicine Program

750 Agronomy Road, Suite 2701
1186 TAMU
College Station, TX 77843-1186

Tel. 979.458.1467 Fax. 979.862.3176
http://rcb.tamu.edu

UNIVERSIDADE DE SÃO PAULO
Instituto de Física de São Carlos

COMISSÃO DE ÉTICA NO USO DE ANIMAIS

CERTIFICADO

Certificamos que a proposta intitulada "Inativação fotodinâmica da pneumonia bacteriana utilizando nebulização do fotossensibilizador e iluminação externa: cinética, segurança e eficácia em modelo porcino ", protocolada sob o CEUA nº 8416011020, sob a responsabilidade de **Giulia Kassab** *e equipe; Ana Júlia Barbosa Tomé; Flávio Pola dos Reis; Gabriel Jasinevicius; Hilde Harb Buzzá; Johan Sebastian Diaz Tovar; Natalia Mayumi Inada; Prof. Cristina Kurachi; Prof. Paulo Manuel Pego Fernandes; Susimeire Gomes; Vanderlei Salvador Bagnato* - que envolve a produção, manutenção e/ou utilização de animais pertencentes ao filo Chordata, subfilo Vertebrata (exceto o homem), para fins de pesquisa científica ou ensino - está de acordo com os preceitos da Lei 11.794 de 8 de outubro de 2008, com o Decreto 6.899 de 15 de julho de 2009, bem como com as normas editadas pelo Conselho Nacional de Controle da Experimentação Animal (CONCEA), e foi **aprovada** pela Comissao de Etica no Uso de Animais da Instituto de Fisica de Sao Carlos - Universidade de Sao Paulo (CEUA/IFSC) na reunião de 19/10/2020.

We certify that the proposal "Photodynamic Inactivation of Bacterial Pneumonia using Nebulization of the Photosensitizer and External Illumination: kinetics, safety and efficacy in the porcine model", utilizing 25 Swines (25 females), protocol number CEUA 8416011020, under the responsibility of **Giulia Kassab** *and team; Ana Júlia Barbosa Tomé; Flávio Pola dos Reis; Gabriel Jasinevicius; Hilde Harb Buzzá; Johan Sebastian Diaz Tovar; Natalia Mayumi Inada; Prof. Cristina Kurachi; Prof. Paulo Manuel Pego Fernandes; Susimeire Gomes; Vanderlei Salvador Bagnato* - which involves the production, maintenance and/or use of animals belonging to the phylum Chordata, subphylum Vertebrata (except human beings), for scientific research purposes or teaching - is in accordance with Law 11.794 of October 8, 2008, Decree 6899 of July 15, 2009, as well as with the rules issued by the National Council for Control of Animal Experimentation (CONCEA), and was **approved** by the Ethic Committee on Animal Use of the Physics Institute of Sao Carlos - Sao Paulo University (CEUA/IFSC) in the meeting of 10/19/2020.

Finalidade da Proposta: Pesquisa (Acadêmica)

Vigência da Proposta: de 11/2020 a 08/2022 Área: Grupo de Óptica / Fcm

Origem:	Animais provenientes de estabelecimentos comerciais						
Espécie:	Suínos	sexo:	Fêmeas	idade:	7 a 15 semanas	N:	25
Linhagem:	Landrace			Peso:	28 a 32 kg		

Local do experimento: Todos os experimentos serão realizados no laboratório LIM/09 da Faculdade de Medicina da USP, em São Paulo

Sao Carlos, 14 de abril de 2022

Prof. Dr. Fernando Fernandes Paiva
Coordenador da Comissão de Ética no Uso de Animais
Instituto de Fisica de Sao Carlos - Universidade de Sao Paulo

Profa. Dra. Ana Paula Ulian de Araújo
Vice-Coordenadora da Comissão de Ética no Uso de Animais
Instituto de Fisica de Sao Carlos - Universidade de Sao Paulo

Av. Trabalhador Sao-Carlense, 400 - Pq. Arnold Schimdt, CEP: 13566-590 - Sao Carlos/SP. - tel: 55 (16) 3373-6673 / fax: ---
Horário de atendimento: 2ª a 6ª das 08h às 12h e 13h30 às 17h30 : e-mail: ceua@ifsc.usp.br
CEUA N 8416011020

Faculdade de Medicina da Universidade de São Paulo
Avenida Dr. Arnaldo, 455
Pacaembu – São Paulo – SP

COMISSÃO DE ÉTICA NO USO DE ANIMAIS

Certificamos que a proposta intitulada **"Inativação fotodinâmica da pneumonia bacteriana utilizando nebulização do fotossensibilizador e iluminação externa: cinética, segurança e eficácia em modelo porcino"** registrada com o **nº 1597/2020**, sob a responsabilidade de **Paulo Manuel Pêgo Fernandes** e **Giulia Kassab**, apresentada pela Comissão Científica do InCor - que envolve a produção, manutenção e/ou utilização de animais pertencentes ao filo Chordata, subfilo Vertebrata (exceto humanos), para fins de pesquisa científica (ou ensino) - encontra-se de acordo com os preceitos da Lei nº 11.794, de 8 de outubro de 2008, do Decreto nº 6.899, de 15 de julho de 2009, e com as normas editadas pelo Conselho Nacional de Controle de Experimentação Animal (CONCEA), e foi aprovada pela COMISSÃO DE ÉTICA NO USO DE ANIMAIS (CEUA) da Faculdade de Medicina da USP em 23/11/2020

Finalidade	( ) Ensino (x) Pesquisa Científica
Vigência da autorização	Início: 21-12-2020 Término: 21-12-2021
Espécie/linhagem/raça	Suíno
Nº de animais	**25**
Peso/Idade	7-15 semanas
Sexo	fêmeas
Origem	Granja RG

A CEUA FMUSP solicita que ao final da pesquisa seja enviado Relatório com todas as atividades.

CEUA-FMUSP, 23 de novembro de 2020

Dr. Eduardo Pompeu
Coordenador
Comissão de Ética no Uso de Animais